Expression, localization, and interaction studies of the plastidic PII protein from *Arabidopsis thaliana*

Dissertation

der Mathematisch-Naturwissenschaftlichen Fakultät
der Eberhard Karls Universität Tübingen
zur Erlangung des Grades eines
Doktors der Naturwissenschaften
(Dr. rer. nat.)

vorgelegt von
Natalie Krieger
aus Kamyschin/ Russische Föderation

Tübingen
2020

Gedruckt mit Genehmigung der Mathematisch-Naturwissenschaftlichen Fakultät der Eberhard Karls Universität Tübingen.

Tag der mündlichen Qualifikation:	14.05.2020
Dekan:	Prof. Dr. Wolfgang Rosenstiel
1. Berichterstatter:	Prof. Dr. Klaus Harter
2. Berichterstatter:	Prof. Dr. Karl Forchhammer

1 Table of Contents

2 Index Pictures

3 Index Pictures Appendix

4 Index Tables

Abbreviations

2-OG	2-oxoglutarate, α-ketoglutarate
AA	amino acid
ACCase	Acetyl-CoA carboxylase
ADP	Adenosine diphosphate
A. tumefaciens	*Agrobacterium tumefaciens*
A. thaliana	*Arabidopsis thaliana*
Arg	Arginine
Asp	Aspartate
Atg8e	AUTOPHAGY 8E (At2g45170)
Atg8g	AUTOPHAGY 8G (At3g60640)
ATP	Adenosine triphosphate
PII	*A. thaliana* PII, AtGLB1, AtPII
BADC	Biotin attachment domain-containing
BCCP	Biotin carboxyl carrier protein
BiFC	Bimolecular fluorescence complementation
C	carbon
CLSM	Confocal Laser scanning microscope
cPII	CDS of PII
cTP	chloroplast transit peptide
DAO	D-amino acid oxidase
DAPI	4′, 6-Diamidin-2-phenylindol
DAT1	D-amino acid transaminase 1
DXR	Deoxyxylulose reductoisomerase
DXS	Deoxyxylulose synthase
E. coli	*Escherichia coli*
FLIM	fluorescence lifetime imaging microscopy
FRET	Förster resonance energy transfer
GBSSI	Granule-bound starch synthase 1
GFP	Green-Fluorescent protein
GGPPS11	Geranylgeranyl diphosphate synthase 11
Gln	Glutamine
Glu	Glutamate
gPII	genomic PII

Abbreviations

GS	glutamate synthetase
GUS	β-glucuronidase
htACCase	heteromeric Acetyl-CoA carboxylase
Ile	Isoleucine
IRF	instrument response function
Leu	Leucine
Lys	Lysine
MassSpec	Mass spectrometry
Met	Methionine
MS	Murashige and Skoog
N	Nitrogen
N. benthamiana	*Nicotiana benthamiana*
NAGK	N-acetyl-L-glutamate kinase
NBR1	Neighbour of BRCA1 GENE 1 (At4g24690)
Phe	Phenylalanine
PPT	Phosphinothricin/ IUPAC: (RS)-2-Amino-4-(hydroxy (methyl) phosphonoyl) butanoic acid
rBiFC	ratiomeric Bimolecular Fluorescence Complementation
RFP	Red-Fluorescent Protein
Ser	Serine
Thr	Threonine
Tyr	Tyrosine
UMP	Uranyl monophosphate
UDP	Uranyl diphosphate
UTP	Uranyl triphosphate
X-Gluc	5-bromo-4-chloro-3-indolyl-glucuronide
YFP	Yellow-Fluorescent Protein

Zusammenfassung

Die Perzeption und Regulation des zellulären Stickstoff- (N) und Kohlenstoff-(C) Gehalts ist essentiell für alle lebenden Organismen. Dabei soll die Superfamilie der PII Proteine, die hochkonserviert in Bakterien, Archaea, Algen und Pflanzen ist, eine entscheidende Rolle einnehmen. Aufgrund von Studien in Bakterien geht man davon aus, dass PII ein Sensor für den Stickstoff- und Kohlenstoff-Status ist. Obwohl die Funktion des PII Proteins in Bakterien relativ gut charakterisiert ist (Forchhammer and Selim, 2019), ist sehr wenig über diese Funktion in Pflanzen und vor allem in *Arabidopsis thaliana* (*A. thaliana*) bekannt.

Um die Funktion des *A. thaliana* PII-Proteins zu verstehen, habe ich mich auf Expressions-, Lokalisations- und Interaktionsstudien fokussiert. Ich konnte zeigen, dass sich die Expression der *PII* mRNA abhängig von anorganischem Stickstoff unter Dauerlicht verändert. Physiologische Untersuchungen an *PII*-knockdown Mutanten, sowie an *PII*-Überexpressions-Linien, zeigten keine Anhaltspunkte für eine Deregulation des C/N-Stoffwechsels. Diese Beobachtung lässt eine zentrale Rolle des PII-Proteins für diese Prozesse in Pflanzen wenig wahrscheinlich erscheinen.

Des Weiteren konnte ich zeigen, dass PII in Foci in Plastiden sowie im extra-plastidären Raum in Vesikel-ähnlichen Strukturen lokalisiert, welche in Zusammenhang mit dem Proteinumsatz stehen könnten. Zudem konnte ich ausschließen, dass PII an Nukleoide und Stärkekörner lokalisiert. PII co-lokalisiert nicht nur mit den zuvor bekannten Interaktionspartnern N-Acetyl-L-Glutamat Synthase (NAGK), Biotin Carboxyl Transport Protein 1 (BCCP1), Biotin/Lipoyl Anhaftungsdomäne enthaltenden (BADC) Proteinen BADC2 und BADC3 in Plastiden, sondern auch mit der Körnchen-gebundenen Stärkesynthase I (GBSSI), der D-Aminosäure Transaminase 1 (DAT1), der kleinen Rubisco Untereinheit RBCS3B, sowie der Deoxyxylulose Synthase (DXS), der Deoxyxylulose Reductoisomerase (DXR) und partiell mit der Geranylgeranyl Diphosphat Synthase 11 (GGPPS11). Mittels FRET-FLIM und BiFC konnte sogar eine Interaktion von PII mit sich selbst, NAGK, BCCP1, GBSSI, DAT1, RBCS3B, DXS und DXR festgestellt werden.

Das Lokalisierungsmuster und die Interaktionen, die für das *A. thaliana* PII festgestellt wurden, sind ein Indiz für weitere bisher unbekannte Funktionen des PII Proteins in *A. thaliana*.

Summary

The perception and regulation of the cellular content of nitrogen (N) and carbon (C) is essential for all living organisms. Though the superfamily of PII proteins that are highly conserved in bacteria, archaea, algae and plants, ought to play a crucial role. It is assumed from studies in bacteria that PII is a sensor of the nitrogen and carbon status Although the function of PII in bacteria is well characterised (Forchhammer and Selim, 2019), little is known about these function in plants and especially in *A. thaliana*.

To understand the function of *A. thaliana* PII, I focussed on expression, localization, and interaction studies. Here I show that *PII* mRNA expression changes dependent on inorganic nitrogen under constant light. Physiological studies on *PII* knockdown mutants, and in addition with *PII* overexpression lines, revealed no evidence for the deregulation of the C/N-metabolism. This observation let appear a central role of the PII-protein for these processes in plants less probable.

Furthermore, I could show that PII localizes to foci in plastids and in extraplastidic vesicle-like structures, which could be related to protein turnover. Further, I could exclude that PII localizes to nucleoids and starch granules. I could show that *A. thaliana* PII co-localizes not only with the already known interaction partners N-acetyl-L-glutamate kinase (NAGK), the biotin carboxyl carrier protein 1 (BCCP1) and with the biotin/lipoyl attachment domain containing (BADC) proteins BADC2/3 in plastids but in addition with Granule-bound Starch Synthase I (GBSSI), D-Amino Acid Transaminase 1 (DAT1), one of the small Rubisco subunits RBCS3B, and Deoxyxylulose synthase (DXS), Deoxyxylulose reductoisomerase (DXR) and partially with the Geranylgeranyl diphosphate synthase 11 (GGPPS11). Using FRET-FLIM and BiFC studies, even an interaction of PII with itself, NAGK, BCCP1, GBSSI, DAT1, RBCS3B, DXS and DXR could be observed.

The localization pattern and interactions observed for *A. thaliana* PII indicate further unknown regulatory functions of PII in *A. thaliana*.

1 Introduction

The superfamily of PII proteins is highly conserved in nearly all bacteria, archaea, algae, and plants. It turned out in bacteria that these proteins are of central importance for the regulation of the cellular nitrogen-carbon homeostasis (Ninfa and Atkinson, 2000; Arcondéguy et al., 2001; Ninfa and Jiang, 2005; Leigh and Dodsworth, 2007; Forchhammer, 2008; Sant'Anna et al., 2009). Therefore, the speculation whether PII proteins fulfil a similar function in plants is tempting, which was the starting point of my thesis.

1.1 The PII superfamily

The superfamily of PII proteins is subdivided in the three main groups, GlnB, GlnK and NifI, dependent on sequence similarities, and a proposed fourth group, PII-NG (PII-new group) (Ninfa and Atkinson, 2000; Arcondéguy et al., 2001; Ninfa and Jiang, 2005; Leigh and Dodsworth, 2007; Forchhammer, 2008; Sant'Anna et al., 2009).

PII was first discovered by Shapiro (1969) as a component in peak-II as a glutamate synthetase (GS) deadenylylation stimulator in *Escherichia coli* (*E. coli*) (Shapiro, 1969; Anderson et al., 1970).

The first group GlnB, further referred to as PII, is encoded by *glnB*, which is common in nearly all bacteria, archaea, algae and plants, as the major form of PII proteins (Ninfa and Atkinson, 2000; Arcondéguy et al., 2001).

GlnK, a close homologue of GlnB, is encoded by *glnK* that is absent in cyanobacteria, and forms the second group of PII proteins (Ninfa and Atkinson, 2000; Arcondéguy et al., 2001; Forchhammer, 2004). In most bacteria, *glnK* is linked to *amtB*, which encodes the high affinity ammonium transporter AmtB, composing the *glnK/amtB* operon (van Heeswijk et al., 1996; Thomas et al., 2000).

The third group of PII proteins is encoded by *nifI*. This group is distinct from GlnB and GlnK and only present in nitrogen-fixing anaerobic bacteria and nitrogen-fixing archaea (for review see: Leigh and Dodsworth (2007). There are two different groups of NifI proteins, $nifI_1$ and $nifI_2$, dependent on their linkage to the dinitrogenase genes *nifK* and *nifD*, and the dinitrogenase reductase gene *nifH* (Arcondéguy et al., 2001; Leigh and Dodsworth, 2007).

Sant'Anna et al. (2009) proposed a fourth group of PII proteins named PII-NG (PII new group) present in some bacteria. This group consists of proteins lacking the

PROSITE signature typical for PII proteins and is linked to metal transporters (Sant'Anna et al., 2009).

1.2 Structural features of PII

All PII proteins crystallised to date, form homo- or in some cases heterotrimers composing different PII protein isoforms (de Mel et al., 1994; Carr et al., 1996; Jiang et al., 1997; Xu et al., 1998; Forchhammer et al., 1999; Chellamuthu et al., 2014). Most PII proteins bind to ATP (*A. thaliana* PII in Figure 1 B), 2-OG (first shown for *E. coli PII* by Shapiro (1969); Brown et al. (1971)), and ADP as cofactors. Whereas Mg^{2+}-ATP binding promotes 2-OG binding, ADP binding negatively effects 2-OG binding (Jiang and Ninfa, 2009; da Rocha et al., 2013; Lapina et al., 2018). The ability to bind ADP is lost in plant PII proteins (reviewed in Lapina et al. (2018). The PII proteins GlnB and GlnK show high sequence and structural homology (Son and Rhee, 1987; Harrison et al., 1990; Tsinoremas et al., 1991; Liu and Magasanik, 1993; Reith and Munholland, 1993; van Heeswijk et al., 1995; van Heeswijk et al., 1996; Xu et al., 1998). The interaction site of both proteins to other proteins is the T-Loop, whereas the B-loop is important for PII homo- or heterotrimer formation (Figure 1) (Jiang et al., 1997; Jiang et al., 1997).

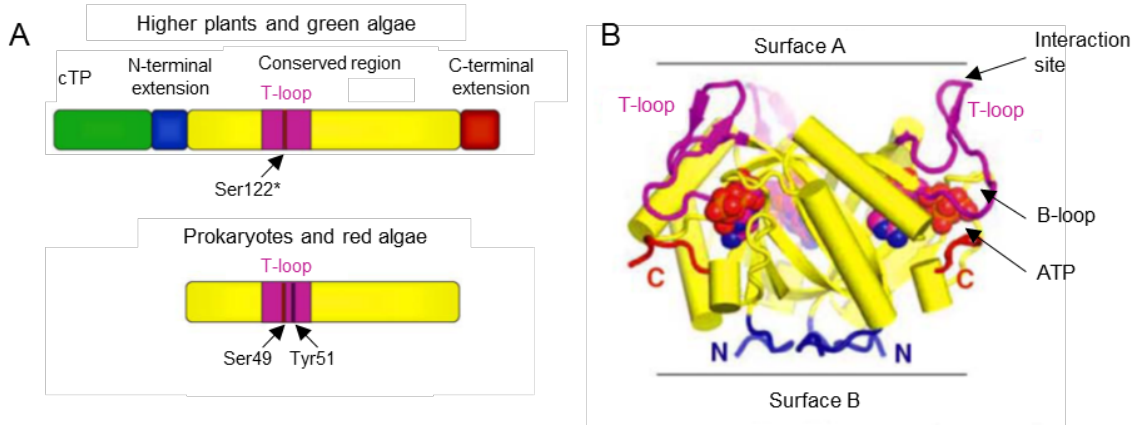

Figure 1: Scheme of conserved domains of PII proteins and crystal structure of *A. thaliana* PII.

A) Scheme of conserved PII domains in higher plants and green algae (upper panel), and prokaryotes and red algae; chloroplast transit peptide (cTP) in green, N-terminal extension in blue, and C-terminal extension in red are unique to higher plants and green algae. Conserved region in yellow with T-loop in magenta. Conserved Residues within the T-loop: Ser49 (phosphorylated) and Tyr51 (uridylylated) in prokaryotes and red algae, and corresponding Ser in higher plants and green algae (Ser122* in *A. thaliana* PII (Smith et al., 2004)). B) Crystal structure of *A. thaliana* PII. Surface A represents site of interaction, comprising the T-loop. B-loop important for PII homo- or heterotrimer formation (Jiang et al., 1997; Jiang et al., 1997). Surface B comprises the N-terminus of PII. A) and B) are modified from Uhrig et al. (2009).

In enteric bacteria, PII is post-translationally modified by uridylylation at position Tyr51 (Figure 1 A) by the bifunctional protein uridylyltransferase/ uridylyl-removing

enzyme UTase/UR dependent on the nitrogen (N) and carbon (C) level (Brown et al., 1971; Mangum et al., 1973; Adler et al., 1975; Engleman and Francis, 1978; Francis and Engleman, 1978; Rhee et al., 1978; Mura et al., 1981; Mura and Stadtman, 1981; Garcia and Rhee, 1983; Bueno et al., 1985; Son and Rhee, 1987; Kamberov et al., 1995). *Synechococcus* and *Synechocystis* PII, although harbouring Tyr51, are not uridylylated at this position but are phosphorylated at Ser49 (Figure 1 A) (Forchhammer and Tandeau de Marsac, 1994, 1995; Forchhammer and Tandeau de Marsac, 1995a; Hisbergues et al., 1999; Spät et al., 2015). Post-translational phosphorylation and thereby amount of phosphorylated PII in the trimer is dependent on nitrate, ammonium, and inorganic carbon level. Low nitrate, nitrite, and ammonium and high 2-OG concentrations lead to phosphorylation of PII, whereas increasing N concentrations lead to intermediate to full dephosphorylation (Forchhammer and Tandeau de Marsac, 1995; Forchhammer and Tandeau de Marsac, 1995a; Irmler et al., 1997; Forchhammer, 2004; Kloft et al., 2005).

Phosphorylation of PII was not detected so far in other cyanobacteria (reviewed in: Forchhammer and Selim (2019)), and evidence is missing for phosphorylation of Ser49 at corresponding Ser122 in *A. thaliana* (Figure 1 A) (Smith et al., 2004). *A. thaliana* and *Castor bean* PII are lacking the Tyr corresponding to the uridylylation site at position 124 and harbour a Phe instead (Hsieh et al., 1998).

1.3 PII in bacteria

In *E. coli*, PII interacts at high Gln levels with the histidine kinase and phosphatase NtrB, part of the *E. coli* two-component system, which in turn dephosphorylates the enhancer-binding transcription factor NtrC (Weiss and Magasanik, 1988; Ninfa and Bennett, 1991; Ninfa et al., 1993). By this, transcription of *glnA* is suppressed, which encodes GS. PII binds to the bifunctional GS adenylyltransferase (ATase) that adenylylates GS leading to its inactivation. At low ammonium level, 2-OG concentrations increase and Gln level decrease. PII gets uridylylated, interacts with ATase, leading to the activation of GS by deadenylylation. Uridylylated PII cannot interact with NtrB, which in turn leads to the phosphorylation of NtrC by NtrB and the initiation of *glnA* transcription (Shapiro, 1969; Brown et al., 1971; Mangum et al., 1973; Bueno et al., 1985; Ninfa and Magasanik, 1986; Son and Rhee, 1987; Weiss and Magasanik, 1988; Atkinson et al., 1994; Kamberov et al., 1994; Kamberov et al., 1995).

In cyanobacteria, PII interacts with the transcriptional co-activator PII-interacting Protein X (PipX) in a 2-OG dependent manner (Burillo et al., 2004; Espinosa et al., 2006). PipX interacts with the global transcription factor NtcA, which regulates gene expression in an N dependent manner as of e.g. PII, nitrogen-scavenging transporters, GS and GOGAT (Espinosa et al., 2006; Espinosa et al., 2007; Giner-Lamia et al., 2017). PipX interacts with PII, preferentially bound to ADP, at low or intermediate 2-OG levels, grown on ammonia or nitrate. Alternatively, PipX interacts with NtcA, bound to 2-OG, under intermediate or high 2-OG levels grown on nitrate or N starvation, thereby NtcA is activated (Espinosa et al., 2006; Llácer et al., 2010; Zeth et al., 2014). Under N deprivation, activated NtcA increases *PII* expression (Giner-Lamia et al., 2017). Localization studies of PII and PipX in *Synechococcus* revealed, localization of both proteins in foci at night at a putatively low ATP/ADP ratio (Espinosa et al., 2018), that was shown to be important for interaction of PII with PipX (Zeth et al., 2014; Luddecke and Forchhammer, 2015).

The first observed interaction partner of PII in cyanobacteria was the N-acetyl-L-glutamate kinase (NAGK), identified in a yeast-two hybrid screen using *Synechococcus sp.* PCC 7942 proteins (Burillo et al., 2004; Heinrich et al., 2004). NAGK, encoded by *argB*, is a key enzyme of the ornithine/arginine pathway, catalysing the reaction from N-acetyl-L-glutamate to N-acetyl-L-glutamate-phosphate and feedback regulated by L-Arg (reviewed in Cunin et al. (1986); Caldovic and Tuchman (2003)). The complex formation of two PII homotrimer with two NAGK homotrimer in a sandwich-like conformation promotes a higher enzyme activity of NAGK, which is furthermore slower feedback regulated by L-Arg (Maheswaran et al., 2004; Llácer et al., 2007; Beez et al., 2009). The ability of PII to bind 2-OG is dependent on Mg^{2+}-ATP presence, whereas this is not the case for PII in the PII-NAGK complex. 2-OG at low concentration leads to an increased activity of NAGK in the PII-NAGK complex. Only dephosphorylated PII binds to NAGK with high affinity. ADP and 2-OG bound to all three PII proteins in the trimer lead to the dissociation of the two interaction partners (Heinrich et al., 2004; Maheswaran et al., 2004; Beez et al., 2009; Fokina et al., 2010).

The interaction of PII with the biotinylated BCCP subunit of the ACCase, leading to its inhibition, was recently observed in *E. coli* and *Synechocystis sp.* PCC 6803 (Rodrigues et al., 2014; Gerhardt et al., 2015; Hauf et al., 2016). This inhibitory effect is negatively regulated by 2-OG and uridylylation or phosphorylation of PII,

respectively (Rodrigues et al., 2014; Gerhardt et al., 2015; Hauf et al., 2016). In *Synechococcus sp.* PCC 7942, ACCase activity increases and thereby increased levels of lipid bodies could be observed when PII is absent (Verma et al., 2018). It is proposed, that PII regulates ACCase activity dependent on the carbon levels in the cells and in turn regulates the distribution of acetyl-CoA and 2-OG to the TCA cycle, GS/GOGAT cycle or fatty acid production (Forchhammer and Selim, 2019).

1.4 PII in algae

Genome mapping of the red alga *Porphyra purpurea* revealed a *glnB* sequence encoded in its chloroplast genome (Reith and Munholland, 1993), whereas PII is absent in other red algae genomes. In green algae and plants, PII is nuclear-encoded but plastid localized (Hsieh et al., 1998; Uhrig et al., 2009; Baud et al., 2010; Ermilova et al., 2013). In contrast to prokaryotes and red algae, green algae and higher plant PII reveal an additional N-terminal chloroplast transit peptide and domain extensions at the N- and C-terminus. The latter harbours the Q-loop that binds at low affinity to L-Gln (Figure 1) (Uhrig et al., 2009; Chellamuthu et al., 2014). *Porphyra purpurea* PII acts in a ATP/ADP and 2-OG dependent manner, interacts with NAGK, and increases its activity independent of L-Gln (Lapina et al., 2018). This is in contrast to the non-photosynthetic green alga *Polytomella parva* in which PII and NAGK interact in an effector molecule independent manner, but NAGK activation is glutamine-dependent as in most green algae and higher plants (Chellamuthu et al., 2014; Selim et al., 2019). The PII protein of the closely related green algae *Chlamydomonas reinhardtii* (*Cr*) (Ermilova et al., 2013) was shown to interact with NAGK (Chellamuthu et al., 2014) and in addition, with the BCCP subunit of the ACCase, thereby negatively regulating lipid body formation (Zalutskaya et al., 2015).

PII of the green microalga *Myrmecia incisa* interacts with NAGK but not with BCCP1/2 in a yeast-two hybrid screen (Li et al., 2017). In addition, NAGK activity first increases and then decreases under N deprivation when 2-OG level increase and the PII-NAGK complex is disassembled (Li et al., 2017).

1.5 PII in plants

1.5.1 PII expression

In contrast to bacteria, the role of PII in plants is barely understood. An *in planta* PII-like protein (further referred as PII) *from A. thaliana* was first described by Hsieh et al. (1998). In *A. thaliana*, PII is a plastid-localized protein encoded by *GLB1* (further

referred as *PII*), a single copy gene on chromosome IV of the nuclear genome (Hsieh et al., 1998). This is in contrast to the red alga *Porphyra purpurea*, where *PII* is plastome-encoded (Reith and Munholland, 1993).

Expression of *PII* was shown to be positively regulated by light and sucrose. Addition of mannitol showed only a slight increase in PII expression in light, implying no dependency of *PII* expression to osmotic stress (Hsieh et al., 1998). *PII* expression is down regulated by dark and metabolites such as Gln, Glu and Asp in light on additional sucrose supply. In contrast, addition of sucrose in dark led to an increased expression (Hsieh et al., 1998). In addition, *PII* expression was shown to be affected by the transcription factor WRINKLED1 (WRI1), inducing expression of genes involved in fatty acid metabolism like BCCP1 (Baud et al., 2010).

1.5.2 PII localization

PII localization in chloroplasts in *A. thaliana* was first shown by Western blot analyses (Hsieh et al., 1998). PII from green algae and plants possess an N-terminal extension, predicted to be a chloroplast transit peptide by ChloroP (Nielsen et al., 1997; Emanuelsson et al., 1999; Emanuelsson et al., 2000), that is missing in bacteria (for review (Uhrig et al., 2009)). In *Oryza sativa* leaves, OsPII tagged with the Green-Fluorescent Protein (GFP) localized to chloroplasts (Sugiyama et al., 2004). Chloroplast-localization of AtPII was observed by immunohistochemically staining in *A. thaliana* suspension cells and seeds (Chen et al., 2006; Baud et al., 2010).

1.5.3 Phenotype of PII mutants

To date, the role of PII in plants is still cryptic. Hsieh et al. (1998) could show dependency of *PII* expression in *A. thaliana* on sucrose and light and described an increased anthocyanin content in *PII* overexpression lines when grown on ½ MS media with 3% sucrose and 1 mM Gln as sole N source (Hsieh et al., 1998). In the past years, two T-DNA insertion lines of *PII*, *PIIV1* (Ws-0) and *PIIS2* (Col-0), were characterized (Ferrario-Mery et al., 2005). *PIIV1* is a knockdown mutant, whereas *PIIS2* is a knockout mutant with a T-DNA insertion in the fourth intron (Ferrario-Mery et al., 2005). Both mutants did not show a phenotype under non-limiting conditions, but higher sensitivity induced by higher nitrite uptake and accumulation on seed germination and seedling growth (Ferrario-Mery et al., 2005; Ferrario-Mery et al., 2008). In response to ammonium resupply, both mutants showed reduced L-Arg, citrulline and ornithine contents after N starvation (Ferrario-Mery et al., 2006).

Under salt stress in *Oryza sativa*, downregulated PII contributed to an accumulation of amino acids and decrease of protein concentration (Xu et al., 2016). In *Lotus japonicus*, PII overexpression led to decreased N fixation under low N conditions. Under high N conditions, increased number of nodules as well as decreased ethylene content and increased citrulline content in nodules was observed (D'Apuzzo et al., 2015).

1.5.4 Interaction partners of plant PII

The interaction of PII with itself and the N-acetyl-L-glutamate kinase (NAGK), a key enzyme of the arginine biosynthesis, was first observed in Yeast-2 hybrid screens for *Synechococcus sp.* Strain PCC 7942, *A. thaliana* and *Oryza sativa* PII. This interaction is conserved from cyanobacteria to land plants and displays the best characterized interaction of plant PII (Burillo et al., 2004; Heinrich et al., 2004; Sugiyama et al., 2004; Chen et al., 2006; Ferrario-Mery et al., 2006; Mizuno et al., 2007; Beez et al., 2009; Feria Bourrellier et al., 2009; Chellamuthu et al., 2013; Chellamuthu et al., 2014; Lapina et al., 2018; Selim et al., 2019).

Crucial for the organisms in which PII interacts with NAGK found so far, is the hexameric structure of NAGK formed by two trimers (Ramón-Maiques et al., 2006). It was shown that NAGK plays a role in gametophyte function and embryo-development and indeed localizes to plastids in *A. thaliana* (Huang et al., 2017).

The interaction of *A. thaliana* PII and NAGK was shown to be dependent on Mg^{2+}-ATP binding of PII and leads to a reduced feedback regulation of NAGK by L-Arg (Chellamuthu et al., 2014). NAGK activation by PII is independent of L-Gln in *A. thaliana*, in contrast to other analysed green algae and plants, as *Brassicaceae* PII lacks three crucial AA in the Q-loop of the C-terminus and is thereby not able to bind L-Gln directly (Chellamuthu et al., 2014). In comparison to cyanobacteria, binding of 2-OG to PII was shown to have no effect on complex formation with NAGK (Chen et al., 2006; Ferrario-Mery et al., 2006). In *in vitro* assays, another study suggests that low amounts of 2-OG bound to AtPII might still be sufficient to perpetuate complex stability with NAGK, whereas the dissociation of AtPII from AtNAGK require lower 2-OG level in presence of NAG and L-Arg (Beez et al., 2009). In a pull-down assay performed with recombinant AtPII lacking the chloroplast transit peptide (cTP) sequence, purified from *E. coli*, NAGK and five new putative interaction partners were found. The putative interaction partners resembled two biotin carboxyl carrier proteins BCCP1 and BCCP2, a subunit of the plastid-localized

heteromeric Acetyl-CoA carboxylase (htACCase), catalysing the reaction of acetyl-CoA to malonyl-CoA, and three BCCP-like (Biotin/lipoyl attachment domain-containing (BADC)) proteins (Feria Bourrellier et al., 2010). The interaction of PII with the BCCP subunit of htACCase was shown to regulate htACCase activity negatively in *in vitro* assays in the presence of Mg^{2+}-ATP, whereas 2-OG reverse the inhibition of htACCase by PII (Feria Bourrellier et al., 2010). BCCP1 and BCCP2 were shown to have unidirectional redundant functions. BCCP1 is the main form and may fulfil BCCP2 functions but not *vice versa*. BCCP2 cannot complement *bccp1* null alleles that are embryo lethal due to defects in gametophyte and pollen development (Li et al., 2011). The BADC proteins were shown to be antagonists to the BCCP proteins and irreversibly bind and inhibit the htACCase activity (Salie et al., 2016; Keereetaweep et al., 2018).

1.6 Aim of the work

The bacterial PII protein is a well-characterized protein involved in sensing of the carbon/nitrogen balance and the energy status (Ninfa and Atkinson, 2000; Ninfa and Jiang, 2005; Commichau et al., 2006; Huergo et al., 2013; Forchhammer and Selim, 2019). Although the PII protein is conserved throughout evolution, its function in plants is still cryptic.

To elucidate the function of the *A. thaliana* PII, I focused on expression, localization, and interaction studies.

Light and sucrose were shown to have a positive effect on PII expression, whereas certain L-AA have a negative effect on PII expression (Hsieh et al., 1998). To investigate the effect of inorganic N with or without sucrose in constant light, the activity of the *PII* promoter using a promoter GUS assay in stably transformed *A. thaliana* lines should be performed.

The phenotype of the *PII* mutants *PIIVI* and *PIIS2* was shown to be unaffected in regards of non-limiting conditions, whereas both mutants showed higher sensitivity to nitrite (Ferrario-Mery et al., 2005). To determine whether the PII mutant line *PIIS2* display any measurable phenotype in regard to inorganic N and sucrose availability, phenotypic analyses of this line grown under four different light conditions under limiting and non-limiting N/sucrose conditions and the growth phenotype with certain L-AA as additional N source, would give a hint on PII function. Furthermore, phenotypical analyses of PII rescue and overexpression lines should be performed.

A. thaliana PII was shown in immunohistochemical analyses to localize to plastids (Chen et al., 2006; Baud et al., 2010). The subcellular localization pattern of PII was not shown before in living plants. To study this localization pattern, localization analysis of PII fused to fluorescent proteins in transiently transformed *N. benthamiana* and stably transformed *A. thaliana* not only under non-limiting growth conditions but also under differential temperatures and light qualities should give a hint on PII action.

The interaction partners of *A. thaliana* PII, NAGK, BCCP1/2 and BADC1-3 were analysed in *in vitro* studies (Burillo et al., 2004; Chen et al., 2006; Ferrario-Mery et al., 2006; Mizuno et al., 2007; Beez et al., 2009; Feria Bourrellier et al., 2009; Feria Bourrellier et al., 2010). To verify these interactions *in vivo*, first, co-localization experiments of PII with the known interaction partners in transiently transformed *N. benthamiana* and second, interaction studies using a Bimolecular Fluorescence Complementation (BiFC) assay (Grefen and Blatt, 2012) and Förster Resonance Energy Transfer (Forster, 1946) coupled with Fluorescence Lifetime Imaging Microscopy (FRET-FLIM) (Harter et al., 2012; Bücherl et al., 2014; Laptenok et al., 2014; Peter et al., 2014; Hecker et al., 2015) should be performed. These *in vivo* co-localization and interaction studies would show that the proteins indeed co-localize and interact in plastids. In addition, co-immunoprecipitation of PII with its interactome from stably transformed *A. thaliana* using GFP-traps (ChromoTek) could further verify these observations.

2 Results

2.1 Expression studies of *PII*

The expression of *AtGLB1*, hereinafter referred to as *PII*, is induced by light and sucrose and decreased by addition of L-Glu and L-Gln and in darkness (Hsieh et al., 1998). Although PII expression was shown to be affected by light, sucrose and amino acids, this was only shown in whole seedlings (Hsieh et al., 1998), and not in single organs.

2.1.1 PII expression is induced under non-limiting N/C and decreases under limiting N/C conditions

To analyse how *PII* is affected by inorganic nitrogen (N), I generated *A. thaliana* lines expressing β-glucuronidase (GUS) under the control of the endogenous *PII* promoter (*pPII*) of a size of 269 bp. The length of the promoter resembles the sequence between the annotated start codon of At4g01897 (3'-5') and the *PII* (At4g01900) start codon.

The promoter-GUS assays were performed in 10-day old seedlings using an *A. thaliana* line expressing GUS under the Cauliflower Mosaic Virus promoter (*p35S*) as a control.

Seedlings grown on varying N and sucrose concentrations under constant light revealed differential activity of *pPII* in the cotyledons, leaves, hypocotyl and the root after GUS staining (Figure 2). Seedlings grown in constant light with 19.7 mM N (amount of NO_3^- and NH_4^+ in ½ MS) and additional sucrose as carbon (C) source, show induction of the *pPII* mainly in cotyledons and first leaves. Additionally, promoter activity could be observed in the hypocotyl and partially in the root (Figure 2 A). The absence of sucrose addition leads to decreased promoter activity in cotyledons and first leaves, whereas activity in the hypocotyl and the root is not changed (Figure 2 B). The activity of *pPII* decreases under N limitation in comparison to non-limiting conditions (Figure 2 C-D). Furthermore, combined N and C limitation leads to hardly visible *pPII* activity (Figure 2 D). These observations show strong dependency of *pPII* activity not only to sucrose and light (Hsieh et al., 1998) but also to N levels.

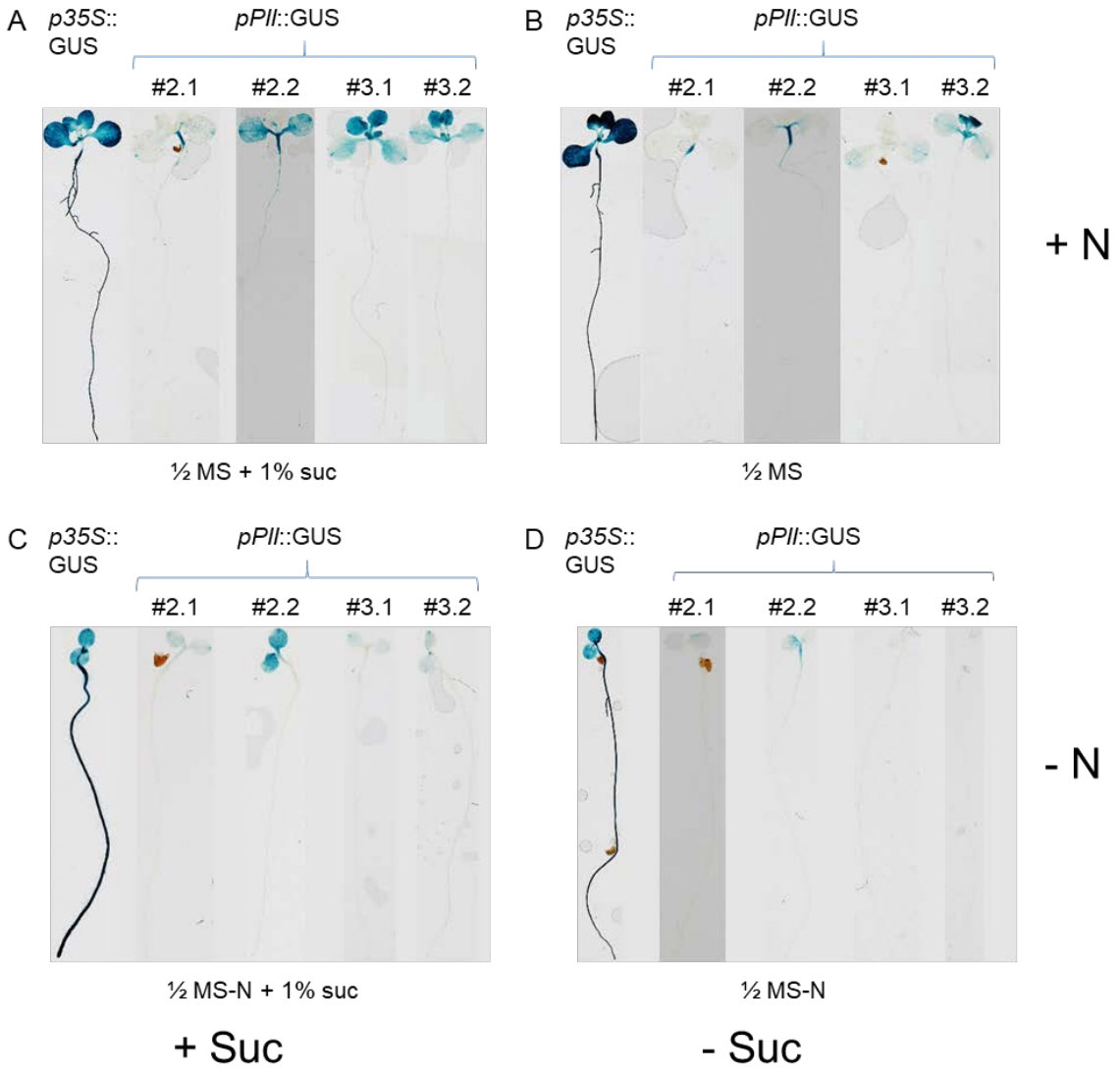

Figure 2: N and sucrose control *pPII* activity.
GUS expression in 10-day old seedlings grown on A) ½ MS + 1% sucrose, B) ½ MS, C) ½ MS-N + 1% sucrose, D) ½ MS-N in constant light. Seedlings expressing GUS *p35S* or the 269 bp long *pPII.* GUS staining performed for ~42 h.

2.2 Phenotypical analyses of PIIS2

Ferrario-Mery et al. (2005) showed, that the PII mutant lines *PIIS2* and *PIIV1* had no phenotype under non-limiting conditions, but showed higher sensitivity to nitrite (Ferrario-Mery et al., 2005).

2.2.1 Effect of carbon and nitrogen metabolism under different light conditions on *PIIS2* mutants

The *PII* promoter activity revealed dependency of *PII* expression under varying N and C concentrations in seedlings (Figure 2). To analyse whether this effect is visible not only on promoter activity but also on protein level, I first performed a growth assay with Col-0 seedlings to assess the minimal N concentration at which Col-0 seedlings are still able to survive (Figure 3).

The growth assay revealed that at an N concentration of approximately 5 mM N in liquid ½ MS+1% sucrose, Col-0 seedlings showed slightly smaller seedlings with partially increased anthocyanin content (Figure 3).

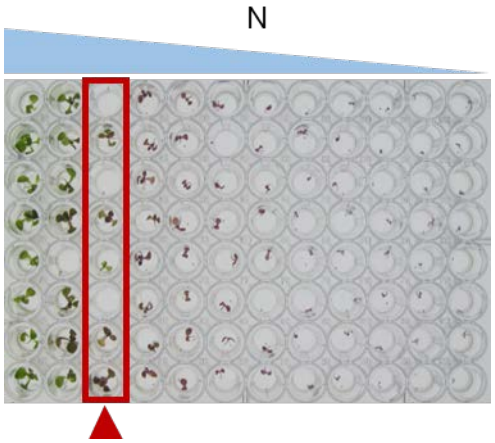

Figure 3: Col-0 show minor growth defects at 4.93 mM N.
Col-0 seedlings grown for 14 days in liquid ½ MS-N with or without additional N (NH_4NO_3 and KNO_3 as N source). ½ MS-N + 19.7 mM N diluted 1:1 with ½ MS-N. First lane represents 19.7 mM N to ~ 0.019 mM N in second last lane. Last lane represents 0 mM N.

Therefore, I performed growth assays of Col-0 and *PIIS2* on ½ MS-N +/- 1% sucrose with either 4.93 mM or 19.7 mM N under constant light, long day, short day or darkness on solid media (Figure 4). Measurement of root length revealed no significant growth differences between Col-0 and *PIIS2* in root length, whereas hypocotyl length was significantly prolonged in *PIIS2* grown on ½ MS-N+4.93 mM N in dark (Figure 4). No significant growth difference was observed in the other tested conditions (Figure 4) and 4.93 mM N in solid medium revealed less growth defects as in liquid medium.

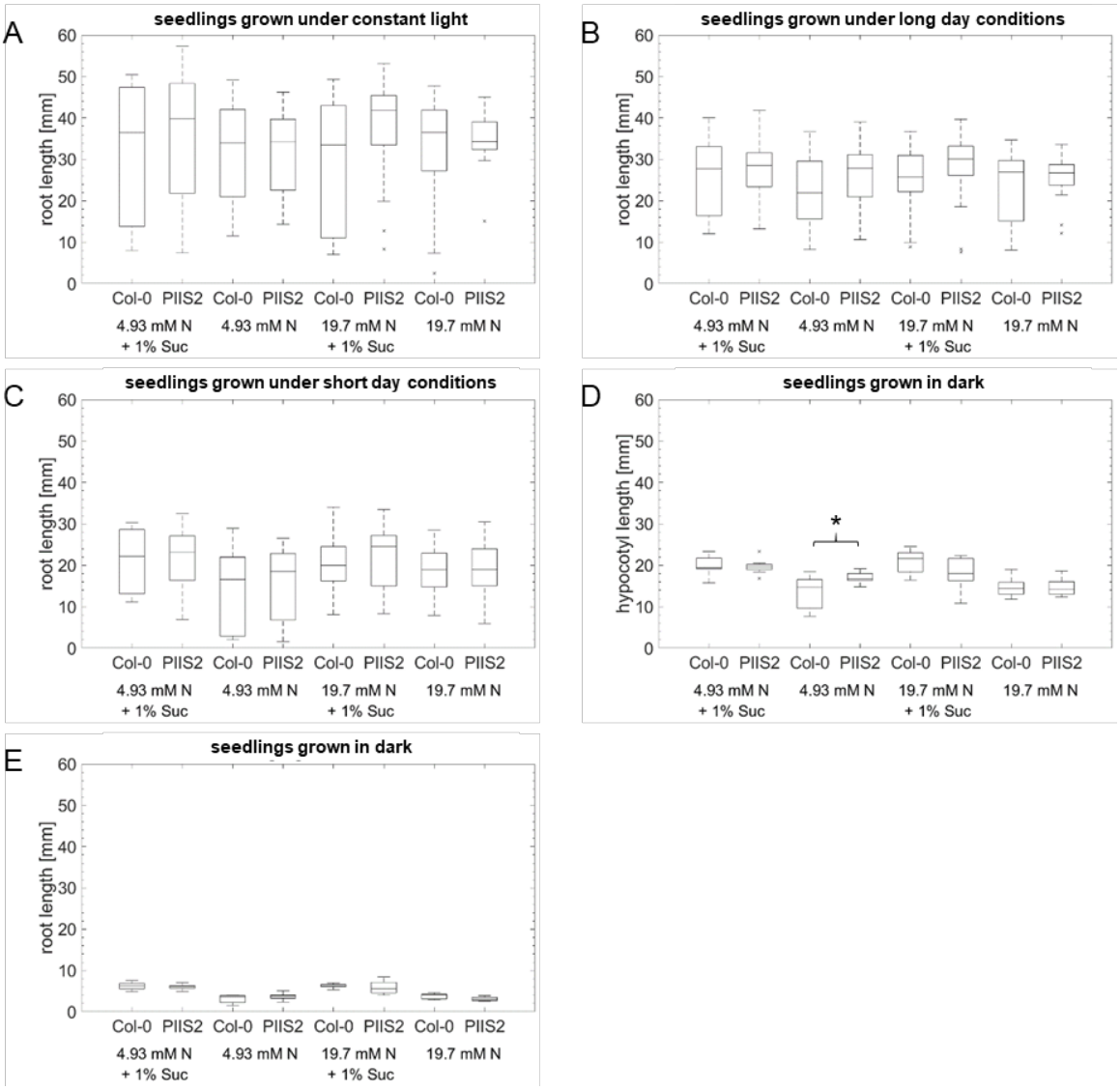

Figure 4: Effect of N/C limiting conditions under differing light conditions on root length of Col-0 and *PIIS2*

Root length [µm] of Col-0 and *PIIS2* grown for 10 days on ½ MS-N media containing either 19.7 mM or 4.93 mM N +/- 1% sucrose grown under constant light (A), long day (B), short day (C) or dark conditions (D, E). For dark conditions additionally to hypocotyl length (D), root length (E) was measured. Asterisk indicate $p < 0.05$.

Therefore, I repeated the growth assay with ½ MS+1% sucrose containing 0 mM or 19.7 mM N (Figure 5). Analysis of root length revealed significant differences under long day conditions on ½ MS-N+1% sucrose, where Col-0 showed a strong decrease in root length but sample size was low (n=8; Figure 5 B). Under dark, *PIIS2* seedlings showed only a minor but still significant reduction in hypocotyl length in comparison to Col-0 on ½ MS+1% sucrose (Figure 5 D). *PIIS2* and Col-0 showed no significant differences in root length under constant light and short day (Figure 5 A and C).

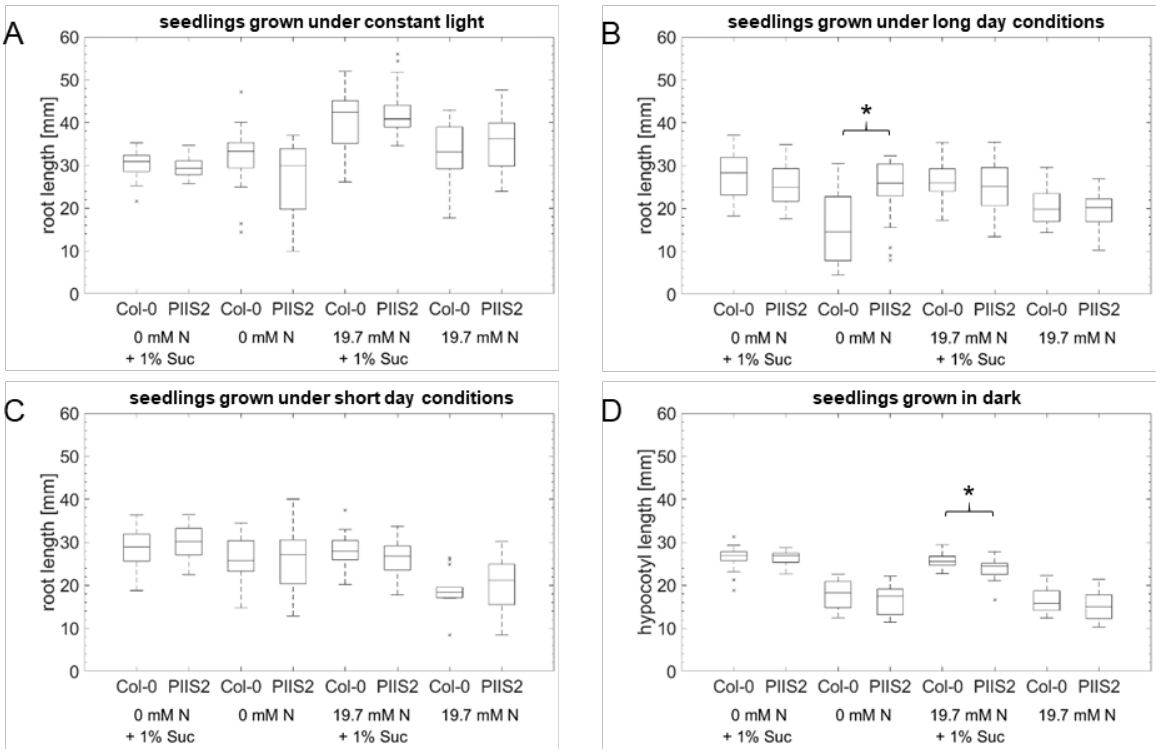

Figure 5: Growth assay under N/C limiting conditions in varying light conditions
Col-0 and *PIIS2* grown for 10 days on ½ MS-N media with 19.7 mM or 0 mM N +/- 1% sucrose under constant light (A), long day (B), short day (C) or dark (D) conditions. For all light conditions except dark, root length was measured. For dark grown seedlings, hypocotyl length was measured. Asterisk indicate $p < 0.05$.

2.2.2 Sensitivity screen with amino acids as N source

PII expression is influenced by amino acids (Hsieh et al., 1998). To answer the question whether amino acids as N source result in a changed phenotype, I grew Col-0 and *PIIS2* on N limiting and non-limiting N conditions with or without L-Gln, L-Glu and L-Arg as additional N source. In these analyses no phenotypical changes could be observed (Figure A 2).

2.3 Generation and genetic analyses of PII mutants

As phenotypical differences between Col-0 and *PIIS2* were barely perceivable in the tested conditions, the question arose whether *PIIS2* is really a knockout mutant. To verify this, RNA from seedlings of Col-0 and *PIIS2* was extracted and reverse transcribed. Full-length transcript of *PII* in *PIIS2* was detectable using five-times more PCR product, exhibiting that *PIIS2* is in fact not a knockout but a knockdown mutant (Figure 6).

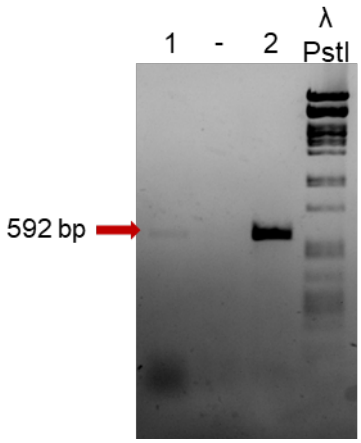

Figure 6: *PII* mRNA expression in *PIIS2* and Col-0
RT-PCR analysis of full-length *cPII* cDNA fragment in *PIIS2* (1) and Col-0 (2) of 14-day-old seedlings grown under long day conditions. 12.5 µL of *PIIS2* and 2.5 µL of Col-0 PCR-Product were loaded on 1% Agarose-Gel.

2.3.1 Generation of PII CRISPR/Cas line

As mRNA expression of *PII* in *PIIS2* was still detectable, I started to generate CRISPR/Cas knockout lines for *PII* with two template DNA sequences (Figure 7 A). Analysis of T1 plants transformed with either Construct 1 or Construct 2 in MTN2966 revealed detectable CRISPR events neither by amplification, nor by sequencing. As single vectors of CRISPR/Cas constructs revealed no CRISPR event, I generated vectors carrying both constructs in tandem.

The first trials of generating a PII knockout mutant yielded in no detectable CRISPR event. As the knockout mutation of the D-amino acid transaminase (DAT1) is not lethal (Suarez et al., 2019), I used *DAT1* as a control. To test whether *PII* knockout could be lethal, I used CRISPR/Cas template DNA sequences from Li et al. (2013). Both template DNA sequences locate to the fourth exon of DAT1 (Figure 7 B). To have an additional marker for selection of transformants, we obtained a CRISPR/Cas vector of Christopher Grefen's group (ZMBP, University of Tübingen) carrying a fluorescing seed marker. Double constructs for PII and DAT1 were transformed in MTN2966 and FastRed-CRISPR/Cas. The analyses of these transformants is in progress.

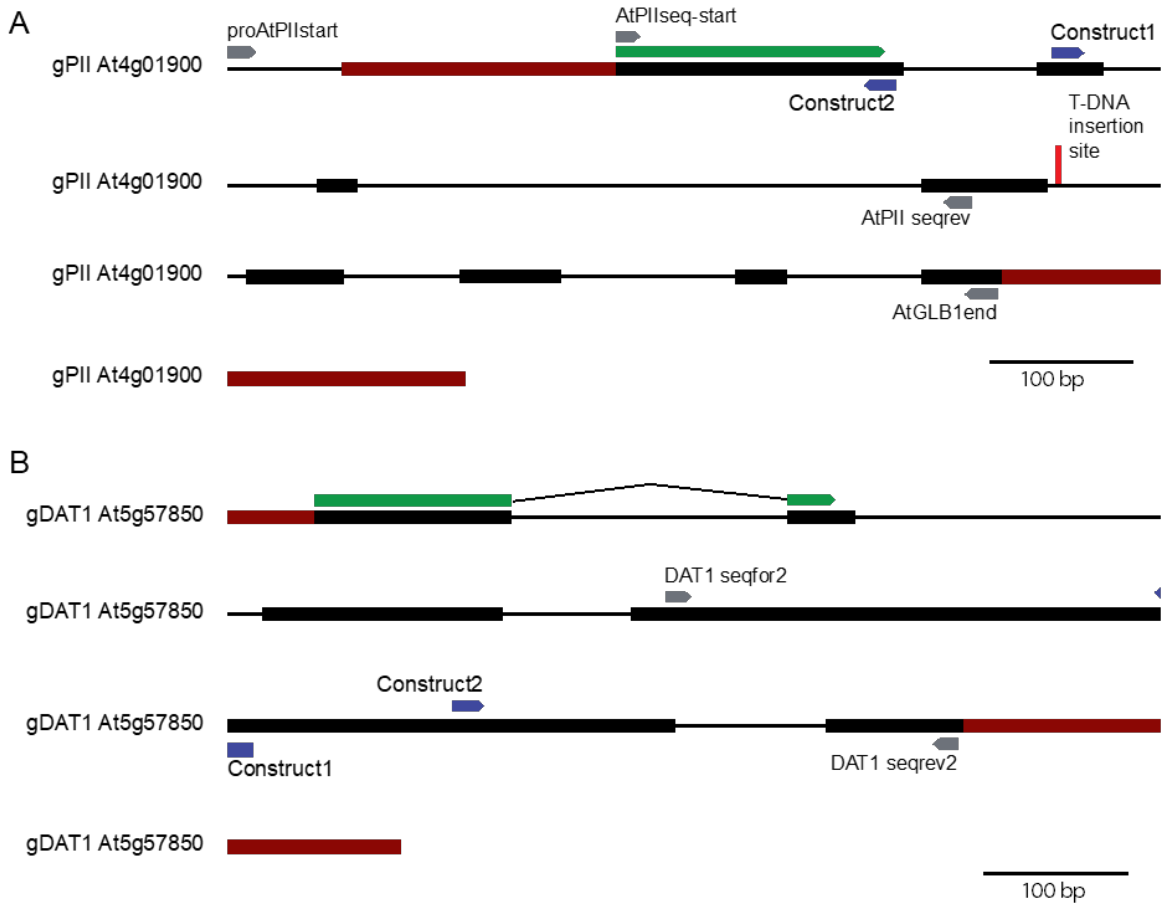

Figure 7: Genomic sequence of *A. thaliana PII* and *DAT1*.
Genomic DNA sequences of A) *PII* and B) *DAT1*.
Exons: black bars; introns: black lines; chloroplast transit peptide: green; primer binding sites: blue; 5'UTR and 3'UTR: red; CRISPR/Cas9 template binding sites: dark violet; T-DNA insertion site: red upright line. Scale bar represents 100 bp.

2.3.2 No obvious phenotypic change of *PII*-overexpressor lines, rescue lines and knockdown mutant

As the published knockdown and knockout mutants *PIIV1* and *PIIS2* displayed no apparent phenotype under nutrient non-limiting conditions (Ferrario-Mery et al., 2005).

I tried out if the ectopic overexpression of PII leads to any visible effects. Therefore, I generated several different *PII* overexpression lines in Col-0 WT and *PIIS2* background. The lines were grown under long day conditions. The analysed lines displayed no phenotypic change in rosette leaf stage until onset of flowering (Figure 8 A-B). The individual lines displayed no homogenous phenotype in both approaches (Figure 8; Appendix: Figure A 8, Figure A 9).

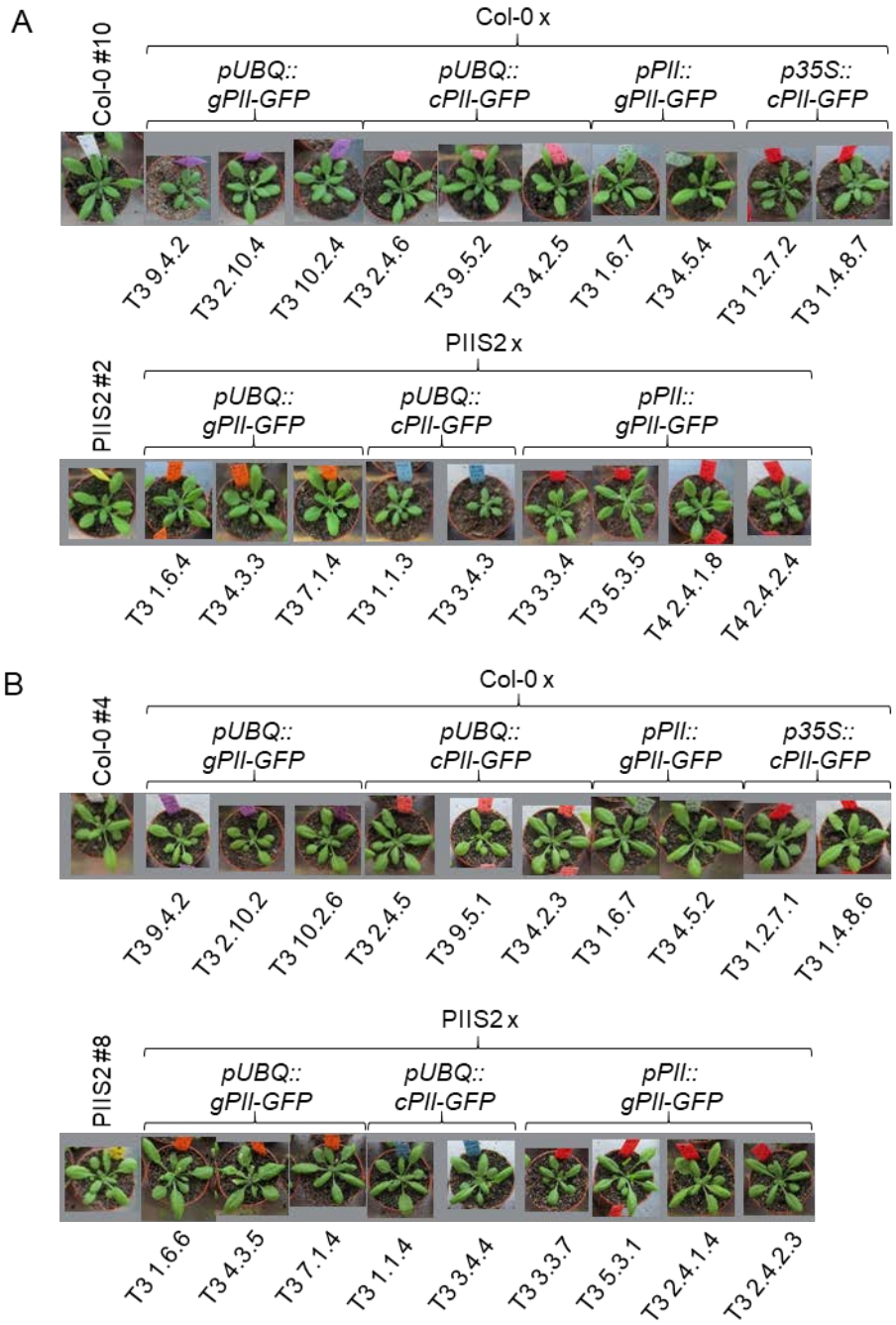

Figure 8: Phenotype of Col-0, *PIIS2* and respective overexpression and rescue lines of T3 and T4 generation.
Rosette leave stage phenotype of 4 ½ weeks old plants grown under long day conditions.
A) Representative plants of first approach. B) Representative plants of second approach.

Analysis of flowering onset revealed a later onset of flowering in approach one (Figure 9 A), but could not be confirmed in the second approach (Figure 9 B). Significant differences in flowering time could be observed for *pUBQ::gPII-GFP* T3 4.3 in *PIIS2* background in both approaches (Figure 9), whereas significant differences of the other lines could only be observed in the second approach (Figure 9 B).

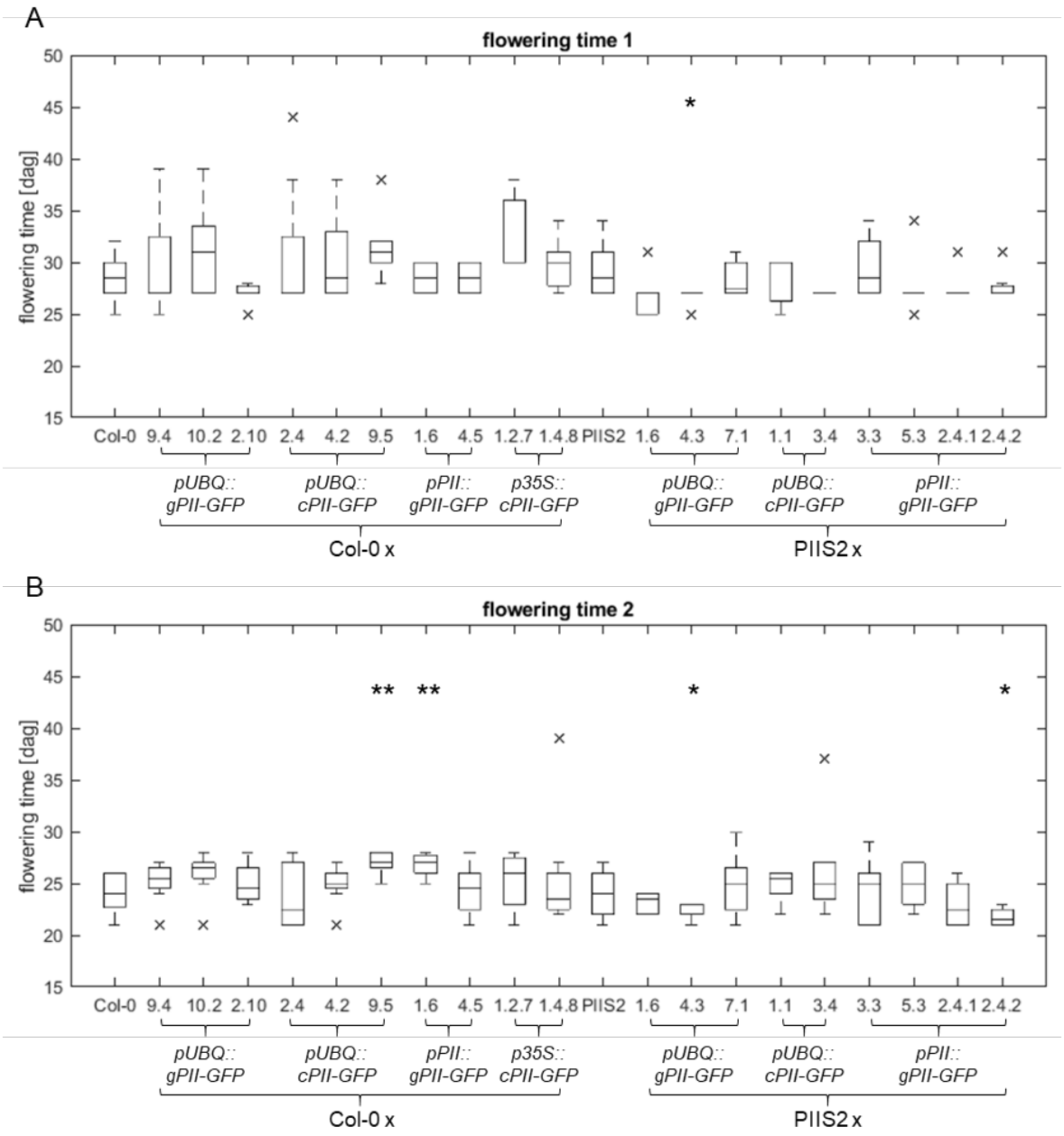

Figure 9: Flowering time of Col-0, *PIIS2* and stable *PII* overexpression and rescue lines in *A. thaliana* Col-0 and *PIIS2* grown under long day conditions.
A) Flowering time of respective lines in first approach. B) Flowering time of respective lines in second approach. Student's t-test revealed significant differences, *: $p < 0.05$, **: $p < 0.01$.

2.4 Localization studies of PII

Although the subcellular localization of PII has been once shown in immunohistochemically analyses (Baud et al., 2010), such *in vivo* studies were still missing, yet. Additionally, the same holds true for *in vivo* interaction studies of PII. Therefore, I performed subcellular localization analyses of *A. thaliana* PII using different promoters, genomic and CDS versions of *PII* tagged with fluorescent proteins in transiently transformed *N. benthamiana* (Figure 10 A, D, E, Figure 11) and stably transformed lines of *A. thaliana* Col-0 (Figure 10 C-D, Figure 11 C).

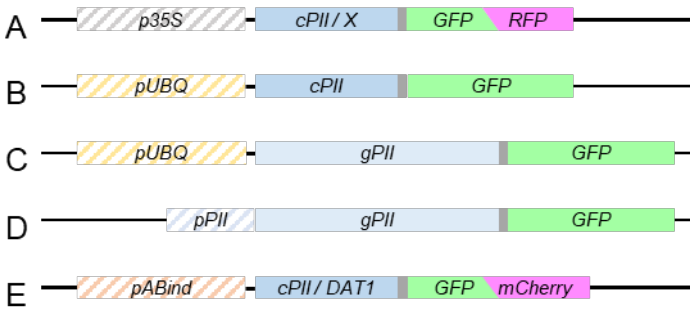

Figure 10: Schematic overview of used promoter, gene and fluorescent protein combination for localization assays of PII in *A. thaliana* and *N. benthamiana*.
A) CDS of PII (cPII) or putative interaction partner (X) tagged with GFP or RFP under the control of the Cauliflower Mosaic virus (CaMV) 35S promoter (*p35S*). B) cPII tagged with GFP under the control of the UBQ10 promoter (*pUBQ*). C) Genomic PII (gPII) tagged with GFP under the control of the *pUBQ*. D) gPII tagged with GFP under the control of its endogenous promoter (*pPII*). E) GFP-tagged cPII or mCherry-tagged DAT1 under the control of an estradiol inducible promoter (*pABind;* generated by Marvin Braun). Diagonal stripes: promoter; grey box: linker sequence.

To analyse the subcellular localization of PII and the influence of the promoter, I made use of four different promoters: *p35S, pUBQ10, pPII and* an estradiol-inducible promoter (*pABind*; (Bleckmann et al., 2010) (Figure 10, Figure 11). I generated six different versions of *PII* expression constructs. The coding DNA sequence (*cPII*) under the control of the *p35S* (Figure 10 A), *pUBQ* (Figure 10 B) and *pABind* (Figure 10 E) and additionally the genomic DNA sequence (*gPII*) under control of *pUBQ* (Figure 10 C) and the endogenous promoter of *PII*, *pPII* (Figure 10 D).

For co-localization analyses with known and putative new interactors, both genes were cloned into 2in1 vectors under the control of *p35S* (Figure 11), single vectors under control of either *p35S* (Figure 10 A) or *pABind* (Figure 10 E). All genes were tagged C-terminally with either GFP, RFP or mCherry (Figure 10, Figure 11).

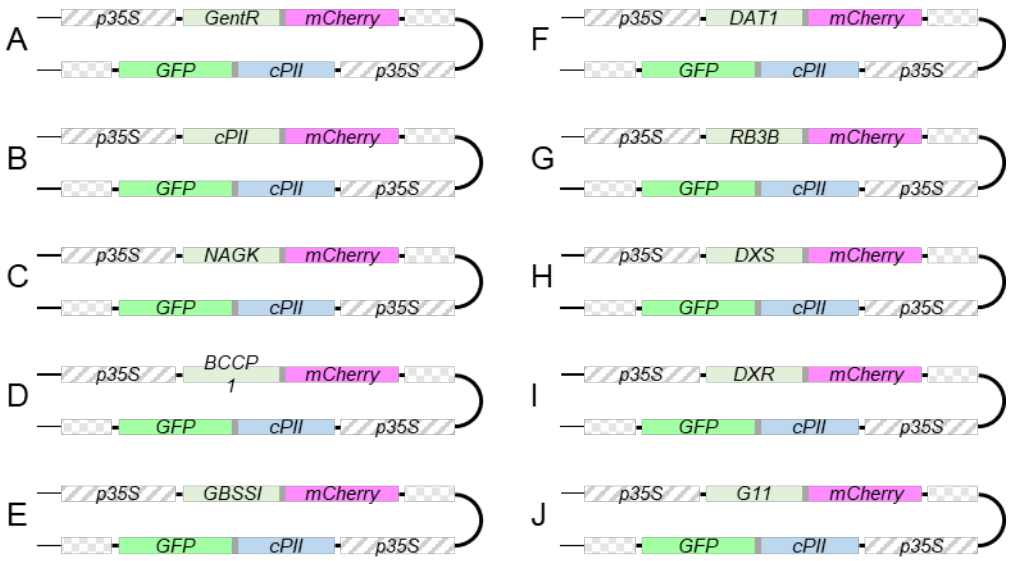

Figure 11: Schematic overview of 2in1 FRET vectors for localization and interaction assays of PII in *N. benthamiana*

PII-GFP with mCherry-tagged A) GentR (Donor-only control), B) PII, C) NAGK, D) BCCP1, E) GBSSI, F) DAT1, G) RBCS3B (RB3B), H) DXS, I) DXR, J) GGPPS11 (G11). CDS versions of single genes. All constructs C-terminally tagged with GFP (only PII) or mCherry under the control of the CaMV 35S promoter. Diagonal stripes: promoter; grey box: linker sequence; dotted box: CaMV 35S terminator.

2.4.1 PII appears as foci in plastids

2.4.1.1 PII localizes in foci in plastids independently of the used promoter

Co-expression of *gPII* (Figure 12 A) or *cPII* tagged with GFP (Figure 12 B) under control of *p35S* with pt-rk (CD3-999; transit peptide of tobacco Rubisco C-terminally tagged with mCherry, (Nelson et al., 2007)) in transiently transformed *N. benthamiana* revealed localization of PII to foci in plastids. Nearly the same localization pattern of PII-GFP was observed for PII-GFP under control of its endogenous promoter in *A. thaliana* (Figure 12 C).

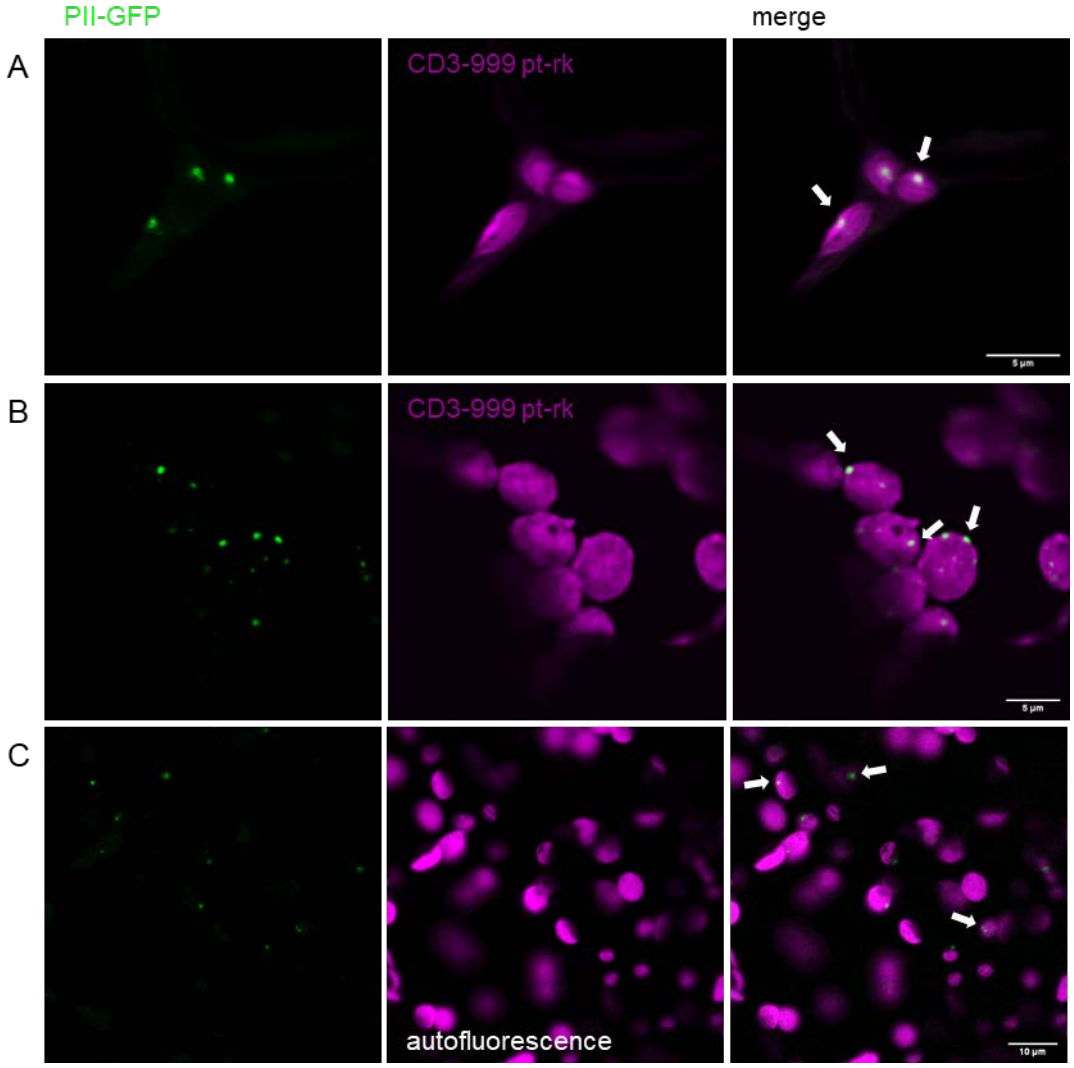

Figure 12: PII-GFP localizes in aggregates to plastids of leaves of transiently transformed *N. benthamiana* and stably transformed *A. thaliana*.

A) GFP-tagged *gPII* under control of *pPII* co-expressed with the mCherry-tagged transit peptide of tobacco Rubisco (CD3-999 pt-rk). B) GFP-tagged *cPII* under control of *p35S* localizes in foci to plastids co-expressing CD3-999 pt-rk. Confocal images were taken 2 days after transient transformation of *N. benthamiana.* Scale bar: 5 µm. C) GFP-tagged *gPII* under control of *pPII* in stably transformed *A. thaliana* localizes in foci to plastids. Magenta displays autofluorescence signal of plastids. Scale bar: 10 µm.

2.4.2 PII co-localizes with known and putative novel interaction partners in plastids

The known interaction partners of PII proteins are quite conserved throughout kingdoms. The interaction of PII with the N-acetyl-L-glutamate kinase (NAGK) is the best-characterized interaction in *A. thaliana* (Chen et al., 2006; Ferrario-Mery et al., 2006; Beez et al., 2009; Feria Bourrellier et al., 2009; Chellamuthu et al., 2014).

To characterize the co-localization pattern of PII with known interaction partners, first the localization pattern of these interaction partners was observed. Localization analyses of NAGK, BADC2 and BADC3 revealed localization to plastids in aggregates when expressed without PII (Figure 13).

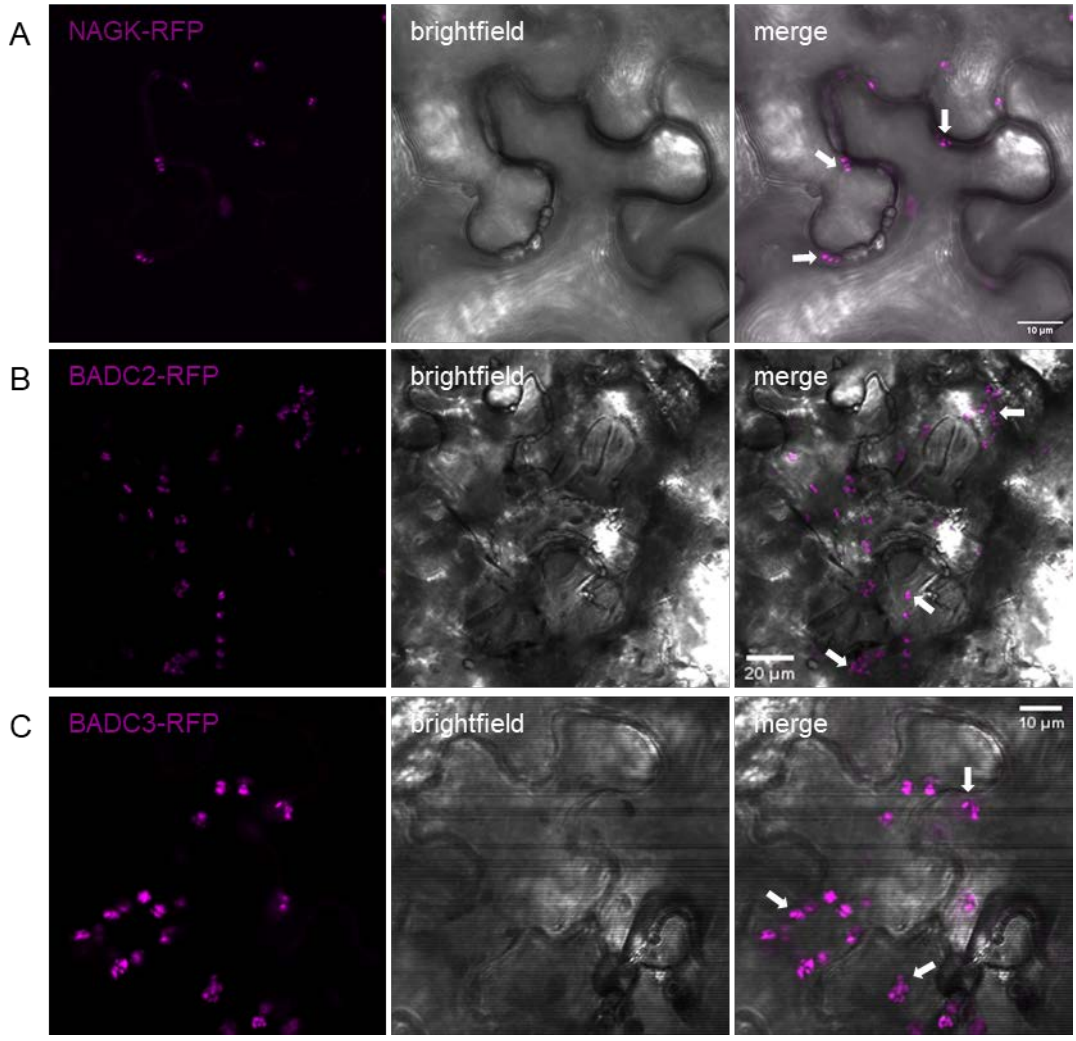

Figure 13: NAGK, BADC2 and BADC3 tagged with RFP localize in aggregates in plastids of transiently transformed *N. benthamiana.*

All genes expressed under the control of the *p35S*. A) NAGK-RFP localizes to plastids. B) BADC2-RFP localizes to plastids. C) BADC3-RFP localizes to plastids. Scale bars: A) and C) 10 µm, B) 20 µm. Confocal images were taken A) 2 days and B)-C) 3 days after transient transformation of *N. benthamiana*. White arrows indicate aggregates in plastids.

Further localization studies revealed co-localization of PII with itself, and the known interaction partners NAGK and BCCP1 in foci and throughout the whole chloroplast (Figure 14 B-D). Co-localization of PII with known interaction partners in foci, led to the question whether PII co-localizes with additional proteins in foci.

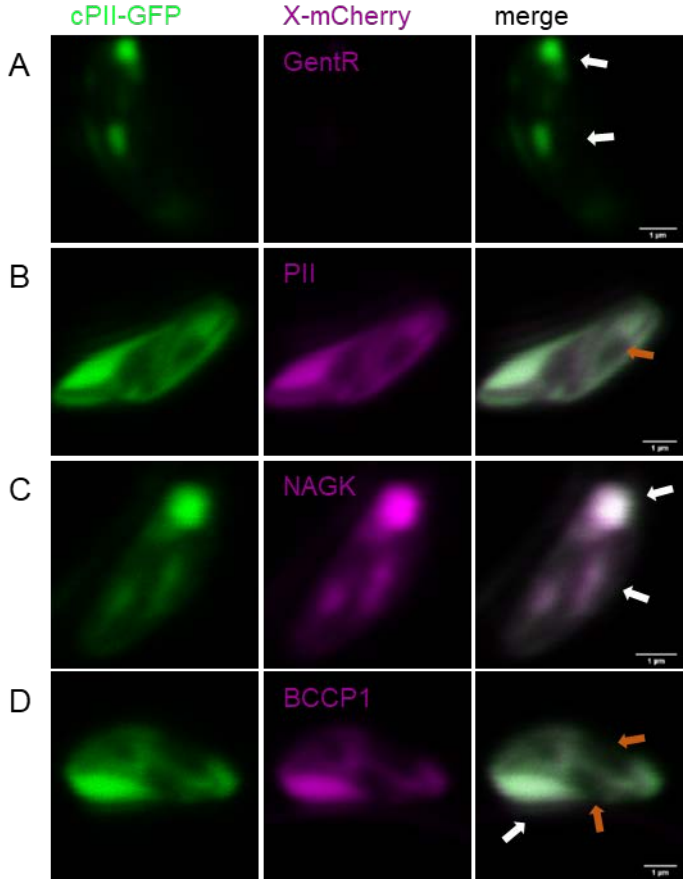

Figure 14: PII co-localizes with known interaction partners in plastids of transiently transformed *N. benthamiana* using 2in1 vectors.
All genes under the control of *p35S*. A) PII-GFP alone localizes to plastids, B) cPII-GFP co-localizes with PII-mCherry. C) cPII-GFP co-localizes with NAGK-mCherry. D) cPII-GFP co-localizes with BCCP1-mCherry.
White arrows indicate aggregates; orange arrows indicate starch granule. Scale bar: 1 µm. Confocal images of single plastids were taken 2 days after transient transformation of *N. benthamiana.*

Co-expression of PII-GFP with BADC2-RFP and BADC3-RFP, two published interactors of PII and antagonists of BCCP1/2 (Feria Bourrellier et al., 2010; Salie et al., 2016; Keereetaweep et al., 2018), confirmed co-localization of PII-GFP with BADC2-RFP (Figure 15 A, B) and with BADC3-RFP (Figure 15 C, D) in foci in plastids.

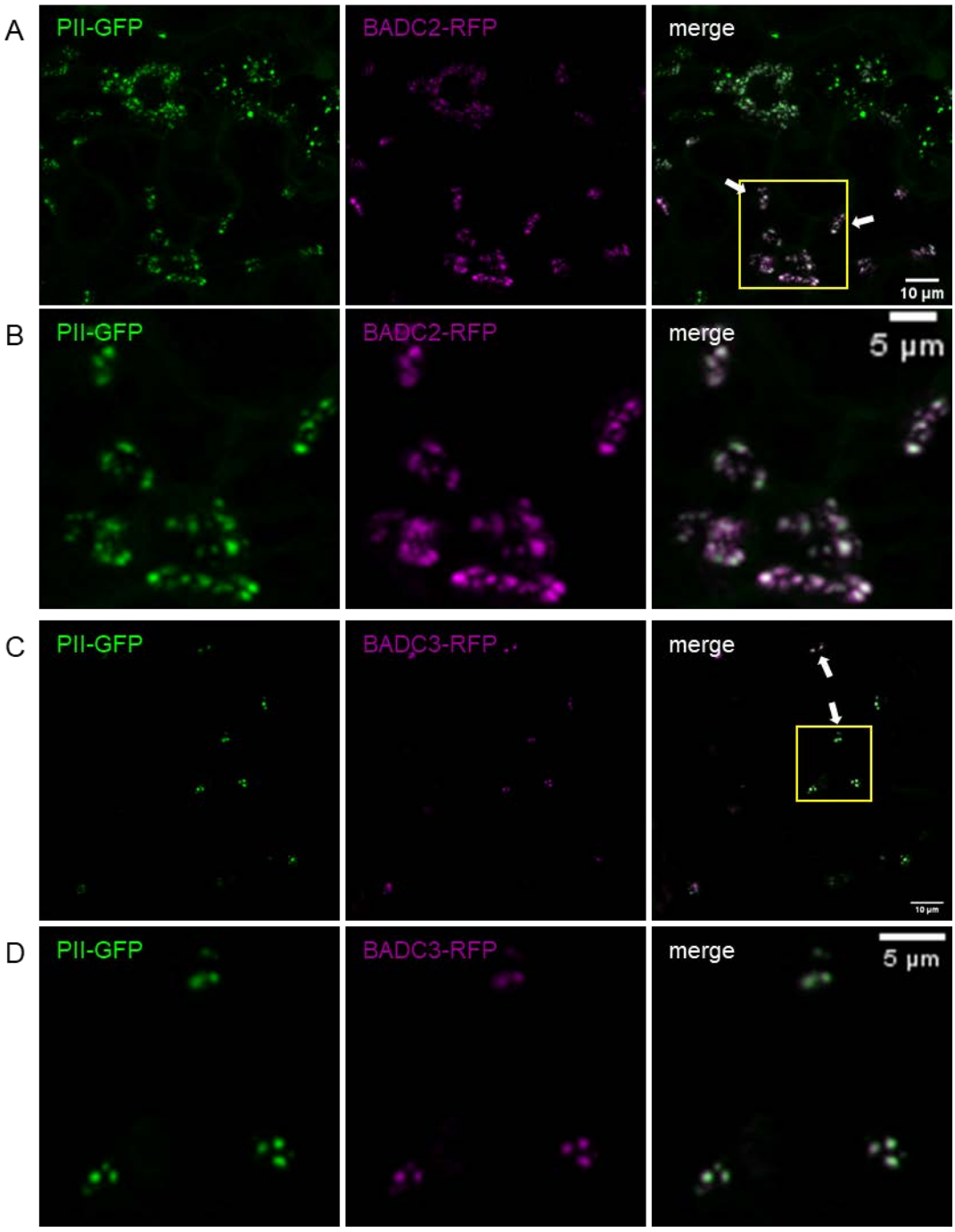

Figure 15: PII-GFP co-localizes to plastids with BADC2-RFP and BADC3-RFP.
A) *cPII-GFP* co-expressed with *BADC2-RFP*. Yellow rectangle indicates close-up view in B). B) Close-up view of A). C) *cPII-GFP* co-expressed with *BADC3-RFP*. Yellow rectangle indicates close-up view in D). D) Close-up view of C). All genes under the control of *p35S* co-expressed for 3 days in transiently transformed *N. benthamiana*. White arrows indicate aggregates. A) and C) Scale bar: 10 µm. B) and D) Scale bar: 5 µm.

2.5 Characterization of the PII foci

The focal accumulation of the PII protein and its interactors in plastids opened the question whether this formation represents suborganellar structures in this compartment.

2.5.1 PII foci are not localizing to nucleoids

It is known for bacterial PII, that it is interacting with PipX (Burillo et al., 2004), a transcriptional co-regulator of the transcription factor NtcA (Espinosa et al., 2006; Chellamuthu et al., 2013). This points to a putative association of plant PII and especially *A. thaliana* PII to nucleoids, although a homologue of PipX is missing in plants (Chellamuthu et al., 2013).

To clarify whether PII localizes to nucleoids, I did a DAPI staining, which was shown to stain plastidic nucleic acids, too (Newell et al., 2012). First experiments indicated co-localization of PII to DAPI stained nucleoids in plastids (Figure 16). A closer look on emission spectra of DAPI and GFP revealed overlay in the analysed range. In addition, the used 405 nm laser did not just excite DAPI but also GFP to comparable extent, indicating bleed-through of GFP signal into the DAPI channel. Yet another difficulty was the blue autofluorescence of plastids.

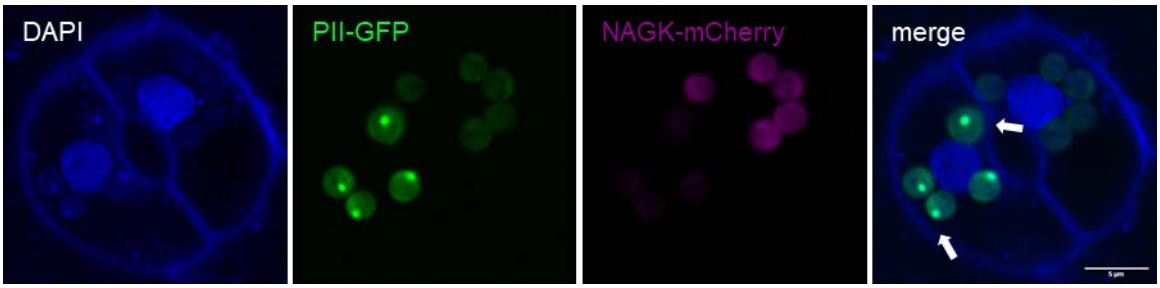

Figure 16: PII-GFP co-localizes with DAPI stained nucleoids in chloroplasts of stomata cells. DAPI stained leaves of stably transformed *A. thaliana* expressing *cPII-GFP* and *NAGK-mCherry* under control of *p35S*. White arrows indicate co-localization of DAPI signal and PII-GFP.DAPI: blue, PII-GFP: green; NAGK-mCherry: magenta; Scale bar: 5 µm.

Krupinska et al. (2014) used YO-PRO™-1, a propidium iodide derivative, to stain nucleoids of plastids. Nucleoid staining with YO-PRO™-1 of transiently transformed *N. benthamiana* leaves with P19 showed nucleoid localization in a punctate pattern in chloroplasts (Figure 17 A). Transiently transformed *N. benthamiana* leaves with PII-RFP exhibit nucleoid staining with YO-PRO™-1 next to PII aggregates in plastids, but no co-localization of PII and nucleoids (Figure 17 B). Therefore, we could exclude that PII is a part of nucleoids in plastids (Figure 14 B, D, Figure 19 A and Figure 17 B).

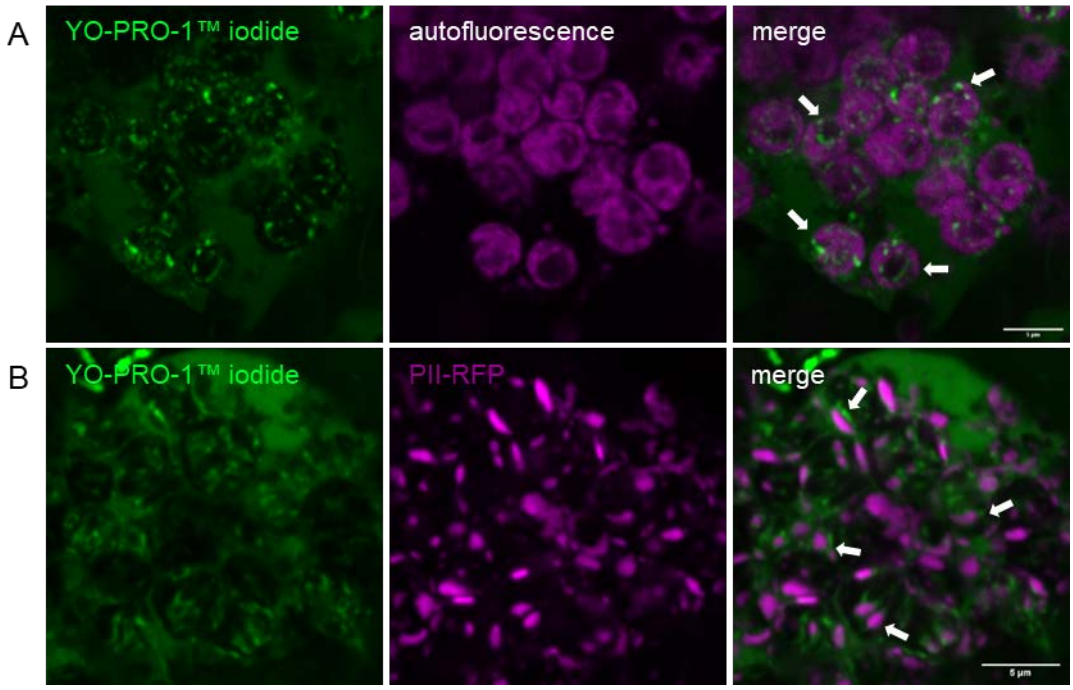

Figure 17: PII-RFP localizes next to nucleoids in chloroplasts of transiently transformed *N. benthamiana* mesophyll cells.
A) YO-PRO™-1 Iodide stained nucleoids in transiently transformed *N. benthamiana* leaves with P19. Magenta indicates autofluorescence. B) YO-PRO™-1 Iodide stained nucleoids in transiently transformed *N. benthamiana* leaves expressing *cPII-RFP* under control of *p35S*. YO-PRO™-1 Iodide depicted in green. White arrows: nucleoids. 3 days after transient transformation in *N. benthamiana* leaf disks were fixed overnight and were stained with YO-PRO™-1 Iodide for 15 min.

2.5.2 PII foci are not localizing on starch granules

Another explanation for the localization pattern of PII-GFP in foci in plastids would have been that they are part of starch granules. To test this hypothesis, I co-expressed PII with the granule-bound starch synthase I (GBSSI) that localizes to plastids and catalyses the reaction from ADP/UDP-Glucose to amylose (Nelson and Rines, 1962; Szydlowski et al., 2009)(for review: Ball et al. (1998)).

GBSSI-GFP localizes to plastids in *N. benthamiana* (Figure 18 A, Figure A 11 A). Co-localization analyses of PII-GFP with GBSSI-mCherry revealed co-localization of both in foci to plastids. These foci were not localizing on starch granules but next to them (Figure 19 A). As a putative negative control, the co-localization of PII with the D-amino acid transaminase DAT1 (Suarez et al., 2019) was tested. DAT1 is involved in D-AA metabolism and catalyses the reaction from its major substrate D-Met with pyruvate to D-Ala with 2-OG (Suarez et al., 2019) and is localizing in aggregates to plastids (Figure 18 B, Figure A 11 B).

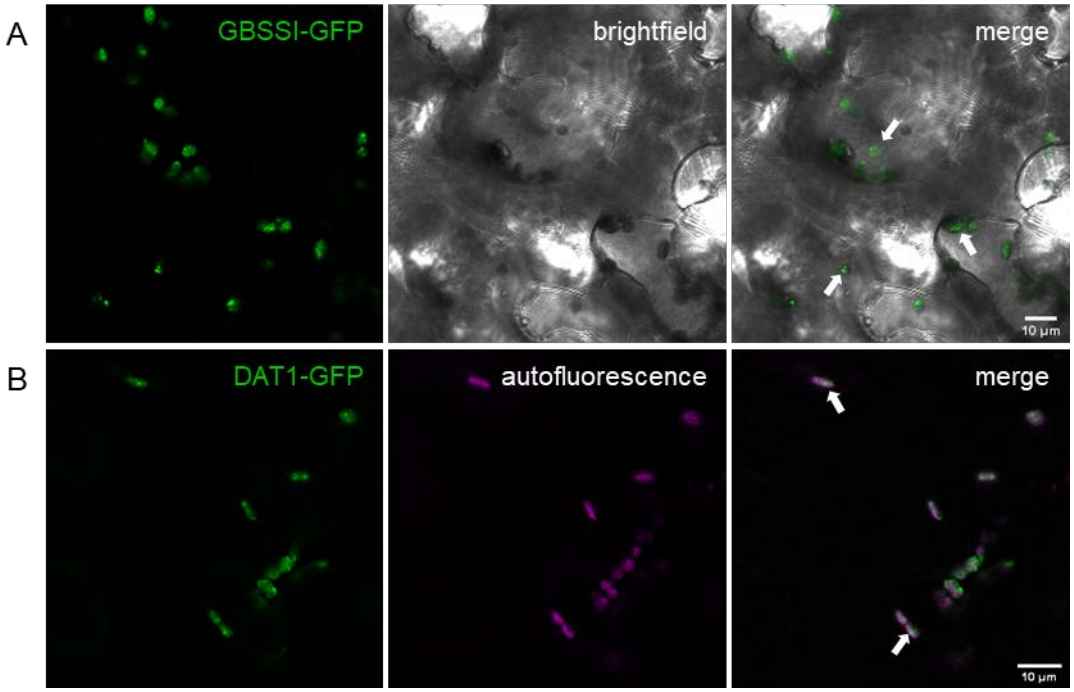

Figure 18: GBSSI and DAT1 tagged with GFP localize to plastids of transiently transformed *N. benthamiana*.
A) GBSSI-GFP localizes to plastids. Expression under the control of the *p35S*. B) DAT1-GFP localizes to plastids. Expression under the control of the *pUBQ*.
White arrows: aggregates in plastids. Scale bars 10 µm. Confocal images were taken A) 2 days and B) 3 days after transient transformation of *N. benthamiana.*

Co-localization of PII-GFP with GBSSI-mCherry and DAT1-mCherry indicates putative interaction (Figure 19 A, B). PII-GFP localization, co-expressed with the known and putative interaction partners, is mainly unchanged in comparison to PII-GFP expressed alone (Figure 14 A).

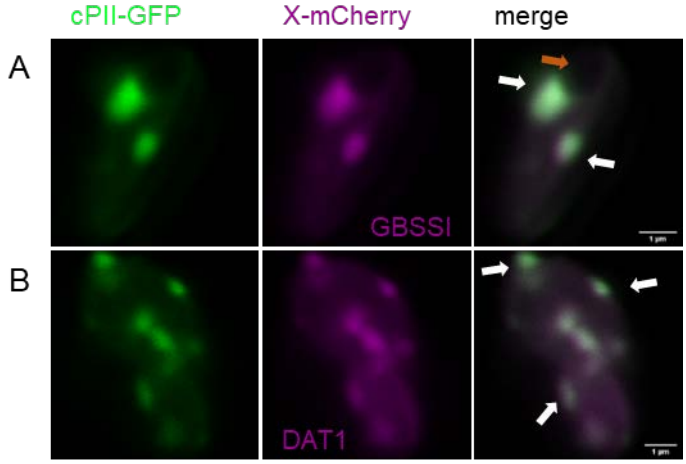

Figure 19: PII co-localizes with putative novel interaction partners in plastids of transiently transformed *N. benthamiana* using 2in1 vectors.
A) cPII-GFP co-localizes with GBSSI-mCherry. B) cPII-GFP co-localizes with DAT1-mCherry. All genes under the control of *p35S.* White arrows indicate aggregates; orange arrows indicate starch granule. Scale bar: 1µm. Confocal images of single plastids were taken 2 days after transient transformation of *N. benthamiana*.

2.5.3 PII localizes in vesicle-like structures at plastids and in cytoplasm

PII-GFP localization was not only observed in plastids but also extra-plastidic in vesicle-like structures (Figure 20). This phenomenon reminds of protein degradation from plastids. To test the hypotheses that PII is part of such structures, I analysed

co-localization of PII to proteins known to be related to autophagy-dependent and -independent protein turn over.

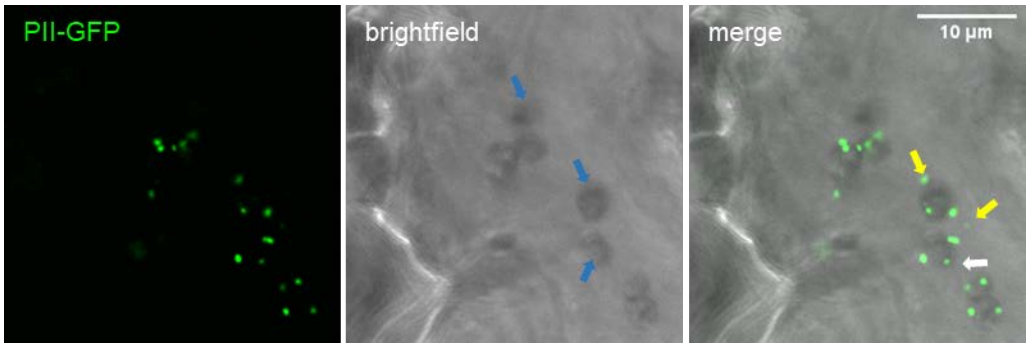

Figure 20: PII-GFP localizes to plastids in foci and in extra-plastidic vesicle-like structures in transiently transformed *N. benthamiana* leaves.
PII-GFP expressed under control of *p35S*. Confocal images were taken 2 days after infiltration. White arrows: foci in plastids; yellow arrows: extraplastidic foci; blue arrows: plastids.

Rubisco localizes in extra-plastidic compartments named Rubisco containing bodies (RCBs), which are involved in autophagy-dependent protein turnover (Chiba et al., 2003; Ishida et al., 2008; Izumi et al., 2010). Localization analyses of RBCS3B-RFP alone revealed localization to plastids in aggregates (Figure 21, Figure A 11).

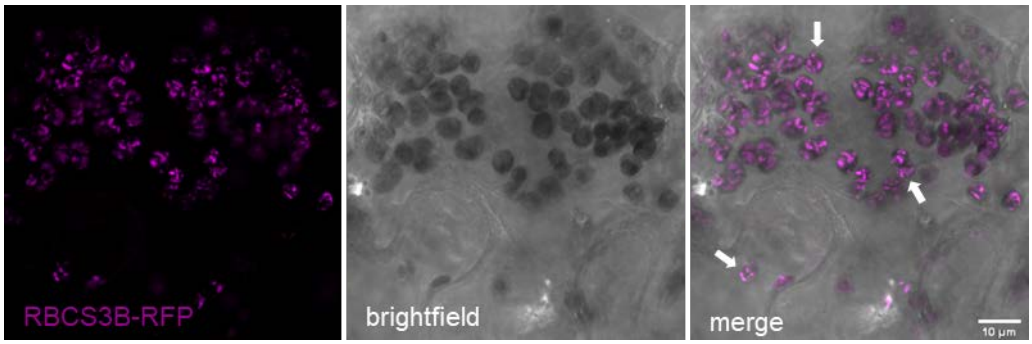

Figure 21: RBCS3B-RFP localizes to plastids in transiently transformed *N. benthamiana* leaf cells.
RBCS3B tagged with RFP was expressed under the control of the *p35S*. RBCS3B-RFP localizes to plastids. White arrows: aggregates in plastids. Scale bar: 10 µm. Confocal images were taken 2 days after infiltration.

Ectopic co-expression of PII-GFP with one of the small subunits of Rubisco, RBCS3B, tagged with RFP revealed extra-plastidic localization of both proteins to vesicle-like structures at plastids and in the cytoplasm (Figure 22 A). We observed extra-plastidic localization of co-expressed PII-GFP not only with RBCS3B-RFP (Figure 22 A) but also with DAT1-RFP (Figure 22 B) in vesicle-like structures at plastids and in the cytoplasm.

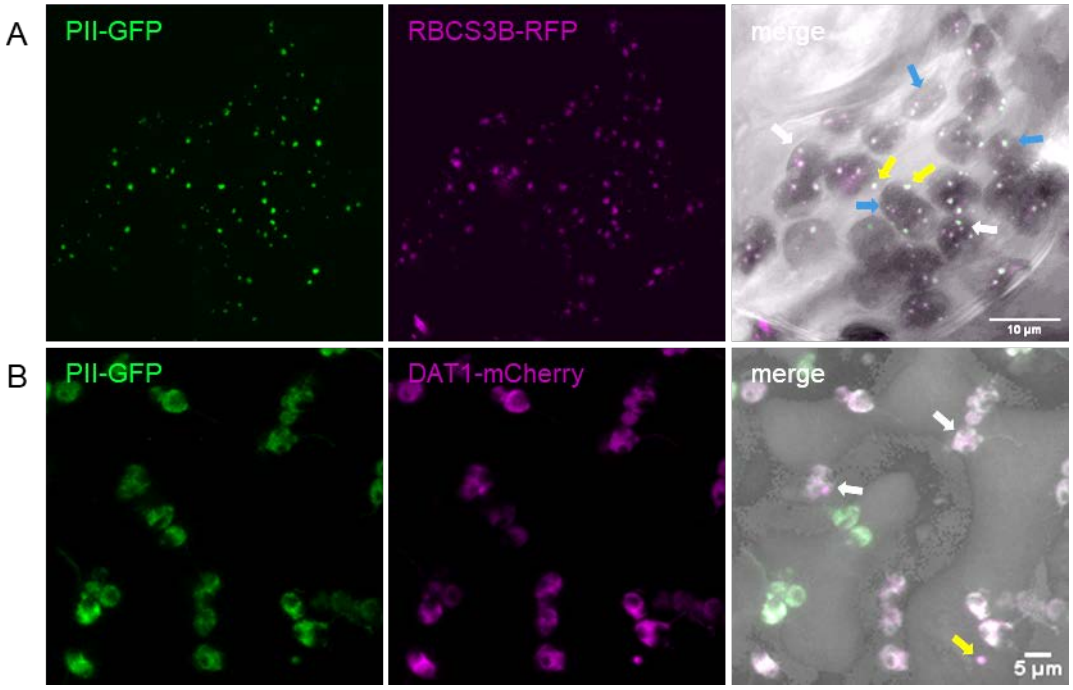

Figure 22: PII localizes in foci in plastids and in vesicle-like structures next to plastids.
A) PII-GFP and RBCS3B-RFP co-localize in foci in plastids and in vesicle-like structures next to plastids, both under the control of *p35S*. Confocal images were taken 2 days after transient transformation of *N. benthamiana* leaves. Scale bar: 10 µm. B) PII-GFP and DAT1-mCherry co-localize throughout the plastid and in the extra-plastidic space. Both under the control of an estradiol-inducible promoter. Estradiol induction 3 days after transient transformation of *N. benthamiana* leaves performed by Marvin Braun. 3D- image generated from Z-stack of confocal images taken 96 h after induction. Scale bar: 5 µm. White arrows: foci in plastids; yellow arrow: extraplastidic localization in vesicle-like structures; blue arrow: plastids.

Perello et al. (2016) showed that the Deoxyxylulose synthase (DXS), the Deoxyxylulose reductoisomerase (DXR) and the Geranylgeranyl-diphosphate synthase 11 (GGPPS11), three proteins of the isoprenoid pathway, localize in different manner in plastids. DXS and DXR localize in foci in plastids (Figure 23 A-B), whereas GGPPS11 localizes throughout the plastid and forms no foci (Figure 23 C) (Perello et al., 2016). The degradation of DXS and DXR is proposed to occur in different pathways (Pulido et al., 2013; Perello et al., 2016; Pulido et al., 2016): DXS degradation takes place via chaperones (Pulido et al., 2013; Pulido et al., 2016), whereas DXR is proposed to be degraded in Chloroplast vesiculation containing vesicles (CCVs), which are autophagy independent (Perello et al., 2016).

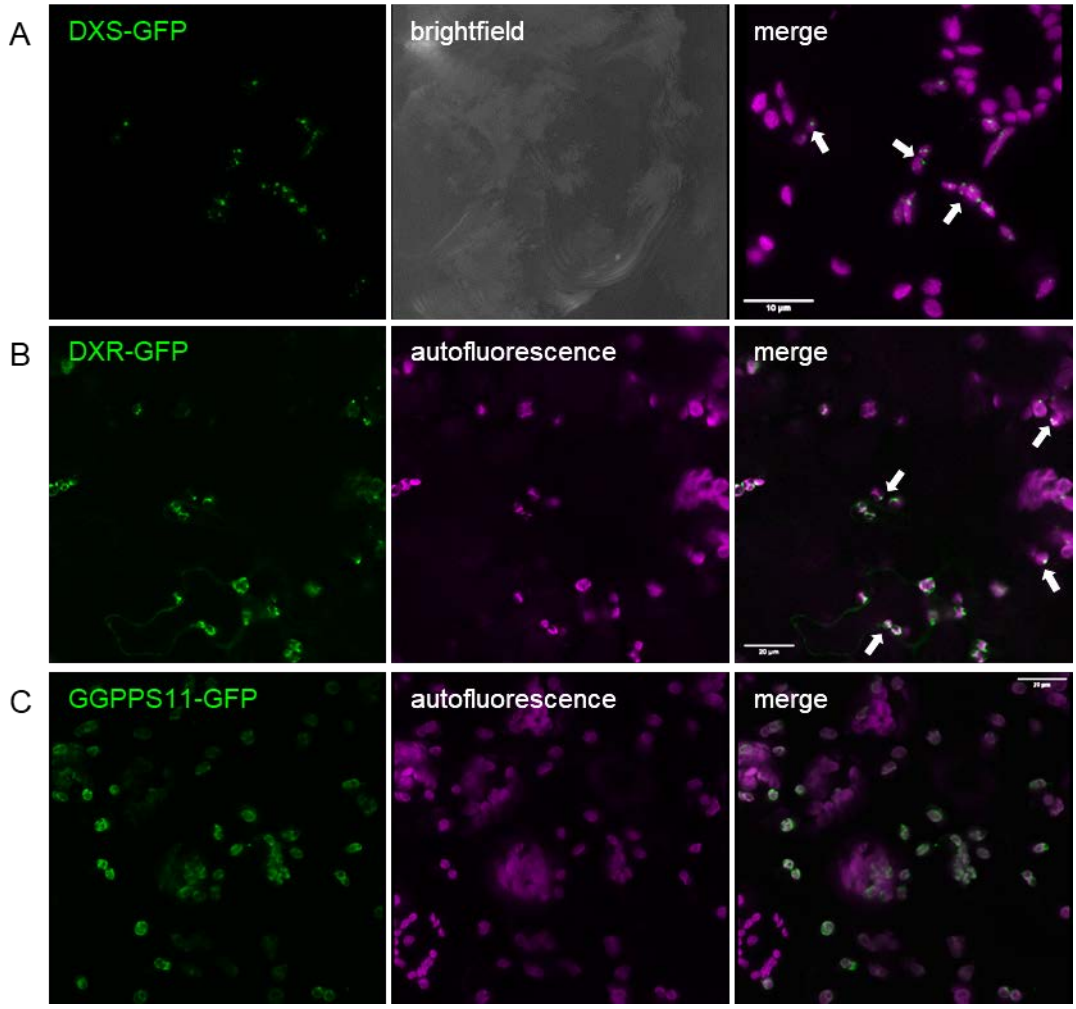

Figure 23: DXS-, DXR-, and GGPPS11-GFP localize to plastids of transiently transformed *N. benthamiana* leaf cells.

A) 3D- image generated from Z-stack of DXS-GFP. DXS-GFP localizes to plastids. B) DXR-GFP localizes to plastids. C) 3D- image generated from Z-stack of GGPPS11-GFP.

Expression of all genes under control of *p35S*. Scale bars: 10 µm. Confocal images were taken 3 days after transient transformation of *N. benthamiana*. White arrows indicate aggregates in plastids.

Co-expression revealed co-localization of PII-RFP with DXS-GFP, DXR-GFP and partially with GGPPS11-GFP in plastids (Figure 24 A-C), as GGPPS11-GFP does not form foci and localizes throughout the plastid (Figure 24 C).

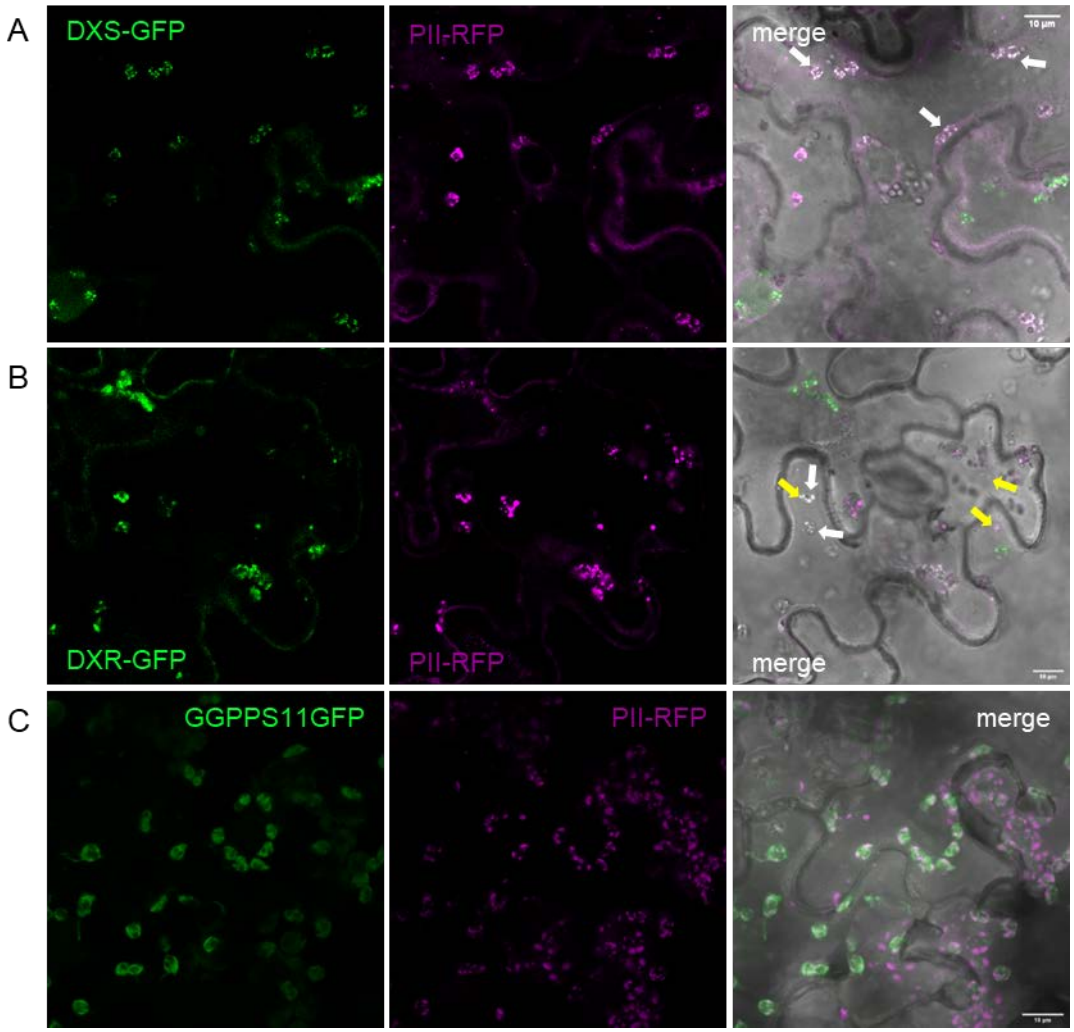

Figure 24 PII co-localizes with DXS, DXR and partially with GGPPS11 in plastids of *N. benthamiana.*

A) DXS-GFP and PII-RFP co-localize in foci in plastids. B) DXR-GFP and PII-RFP co-localize in foci in plastids and in extra-plastidic vesicle-like structures. C) GGPPS11-GFP localizes throughout plastids. PII-RFP localizes in foci in plastids.

White arrow: foci in plastids; yellow arrow: extra-plastidic localization in vesicle-like structures, putative CCVs. Expression of all genes under control of *p35S*. Scale bars: 10 µm. Confocal images were taken 3 days after transient transformation of *N. benthamiana*.

2.5.4 PII is involved in autophagy in *N. benthamiana*

PII putatively localizes not just with potential RCBs (Figure 22 A), which are autophagy-dependent but also with DXR that is degraded via CCVs, to putative CCVs, which are autophagy-independent (Figure 24 B) (Wang and Blumwald, 2014; Perello et al., 2016). As these are two different pathways for protein turnover, I analysed whether PII co-localizes with the cytoplasmic localized autophagy-related proteins Atg8e, Atg8g and NBR1 (Figure 25) (Contento et al., 2005; Hafren et al., 2018; Ustun et al., 2018).

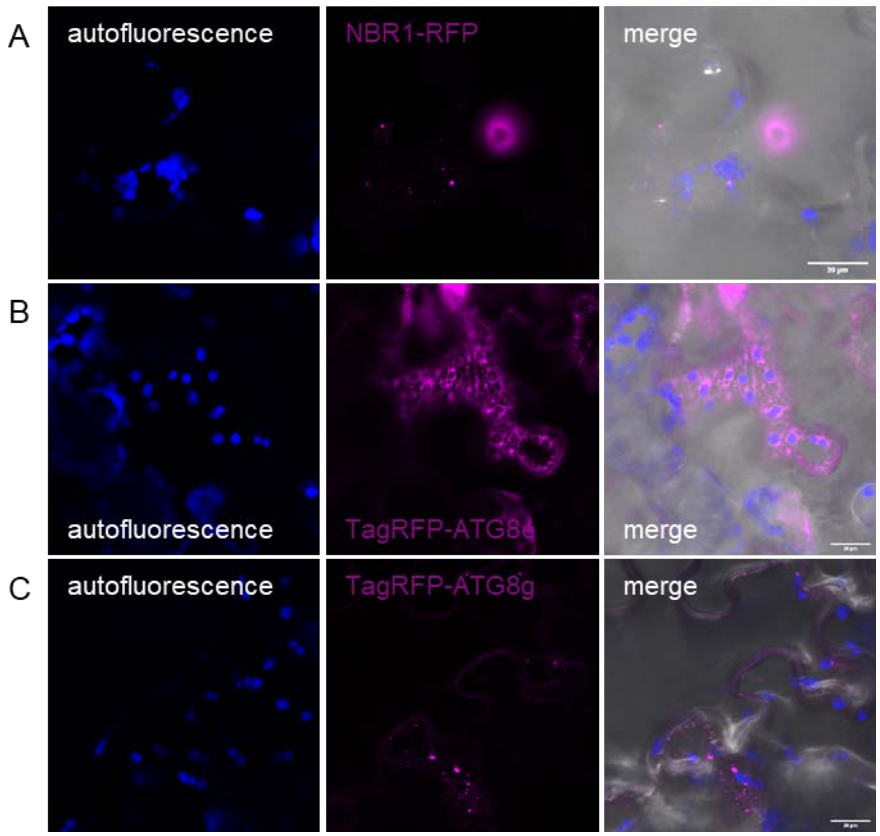

Figure 25: NBR1, Atg8e and Atg8g localize to the cytoplasm in transiently transformed *N. benthamiana* epidermal cells. A) NBR1-RFP localizes to the cytoplasm in vesicle-like structures. B) TagRFP-Atg8e localizes to the cytoplasm. C) TagRFP-Atg8g localizes to the cytoplasm uniformly and in vesicle-like structures. All genes expressed under the control of *p35S*. Scale bar: 20 µm. Autofluorescence indicated in blue.

Co-expression of PII-GFP with NBR1-RFP revealed partial co-localization in aggregates in the cytoplasm (Figure 26 A). The two Atg8 subforms Atg8e and Atg8g tagged with TagRFP localized in aggregates in the cytoplasm but also in a not aggregated form (Figure 25 B-C, Figure 26 B-C). PII-GFP co-localized with both subforms of Atg8 in aggregates in the cytoplasm and appeared in additional aggregates (Figure 26 B-C). The observed co-localization of PII with autophagy-dependent protein turnover may indicate a role of PII in these pathways.

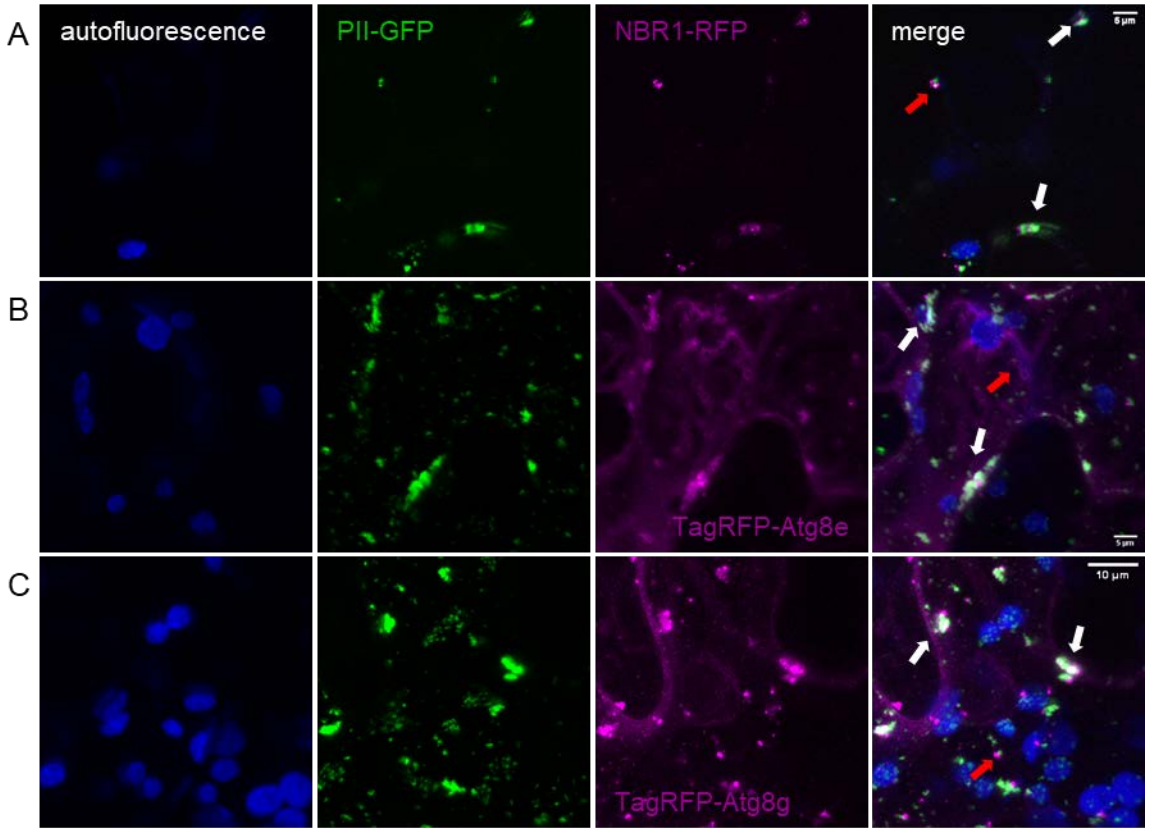

Figure 26: PII-GFP co-localizes partially with autophagy-related proteins NBR1, Atg8e and Atg8g in transiently transformed *N. benthamiana* leaves.
PII-GFP co-expressed with A) NBR1-RFP, B) TagRFP-Atg8e and C) TagRFP-Atg8g under the control of *p35S*. Scale bar: 5 µm A)-B) and 10 µm C). Autofluorescence indicated in blue. White arrows indicate co-localization; red arrows indicate no co-localization. A) Confocal image was taken 2 days after transient transformation of *N. benthamiana*. B)-C) 3D- image generated from Z-stack of confocal images taken 2 days after transient transformation of *N. benthamiana*.

2.6 Dynamics of PII foci formation

PII accumulates in foci but is also found in the rest of the plastid (Figure 14 B, Figure 20 and Figure 22). This led me to the observation that PII-GFP formed foci with NAGK-mCherry within seconds to a few minutes in mesophyll cells of transiently transformed *N. benthamiana* (Figure 27).

Visualization of foci formation kinetics revealed a fast onset of foci formation (Figure 28) within seconds (Figure 28 A) and lead to an increase in foci size within minutes (Figure 28 B). This observation led to the question whether fast foci formation is dependent on light or temperature.

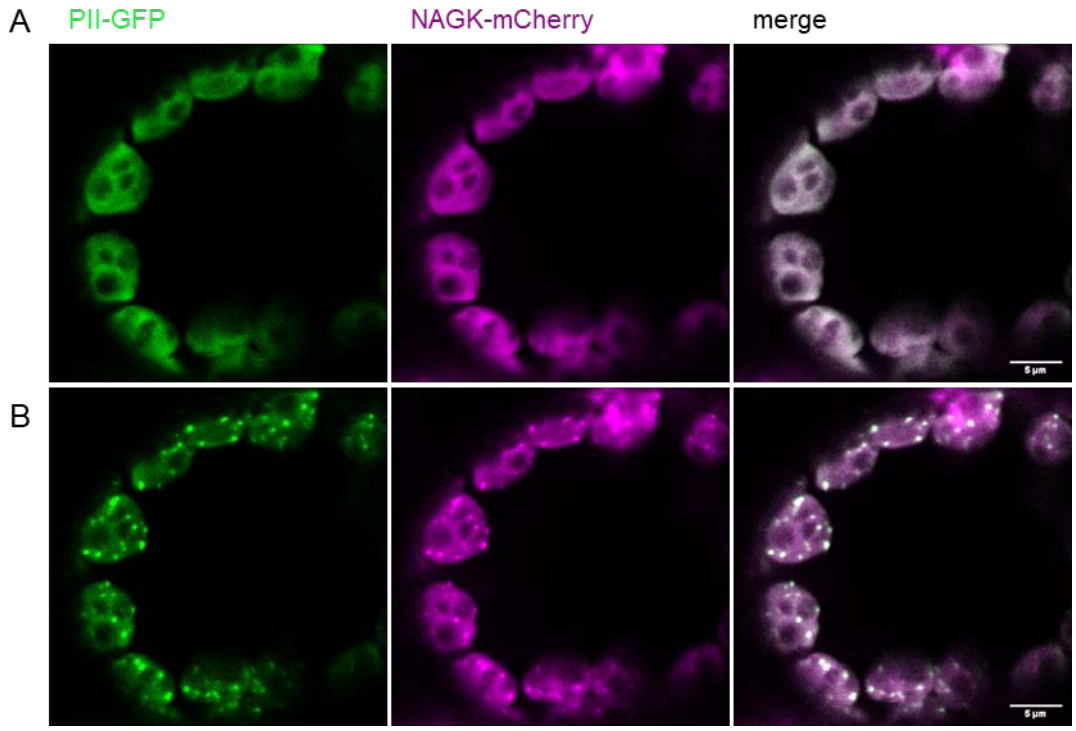

Figure 27: PII-GFP and NAGK-mCherry form foci within seconds in transiently transformed *N. benthamiana* mesophyll cells.

A) PII-GFP and NAGK-mCherry localize throughout plastids. B) PII-GFP and NAGK-mCherry localize throughout plastids and in foci 1 min 36 sec after first image (A). Both genes expressed under the control of *p35S* using the 2in1 FRET vector. Confocal images were taken 2 days after transient transformation of *N. benthamiana*.

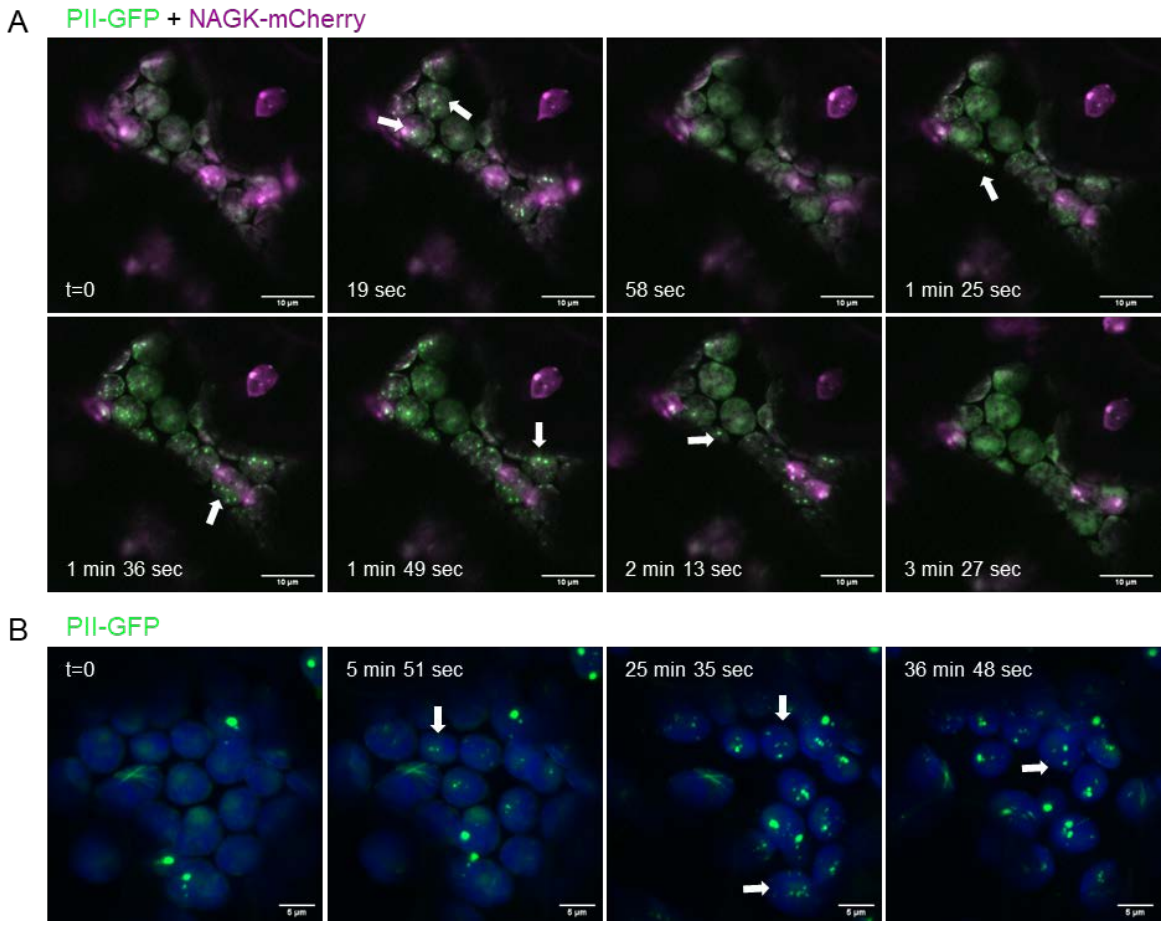

Figure 28: Kinetics of PII foci formation in transiently transformed *N. benthamiana* mesophyll cells.
A) Single plane images of time series of PII-GFP and NAGK-mCherry kinetics. Scale bar: 10 µm. Confocal images were taken 2 days after transient transformation of *N. benthamiana*.
B) Z-Stacks of time series of PII-GFP kinetics. Scale bar: 5 µm. Donor-only 2in1 FRET vector. Confocal images were taken 3 days after transient transformation of *N. benthamiana*.
All genes expressed under the control of *p35S* using the 2in1 FRET vector.

2.6.1.1 PII foci formation is partially dependent on temperature and light

To investigate the dependency of fast foci formation to light or temperature, I analysed stably transformed *A. thaliana* PII-GFP plants expressing *gPII-GFP* under the control of *pUBQ*.

Variation in PII-GFP fluorescence intensity levels in single plants of the analysed line prohibited quantification of this phenomenon. Therefore, only tendencies could be determined of PII foci formation in dependence to temperature and light. We observed PII-GFP forming foci with all tested conditions but not uniformly throughout all plant cells (Figure 29, Figure 30, Figure A 12, Figure A 13). PII-GFP localizes mainly in a uniform manner in the whole chloroplast in mesophyll cells and in foci in stomata cells when grown in dark at 8°C (Figure 29 B, Figure A 12 C-D). An increase in foci formation in chloroplasts of mesophyll cells was observed in dark at 23°C (Figure 29 A, Figure A 12 A-B), which was even more pronounced at 37°C (Figure 29 C, Figure A 12 E-F). Increase of temperature seemed to promote partial foci formation of PII-GFP in chloroplasts of mesophyll cells.

As foci formation is already visible at low temperatures and increases at higher temperatures in dark, I analysed PII-GFP localization exposed to blue, green, red and far-red light (Figure 30, Figure A 13).

Under blue light, PII-GFP localization was mostly uniform throughout the chloroplasts of mesophyll cells with partial additional aggregation (Figure 30 A; Figure A 13 A-B).

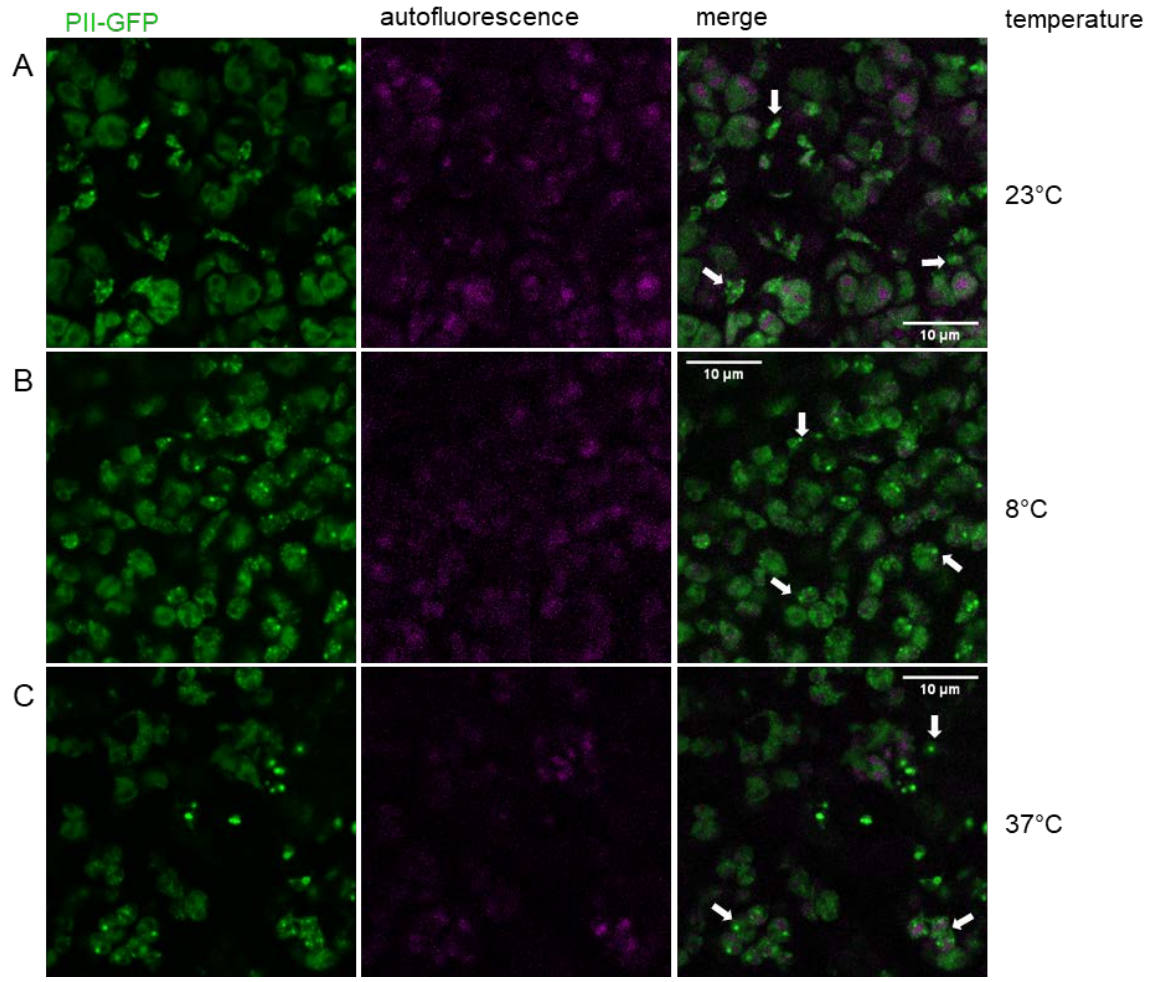

Figure 29: PII-GFP localization changes slightly in 6-day old seedlings after 24h in varying temperature conditions in *A. thaliana* expressing PII-GFP under the control of *pUBQ*.
A) PII-GFP localization after 24h in dark at 23°C. B) PII-GFP localization after 24h in dark at 8°C. C) PII-GFP localization after 24h in dark at 37°C.

Exposing seedlings to green light revealed PII-GFP localization in foci in plastids of stomata or epidermal cells (Figure 30 B). In mesophyll cells, an even distribution throughout plastids could be detected in most cells (Figure 30 B) but foci formation in plastids of mesophyll cells could be observed in few cells (Figure A 13 C-D).

Interestingly, the same pattern in mesophyll cells emerged when exposed to red or far-red light (Figure 30 C, D, Figure A 13 F, H). Still, this pattern could not be observed in all mesophyll cells (Figure A 13 E, G). This indicates at least partial dependency of PII foci formation to light and temperature, which needs to be further examined.

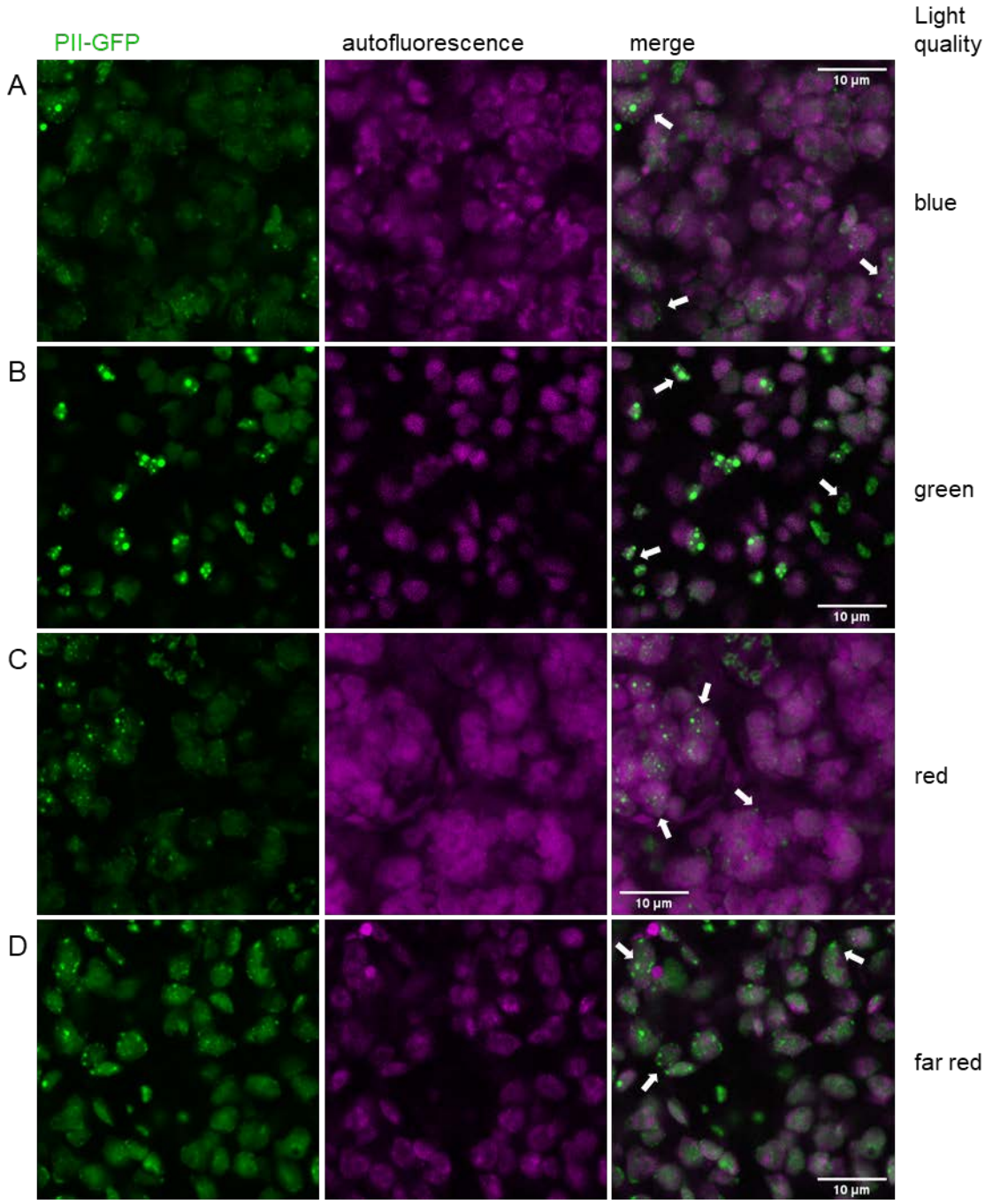

Figure 30: PII-GFP localization changes slightly in 6-day old seedlings after 24h in varying light conditions in *A. thaliana* expressing gPII-GFP under control of *pUBQ*.
A) PII-GFP localization after 24h under blue-light. B) PII-GFP localization after 24h under green light. C) PII-GFP localization after 24h under red light. D) PII-GFP localization after 24h under far-red light. White arrows indicate foci in plastids.

2.7 Interaction studies

The co-localization studies with PII raised the question if these observations are caused by direct interaction. *In vivo* interaction behaviour of plant PII had not been analysed to date. The analyses of interaction partners of AtPII was mainly performed with *in vitro* assays using recombinant PII without cTP (Chen et al., 2006; Feria Bourrellier et al., 2010). To investigate whether PII is interacting with known and putative novel interaction partners *in planta*, I made use of two fluorescent protein-based interaction analysis methods in transiently transformed *N. benthamiana*. First, the Förster Resonance Energy Transfer (FRET) (Forster, 1946) combined with Fluorescence Lifetime Imaging Microscopy (FLIM) and second, the Bimolecular Fluorescence Complementation (BiFC), both utilizing 2in1 vectors (Grefen and Blatt, 2012; Hecker et al., 2015). Additionally, we applied GFP-traps of whole leaf extracts from stably transformed *A. thaliana* Col-0 with PII-GFP under control of the *pUBQ* as an alternative method for interaction analysis.

2.7.1 FRET-FLIM

The co-localization of PII with known and putative novel interaction partners observed in co-localization studies (Figure 14, Figure 15, Figure 19, Figure 22 A, Figure 24) led to the question whether these proteins are in fact interacting with PII. The fluorescence-based analyses using FRET-FLIM reveals whether a drop in the donor-lifetime and thereby an energy transfer to the acceptor occurs. This takes place when the two FP-tagged proteins are in a distance below 10 nm (Peter et al. (2014), for review see Ishikawa-Ankerhold et al. (2012)). FRET-FLIM analyses were used to investigate the reduction of fluorescence lifetime of the analysed PII-GFP co-expressed with known and putative interaction partners fused to mCherry.

FLIM analyses revealed highly significant reduction of GFP fluorescence lifetime using PII-GFP as a donor with itself, NAGK, BCCP1, GBSSI and DAT1 fused to the acceptor mCherry in comparison to PII alone (PII-GFP co-expressed with GentR (Figure 31 A); Figure 31 G). These observations were also made using PII-GFP as a donor with NAGK, RBCS3B, DXS, DXR and GGPPS11 fused to the acceptor mCherry in rapidFLIM studies in comparison to PII alone (Figure 32 A; Figure 32 G). Although PII showed co-localization with DXR in foci in first co-localization studies (Figure 24 B), DXR-mCherry showed no foci formation in plastids using 2in1 vectors (Figure 32 E) and only a slight but significant reduction in GFP fluorescence lifetime in rapidFLIM studies (Figure 32 G). The reduction of GFP fluorescence lifetime

indicates interaction of PII to the tested proteins, which was further verified in BiFC-interaction analyses (Figure 33). The highest reduction in GFP fluorescence lifetime was measured for PII co-expressed with NAGK, indicating a very close proximity of the fluorophores.

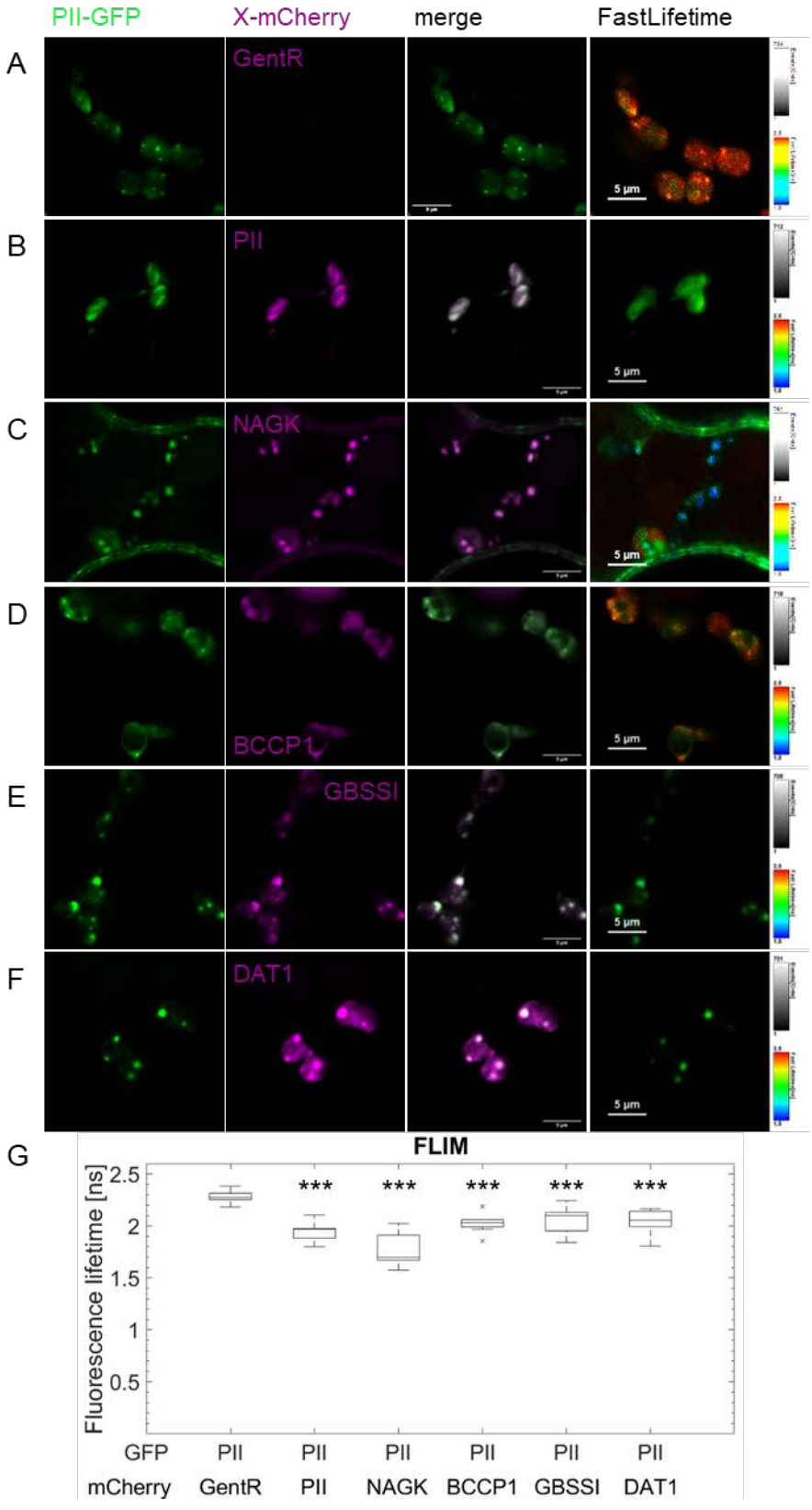

Figure 31: Co-localization and FRET-FLIM analyses of PII interactions with known and novel interaction partners in *N. benthamiana* using 2in1 FRET vectors.
A) PII-GFP alone (Donor-only control). PII-GFP co-expressed with B) PII-mCherry, C) NAGK-mCherry, D) BCCP1-mCherry, E) GBSSI-mCherry and F) DAT1-mCherry. G) Boxplot of GFP-Fluorescence Lifetime decrease obtained in FLIM analyses; students t-test revealed p-values ***<0.001. Expression of all genes under the control of *p35S*. FastLifetime images indicate decrease of GFP fluorescence lifetime depicted by a heat map from 2.5 to 1.0 ns.
Confocal images were taken and FLIM measurement were performed 2 days after transient transformation of *N. benthamiana*.

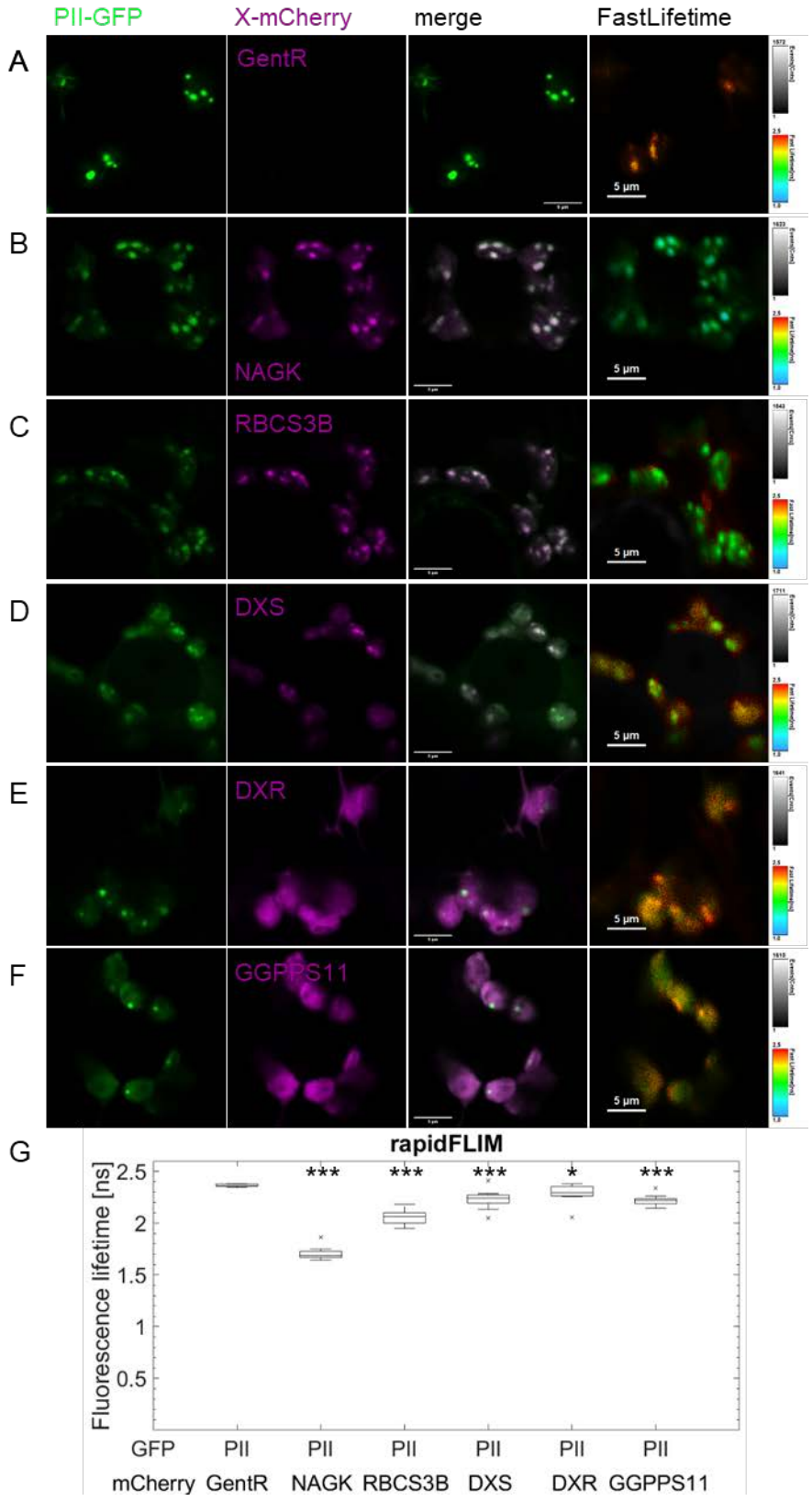

Figure 32: Co-localization and FRET-FLIM analyses of PII interactions with known and novel interaction partners in *N. benthamiana* using 2in1 FRET vectors.
A) PII-GFP alone (Donor-only control). PII-GFP co-expressed with B) NAGK-mCherry, C) RBCS3B -mCherry, D) DXS-mCherry, E) DXR-mCherry and F) GGPPS11-mCherry.
G) Boxplot of GFP-Fluorescence Lifetime decrease obtained from rapidFLIM analyses; student's t-test revealed p-values:* < 0.05, *** < 0.001. Expression of all genes under the control of *p35S*. FastLifetime images indicate decrease of GFP fluorescence lifetime depicted by a heat map from 2.5 to 1.0 ns.
Confocal images were taken and FLIM measurement were performed 2 days after transient transformation of *N. benthamiana*.

2.7.2 BiFC

The reconstitution of YFP using the BiFC approach, is an alternative method to analyse the interaction of two proteins *in vivo* (Hu et al., 2002). Therefore, I performed BiFC analyses in stably transformed *N. benthamiana* using BiFC

constructs of PII with the same interaction candidates as in section 2.7.1 to further confirm the observed interactions.

The reconstitution of YFP exclusively in foci in plastids was observed for all tested constructs (Figure 33 B-I), indicating interaction, except of PII with GGPPS11 (Figure 33 J) and the donor-only control PII co-expressed with GentR (Figure 33 A). Although PII showed close proximity and putative interaction with GGPPS11 in FRET-FLIM (Figure 32 F-G), this could not be verified by BiFC analyses (Figure 33 J).

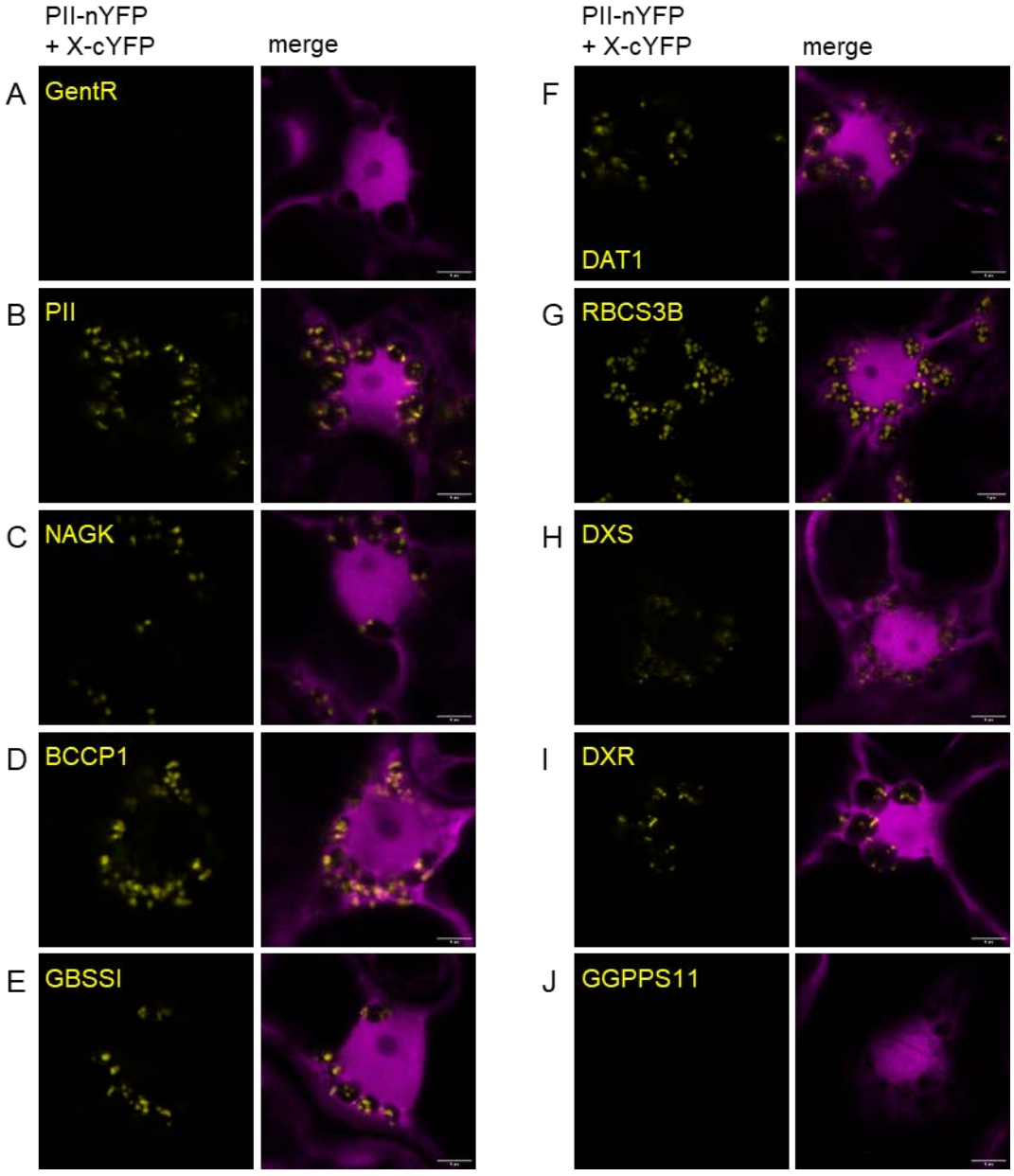

Figure 33: BiFC analyses of PII with known and putative novel interaction partners in transiently transformed *N. benthamiana* using 2in1 BiFC vectors
PII-nYFP co-expressed with C-terminal cYFP-tagged A) PII, B) NAGK, C) BCCP1, D) GBSSI, E) DAT1, F) RBCS3B, G) DXS, H) DXR, I) GGPPS11. M) PII-nYFP alone (Donor-only control) Free mRFP is used as transformation control. Expression of all genes under control of *p35S*. Confocal images were taken 3 days after transient transformation of *N. benthamiana*. Scale bar 5 µm.

2.7.3 GFP-trap

It was not much known before about additional interaction partners of PII besides NAGK, BCCP1/2 and BADC1-3, and possible complex formation involving PII (Chen et al., 2006; Ferrario-Mery et al., 2006; Beez et al., 2009; Feria Bourrellier et al., 2009; Feria Bourrellier et al., 2010; Chellamuthu et al., 2014).

There is evidence for a broader range of putative interaction partners according to our FRET-FLIM and BiFC data (Figure 31, Figure 32 and Figure 33). To further verify this, I performed a GFP-trap assay to pull down interaction partners of PII in *A. thaliana*. The GFP-trap was performed with whole leaf extracts of five-week-old plants overexpressing PII-GFP under the *pUBQ10*. As a negative control, I used *Col-0* expressing pt-gk, the transit peptide of tobacco Rubisco C-terminally tagged with GFP (Nelson et al., 2007).

GFP-trap samples of whole leaf extracts revealed detectable bands for pt-gk at ~50 kDa and for PII-GFP at 15 kDa, ~35 kDa and ~45 kDa (Fraction 6 in Figure 34 A-C). Additional bands could be detected for PII-GFP in Western blot analyses (Figure 34 C). Bands of predicted protein sizes of known and putative interaction partners of PII were cut out and were subjected to targeted mass spectrometry (MassSpec) analyses (Figure 34 B). Control samples were cut out from elution fraction of pt-gk (Figure 34 B).

MassSpec-analysis of protein bands revealed high sequence coverage only for PII, either mGFP5-tagged at ~58.5 kDa, ~45.8 kDa, ~34.5 kDa, ~34 kDa and ~31.2 kDa, or alone at ~17.9 kDa, ~15.5 kDa and ~14.7 kDa (Table 1). The remaining hits resemble none of the known or the putative novel interaction partners of PII (Figure 31, Figure 32, Figure 33 and Table 24: Appendix).

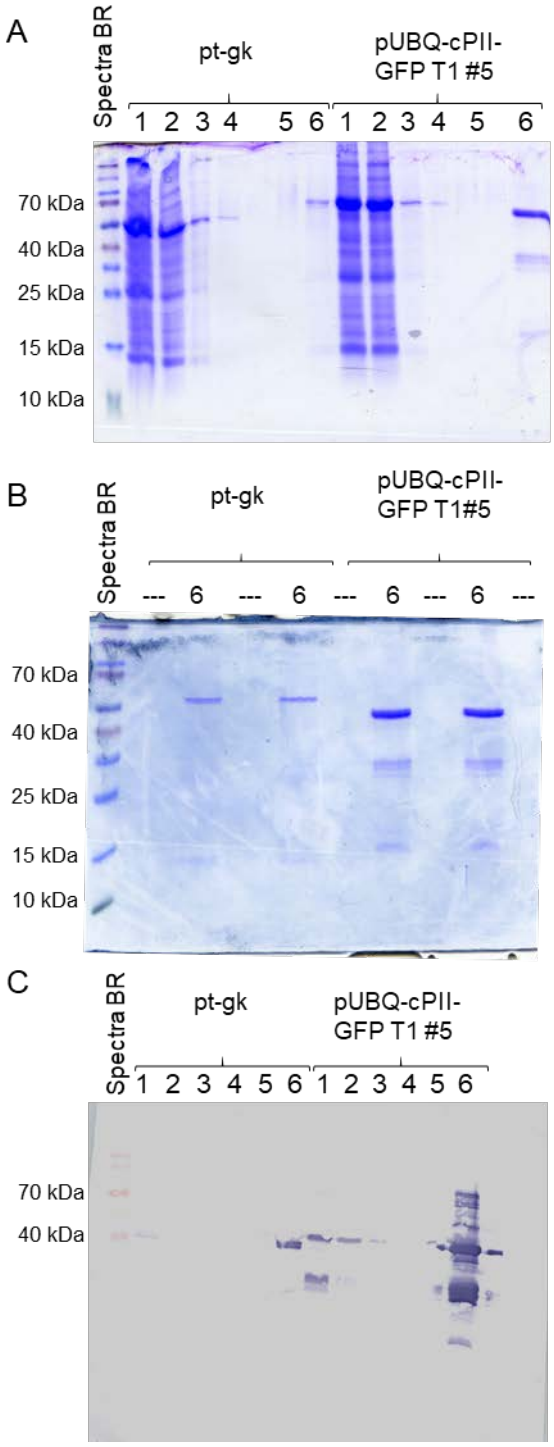

Figure 34: SDS-PAGEs and Western blot of whole leaf extracts followed by GFP-trap from pt-gk (tobacco Rubisco cTP tagged with GFP) and *pUBQ::cPII-GFP* T1 #5 stably transformed in *A. thaliana*.

A) Whole leaf extracts from five-week-old plants. SDS-PAGE of single fractions after GFP-trap.

B) SDS-PAGE of eluates after GFP-trap (see 6 in A) for MassSpec-analyses. Single band detectable for pt-gk in fraction 6 at ~50 kDa. Eluate of cPII-GFP trap revealed bands at ~45 kDa, ~35 kDa and 15 kDa.

C) Western blot of GFP-trapped leaf extracts with α-GFP. For pt-gk single band detectable in fraction 1 and 6 at ~40 -50 kDa. For cPII-GFP bands detectable at ~35 kDa and ~45 kDa in fraction 1, 2 and 6. In elution fraction of cPII-GFP (6) additional bands are detectable.

Fraction 1: Input; 2: Flow-through; 3: Wash 1; 4: Wash 2; 5: Wash 3; 6: Elution. 15 µL per lane.

Table 1: Hits against PII-mGFP5 and PII using MS-Fit ProteinProspector

Protein size SDS-PAGE (kDa)	% coverage	Protein name	Protein size (kDa)
58.5	6.4	PII-mGFP5	52.391
45.8	64.2	PII-mGFP5	52.391
45	14.2	PII-mGFP5	52.391
34.5	26.9	PII-mGFP5	52.391
34	30.5	PII-mGFP5	52.391
31.2	26.7	PII-mGFP5	52.391
17.9	20.9	PII (Nitrogen regulatory protein P-II homolog)	21.276

15.5	51	PII (Nitrogen regulatory protein P-II homolog)	21.276
14.7	15.3	PII (Nitrogen regulatory protein P-II homolog)	21.276

3 Discussion

3.1 The function of PII as C/N sensor in plants

The expression of *PII* is dependent on light and sucrose (Hsieh et al., 1998). We could show that the activity of the *PII* promoter is not only dependent on sucrose and light but in addition on inorganic N (Figure 2). Moreover, limiting N conditions lead to low promoter activity independent of sucrose. Hsieh et al. (1998) showed decreased *PII* levels with organic N sources like AAs in addition to sucrose (Hsieh et al., 1998). We could show that *PII* promoter activity increases with additional inorganic N. Light and sucrose without inorganic N are not sufficient to induce an increased promoter activity (Figure 2). At least for the onset of transcription, these data indicate that not only light and abundance of C sources like sucrose are essential but also inorganic N sources. The activity of the promoter depending on availability of C and inorganic N sources display a fine-tuning already on the transcriptional level. Transcriptional regulation of PII was at least shown for NtcA activated gene expression in cyanobacteria. But in contrast to our data, PII expression in cyanobacteria was induced in N deprived cells (Giner-Lamia et al., 2017).

The mutant line *PIIS2* (Ferrario-Mery et al., 2005) displayed no apparent phenotype under the N and sucrose limiting conditions. The absence of a phenotype led to the question whether *PIIS2* is an actual knockout mutant. RT-PCR of seedlings revealed low but detectable full-length *PII* mRNA in *PIIS2* (Figure 6). As *PII* mRNA was still detectable, *PIIS2* is not a knockout but a knockdown mutant. The detected mRNA may be sufficient for stable PII protein level and therefore, no reproducible changed phenotype is detected under the tested conditions for *PIIS2. PIIS2* is the only characterized *PII* knockout line in Col-0 background (Ferrario-Mery et al., 2005). The effect of *PII* loss on plant development must be repeated with additional mutant lines. Hence, we generated *PII* CRISPR/Cas lines to clarify the role of PII in *A. thaliana*. The characterization of these lines revealed no CRISPR/Cas events so far.

3.2 PII localizes to foci and may be involved in protein turnover

We found *in vivo* that PII tagged with fluorescent proteins under the control of different promoters distributed all over the whole plastid, except of putative starch granules, but mainly in foci in plastids. During my studies I tried to relate this distribution pattern to known suborganellar structures in plastids.

These studies revealed, that PII is not localizing in starch granules, visualised indirectly in co-localization experiments (Figure 19 A). In addition, PII localization to plastoglobuli could be excluded, as PII is not present in the plastoglobuli proteome (Lundquist et al., 2012). Furthermore, we could exclude, that PII localizes to nucleoids in plastids (Figure 17 B), thus a PipX homologue is absent in plants (Chellamuthu et al., 2013).

We observed a fast onset of foci formation within seconds in chloroplasts of *N. benthamiana*. Although there were slight differences in foci formation in *PII* overexpressing *A. thaliana* plants treated with different temperatures in the dark as well as with various light qualities at RT, the dependency of foci formation onset to temperature and light is still an open question. It was proposed, that cyanobacterial PII was modified post-translationally by phosphorylation via changes in the redox-state of plastoquinone in the photosystem II (PSII) (Allen et al., 1981), but not by PSI, in the photosynthetic electron transport chain or by differential ammonia concentrations (Harrison et al., 1990; Tsinoremas et al., 1991). This change was observed after growth of cells at wavelengths preferred by PSII (Harrison et al., 1990). A post-translational modification of *A. thaliana* PII could not be detected so far (Smith et al., 2004), indicating that PII foci formation may not be due to phosphorylation. Another possibility is that foci formation may be due to a change in effector molecule concentrations, as it has been shown for *Synechococcus* PII (Espinosa et al., 2018). It localizes in dark to foci at potentially low ATP to ADP level in a putative inactive stage (Espinosa et al., 2018). Therefore, this foci formation may represent an inactivation of PII or its interactors *in planta*. Binding of PII to 2-OG mediates inactivation of the so far characterized interactions. When the 2-OG level is high in the foci, an opportunity to measure this could be the use of 2-OG, derivatized with *o*-phenylenediamine (OPG), resulting in a fluorescent derivative emitting at 420 nm (McNeill et al., 2005). The concentration or even foci formation of this derivative in the plastids, could give a further hint.

We observed PII localization not only intraplastidic in foci but also extraplastidic in vesicle-like structures. PII co-localizes with DAT1, RBCS3B and DXR intra- and extraplastidic in a putative autophagy dependent and/or independent manner (Figure 36). PII showed partial co-localization with autophagy related proteins. This may be another hint on PII acting as a molecular glue by interacting with many metabolic proteins, thereby either positively or negatively regulating their activity and

putatively “catch” proteins for protein degradation in foci in the cytoplasm. It was shown for RCBs, that a higher number of RCBs could be detected in plants grown on ½ MS without sucrose in comparison to ½ MS with sucrose in dark (Izumi et al., 2010). A first approach could be the growth of stably transformed *A. thaliana* expressing PII-XFP on ½ MS media with and without sucrose and further characterization using fluorescence microscopy (Ishida et al., 2008). Additional treatment with concanamycin A, an inhibitor of the V-ATPase, used for targeting of proteins to the vacuole in a autophagy-dependent manner, could be used (Ishida et al., 2008). When PII-XFP foci are localizing to the vacuole, RBCS3B localization could be analysed in wild type and *PII* knockout lines, as Rubisco is linked to RCBs (Ishida et al., 2008). When RCBs are still detectable in a comparable amount to wild type in the vacuole, at least a direct connection involving PII in RCB formation may be excluded.

The protein turn over via CCVs is autophagy-independent (Wang and Blumwald, 2014). It was presumed for DXR that it is degraded via CCVs (Perello et al., 2016). Microscopic analyses revealed co-localization of PII with DXR in extraplastidic vesicle-like structures. This may indicate PII degradation or involvement in protein turn over via CCVs (Figure 36). Treatment of stably transformed *A. thaliana* expressing PII-XFP with concanamycin A, could lead to a loss in extraplastidic vesicle-like structure and a more diffuse distribution of PII in plastids, as it was reported for CCVs (Wang and Blumwald, 2014). As both scenarios are possible, this experiment should be performed preceding further characterization of the observed extraplastidic vesicle-like structures.

3.3 Putative new functions for PII in plants

3.3.1 PII interacts with proteins involved in diverse metabolic pathways

In the past, interaction analyses of plant PII in yeast-2 hybrid screens or expressed in *E. coli* in a pull-down assay were performed using recombinant PII lacking the transit peptide (Sugiyama et al., 2004; Chen et al., 2006; Ferrario-Mery et al., 2006; Feria Bourrellier et al., 2009; Feria Bourrellier et al., 2010).

Co-expression analyses revealed co-localization of PII with the already known interaction partners NAGK, BCCP1, BADC2 and BADC3. In addition, PII co-localized with GBSSI, DAT1, DXS, DXR and RBCS3B and partially with GGPPS11, which were not described as putative interactors of PII, yet. Using FRET-FLIM and BiFC analyses, I could show that full-length PII is interacting *in vivo* with itself, NAGK

and BCCP1 in transiently expressed *N. benthamiana*. Furthermore, reduction of GFP fluorescence lifetime in FRET-FLIM and reconstitution of YFP in BiFC strongly indicate interaction of PII with GBSSI, DAT1, RBCS3B, DXS and DXR (Figure 36). These interactions were not described before.

All these known and putative interactors are involved in metabolic pathways dependent on C and/or N availability (Krebbers et al., 1988; Dedonder et al., 1993; Szydlowski et al., 2011; Pulido et al., 2013; Perello et al., 2016; Pulido et al., 2016; Suarez et al., 2019). The mRNA expression of *GBSSI* increases during day and decreases at night. The protein level of GBSSI display no significant changes, whereas highest activity of the protein can be observed during day (Tenorio et al., 2003). Targeting of GBSSI to starch granules is dependent on PTST (protein targeting to starch) (Seung et al., 2015). I did not observe localization of GBSSI on starch granules in *N. benthamiana* co-expressed with PII (Figure 19 A, Figure 35 B) as it was described for GBSSI localization in *A. thaliana* (Figure 35 A). The localization pattern of PII co-expressed wih GBSSI reminds of the localization pattern of the starch synthase IV (SSIV) that localizes next to starch granules (Figure 35; Szydlowski et al. (2009).

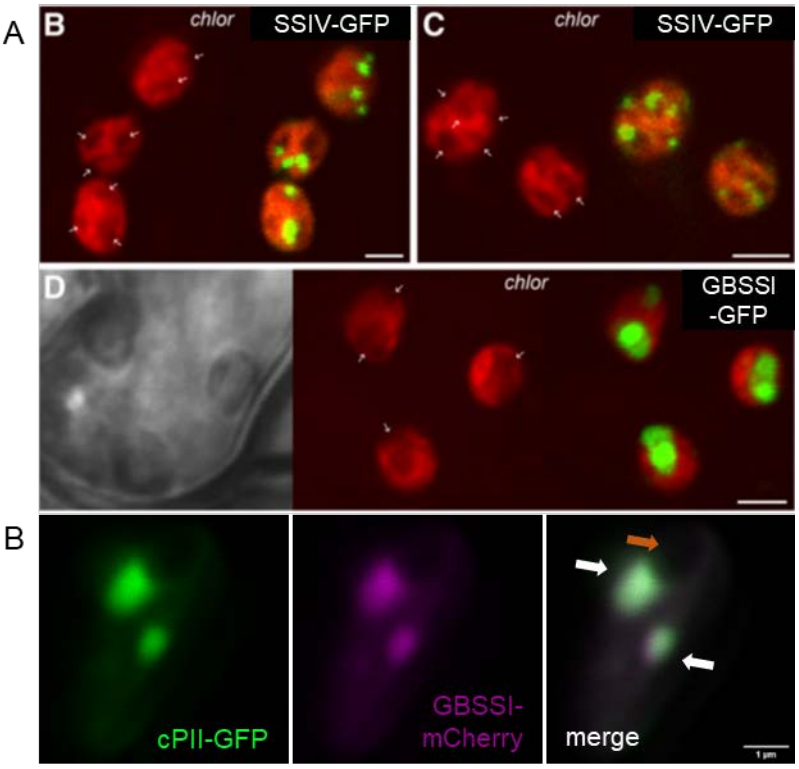

Figure 35: Localization pattern of Starch Synthase IV (SSIV), GBSSI, and GBSSI co-expressed with PII.
A) SSIV-GFP and GBSSI-GFP expressed in A. thaliana. Upper panel: SSIV-GFP localizes next to starch granules. Lower panel: GBSSI-GFP localizes on starch granules. Autofluorescence (chlor). Scale bar 2 µm. Modified from Szydlowski et al. (2009).
B) PII-GFP and GBSSI-mCherry localize next to starch granules indicated by orange arrow. Scale bar 1 µm. Image identical to Figure 19 A.

As *A. thaliana* PTST is not co-expressed with PII-GFP and GBSSI-mCherry, the question remains, whether PII negatively regulates GBSSI activity in the absence of

PTST or acts as a positive regulator of GBSSI. The observed interaction between PII and GBSSI has to be confirmed with co-expressed PTST in day/night cycle.

D-Met is not only the precursor of D-Glu, D-Ala and L-Met (Gördes et al., 2013) but the major substrate of DAT1, preferentially catalysing the reaction from D-Met with pyruvate to D-Ala and 2-OG (Suarez et al., 2019). As PII directly binds 2-OG (Kamberov et al., 1995; Chellamuthu et al., 2014), PII may also sense the levels of 2-OG produced by DAT1, thereby positively or negatively regulating DAT1 by direct interaction. At high levels of 2-OG, all binding sites in the PII trimer are possibly occupied and interaction of PII with DAT1 could be abolished. The activity of DAT1 in presence of PII with 2-OG and/or pyruvate and respective D-AA with additional ATP should be analysed in *in vitro* enzymatic assays.

RBCS3B is a small subunit of Rubisco (Krebbers et al., 1988; Dedonder et al., 1993). Rubisco catalyses the reaction from Ribulose-1,5-bisphosphate with CO_2 to 3-D-Phosphoglycerate or in absence of CO_2, Ribulose-1,5-bisphosphate with O_2 to 2-Phosphoglycolat and 3-D-Phosphoglycerate (for review see Bracher et al. (2017)). I could observe proximity and interaction of PII and RBCS3B in BiFC and FRET-FLIM studies. Rubisco needs bound Mg^{2+} to its carbamatylated L-Lys to be enzymatically active (Bracher et al., 2017). One possibility would be that PII, which directly binds Mg^{2+}, is able to transfer its Mg^{2+} to Rubisco and thereby activate it. Enzymatic activity of Rubisco in presence of PII has to be validated.

We observed co-localization of PII with three proteins of the isoprenoid pathway: DXS, DXR and GGPPS11. Although putative interaction was observed for PII with DXS and DXR, proximity to GGPPS11 was traced but no reconstitution of YFP in BiFC analyses. As these three proteins are part of the isoprenoid pathway (Perello et al., 2016), the effect of PII putatively interacting with DXS and DXR has to be revealed. For this, co-immunoprecipitation of PII with DXS and DXR has to be performed.

Albeit PII was found to interact or at least show proximity to nearly all tested proteins, in MassSpec analyses of GFP-trapped samples none of the known and putative new interaction partners could be found. This finding did not confirm my observations of the interactions of PII, but still did not falsify them. The abundance of the interaction candidates may not be sufficient to detect them in this way. This should be analysed in future experiments. The interactions could be verified

alternatively by the usage of plant extracts of plants expressing PII and the putative interactor in co-immunoprecipitation experiments.

4 Conclusion and Outlook

The promoter activity of *PII* is dependent on C/N availability. To investigate the effect not only on *PII* transcript level but also downstream pathways or regulated pathways, RNAseq experiments should be performed in *PII* knockout and overexpressor lines. Furthermore, Proteomics and Metabolomics experiments of these lines would provide further information on pathways controlled by *PII* directly and indirectly.

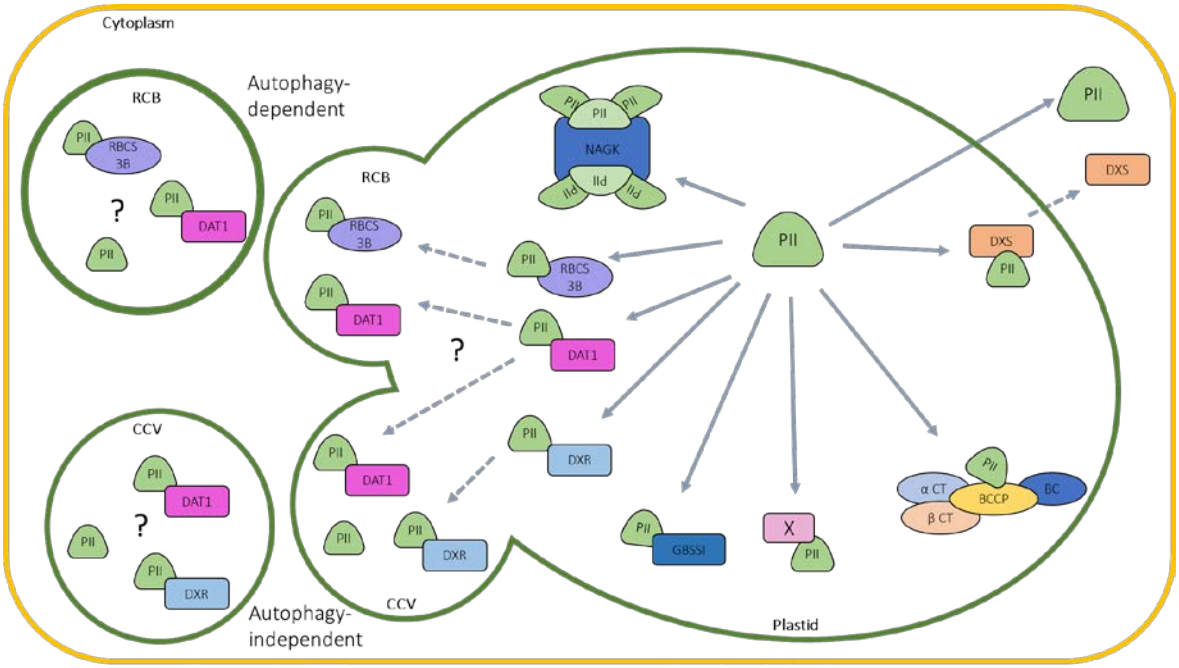

Figure 36: Model of PII action in protein turnover

PII localizes to plastids and interacts with NAGK and BCCP1. Furthermore, it may interact with GBSSI, DAT1, RBCS3B, DXS and DXR. PII could co-localize with RBCS3B to autophagy dependent RCBs. Together with DXR, PII could localize to autophagy independent CCVs. PII could co-localize with DAT1 to either RCBs or CCVs. PII partially co-localizes with the autophagy proteins Atg8e and Atg8g and furthermore with NBR1 in the cytoplasm.

PII forms foci in the intra- and extraplastidic space. This process is very fast, and the stimulus must be validated. One stimulus could be a change in the redox state of the plant, initiated by either light or temperature. Foci did not distribute uniquely in epidermal and mesophyll cells and varied between neighbouring cells and plastids. A small change in the molecular composition or redox state in the single cell or plastid may lead to the fast kinetics. For this, the redox-state of the cell may be crucial by changed levels of ammonia or by photo-damage induced by high light as it was proposed for cyanobacteria (Drath et al., 2008; Dai et al., 2014). In cyanobacteria, a change in the redox-state of PSII or a change in ammonia levels, led to post-translational phosphorylation of PII (Allen et al., 1981; Harrison et al., 1990; Tsinoremas et al., 1991). Nevertheless, since evidence is missing for

phosphorylation of *A. thaliana* PII (Smith et al., 2004), it remains an open question whether PII may sense a change in the redox-state and thereby forms foci. This change can be detected using redox-sensitive fluorescent proteins tagged with specific signal peptides, as Pt-GRX1-roGFP2 (Yu et al., 2013), composing of tobacco Rubisco cTP (Nelson et al., 2007), and NADPH-dependent glutathione/ glutaredoxin (GRX)-reduction oxidation sensitive GFP (Meyer et al., 2007; Gutscher et al., 2008). When a changed redox state of the plastids or even cells can be detected during foci formation, further analyses should be performed to elucidate the responsible effector molecule.

The role of PII in *A. thaliana* remains cryptic although new putative interaction partners and changing subcellular localization patterns could be observed. The new putative interactions should be verified in the future using co-immunoprecipitation before further characterization of these interactions. Upcoming experiments should address dependency and activity of these new interactions on 2-OG and Mg^{2+}-ATP. The proximity of PII with many enzymes involved in various metabolic pathways may reveal new unknown regulatory functions of PII.

The localization and interaction studies and furthermore experiments regarding the phenotype have to be performed in a PII free environment. The endogenous PII from *N. benthamiana* could change the behaviour of *A. thaliana* PII. The co-localization and interaction studies are performed with vectors consisting of the *35S* promoter and plastids have only a small space of few µm, the import of massive amounts of proteins could lead to highly significant reduction of the GFP fluorescence lifetime. This is also true for the BiFC analyses. Co-immunoprecipitation experiments with PII and known and novel interaction partners using the endogenous promoters should be performed with several grams of plant material to further investigate interactions. The lack of known and novel interaction partners after GFP-trap of whole leaf extracts could be due to the low abundance of these proteins. However, as MassSpec analyses was performed only with fragments cut out of the gel, this experiment should be repeated with more leaf material, and with the whole eluate fraction in an untargeted MassSpec approach.

Two hypotheses of PII function *in planta* and especially *A. thaliana* could be mentioned. One is that the new interactions are just a subset of PII interactions and PII positively and/or negatively regulates a wide range of proteins in plastids at high to low affinity. One possibility is that the foci are not the place of activity of the

interactors but maybe aggregation prior to vesiculation and protein turnover (summarized in Figure 36). Another possibility is that interactions and activity of the interactors is high in foci, crowding all necessary effectors and metabolites for the metabolic pathways co-affecting each other.

Second hypothesis includes actual interaction partners of PII, like NAGK, BCCPs, and BADCs, and false-positive interactions by proximity due to protein turnover pathways either autophagy-dependent or –independent with PII acting as a molecular glue or revealing new pathways involving PII as a fine-tuning protein. Quinary structures influence localization and interaction patterns of macromolecules resulting in a crowding effect (Wirth and Gruebele, 2013; Cohen and Pielak, 2017). This may explain the results of the MassSpec analyses of GFP-trapped samples of PII-GFP overexpressing plants, since mainly PII and PII-GFP are present in the eluate fraction (Figure 34, Table 1, and appendix: Table 24).

One possibility to address the crowding effect is to make use of fluorescence recovery after photobleaching (FRAP), as it was shown for thylakoid membrane proteins (Kirchhoff et al., 2008). This method could be used to analyse the dynamics of single protein movement or even movement of multiple proteins.

Although the regulatory function of PII on the intracellular C/N-homeostasis in plants could not be confirmed in this thesis, this question remains open. But especially the described interaction phenomena point to several putative novel functions of PII in *A. thaliana* and should be further investigated.

5 Material and Methods

5.1 Material

5.1.1 Genes

If not specified otherwise, all tested genes were deriving from *A. thaliana.* Sequences were obtained from TAIR, GenBank or Rice genome project.

PII (At4g01900), NAGK (At3g57560), BCCP1 (At5g16390), BADC2 (At1g52670), BADC3 (At3g15690.2), GBSS1 (At1g32900), DAT1 (At5g57850), RBCS3B.1 (At5g38410.1), DXR (At5g62790), DXS (At4g155609), GGPPS11 (G11) (At4g36810), OsPII (Os05g04220.1)

5.1.2 Oligonucleotides

Oligonucleotides (Primers) used during PhD thesis were synthesized by biomers.net GmbH (Ulm, Germany). Complete list of used primers see 7.1.

5.1.3 Vectors

Complete lists of vectors used during this study, see 7.2.

5.1.4 Bacterial Strains

5.1.4.1 Escherichia coli

Table 2: *Escherichia coli* strains used during thesis

Strain	Genotype	origin
NEB5α	fhuA2 a(argF-lacZ)U169 phoA glnV44 a80a(lacZ)M15 gyrA96 recA1 relA1 endA1 thi-1 hsdR17	New England Biolabs (Frankfurt am Main, Germany)
DH5α	F⁻ *endA1 glnV44 thi-1 recA1 relA1 gyrA96 deoR nupG purB20* φ80d*lacZ*ΔM15 Δ(*lacZYA-argF*)U169, hsdR17($r_K^- m_K^+$), λ⁻	Invitrogen Thermo Fisher Scientific (Carlsbad, USA)
TOP10	F- mcrA Δ(mrr-hsdRMS-mcrBC) φ80lacZΔM15 ΔlacX74 nupG recA1 araD139 Δ(ara-leu)7697 galE15 galK16 rpsL(Str^R) endA1 λ-	Invitrogen Thermo Fisher Scientific (Karlsruhe, Germany)
DB3.1	F-gyrA462 endA1 ∆(sr1-recA) mcrB mrrhsdS20(rB-, mB-) supE44 ara14 galK2 lacY1 proA2 rpsL20(Smr) xyl5 ∆leumtl1	Invitrogen Thermo Fisher Scientific (Karlsruhe, Germany)
ccdB-survival	F-mcrA Δ(mrr-hsdRMS-mcrBC) Φ80lacZΔM15 ΔlacX74 recA1 araΔ139 Δ(ara-leu)7697 galU galK rpsL (StrR) endA1 nupG fhuA::IS2	Invitrogen Thermo Fisher Scientific (Karlsruhe, Germany)

5.1.4.2 Agrobacterium tumefaciens

A. tumefaciens strain GV3101 with the genotype C58 (rif R) Ti pMP90 (pTiC58DT-DNA) (gentR) Nopaline was used for transformation of *N. benthamiana* with plant expression vectors carrying genes of interest. For obtained lines used during this study, see 7.3.

5.1.5 Plants

All *Arabidopsis thaliana* wild-type and mutant plants used in this study were ecotype Col-0. For generated lines and obtained lines used in this study, see 7.9.

Nicotiana benthamiana was used for transient transformation of leaves.

5.1.6 Kits and enzymes

5.1.6.1 Kits

Table 3: Kits used during thesis

Kit	application	source
Zymo Quick-RNA MiniPrep Kit	RNA extraction for cDNA synthesis from Col-0	Zymo Research (Irvine, USA)
RNeasy Plant Mini Kit	RNA extraction for cDNA synthesis from Col-0 and PIIS2	QIAGEN N.V. (Venlo, the Netherlands)
pENTR™/D-TOPO®	Cloning of fragments	Invitrogen, Thermo Fisher Scientific (Carlsbad, USA)
Gel extraction MiniPrep Kit	Elution of DNA fragments out of agarose-gel	Genaxxon bioscience GmbH (Ulm, Germany)
GeneJET Gel Extraction Kit	Elution of DNA fragments out of agarose-gel	Thermo Scientific™, Thermo Fisher Scientific (Waltham, USA)

5.1.6.2 Restriction enzymes

All used restriction enzymes were provided by Thermo Fisher Scientific (Karlsruhe, Germany) or New England Biolabs (Frankfurt am Main, Germany).

5.1.6.3 Special enzymes

Table 4: Special enzymes used during thesis

DNA Polymerase	application	source
NEB *Taq* DNA Polymerase	Genotyping, control PCR	New England Biolabs GmbH (Frankfurt am Main, Germany)
Phusion™ High-Fidelity DNA Polymerase	Amplification of genes of interest for cloning into pENTR, and for sequencing	Thermo Fisher Scientific (Waltham, USA)
KOD Hot Start DNA Polymerase	Amplification of genes of interest for BP reaction into pDONR221	Merck KGaA (Darmstadt, Germany)
T4 DNA Ligase	Ligation of fragments for “classical” cloning	Thermo Fisher Scientific (Waltham, USA)
RevertAid H Minus Reverse Transcriptase	cDNA synthesis	Thermo Fisher Scientific (Waltham, USA)
T4 DNA Polymerase	Generation of blunt ends for ligation using 3’-5’ exonuclease activity	Thermo Fisher Scientific (Waltham, USA)
Shrimp Alkaline Phosphatase (SAP)	Dephosphorylation of fragments for “classical” cloning	Thermo Fisher Scientific (Waltham, USA)
Gateway® BP clonase reaction mix	BP reaction	Invitrogen, Thermo Fisher Scientific (Carlsbad, USA)

Gateway® LR clonase reaction mix	LR reaction	Thermo Fisher Scientific (Waltham, USA)

5.1.7 Dyes

Table 5: Dyes used during thesis

Dye	Stock concentration	Subcellular localization	source
DAPI	1 mg/mL	Nucleus, nucleic acids	Gift from FG Müller
YO-PRO™-1 iodide	1 mM	Nucleus, nucleic acids	Thermo Fisher Scientific (Waltham, USA)

5.1.8 Antibodies

Table 6: Antibodies used during thesis

antibody	dilution	organism	company
α-GFP	1:1000	mouse	F. Hoffmann-La Roche AG (Basel, Switzerland)
α-RFP (6G6)	1:1000	mouse	ChromoTek GmbH (Planegg, Germany)
α-RFP	1:3000 – 1:7000	Rabbit	Invitrogen, Thermo Fisher Scientific (Carlsbad, USA)
α-mouse-HRP	1:10000	goat	Sigma-Aldrich (St. Louis, USA)
α-mouse-AP	1:5000	goat	Bio-Rad Laboratories, Inc. (Hercules, USA)
α-rabbit-AP	1:5000 – 1:7000	goat	Bio-Rad Laboratories, Inc. (Hercules, USA)

5.1.9 Media, buffer and solutions

If not specified otherwise, all chemicals used, were purchased from Carl Roth (Karlsruhe, Germany), Sigma-Aldrich (St. Louis, USA), AppliChem GmbH (Darmstadt, Germany) or Thermo Fisher Scientific (Waltham, USA).

5.1.9.1 Growth media

All media were autoclaved after preparation.

5.1.9.1.1 Growth media for bacteria

Lysogeny broth (LB) medium (Luria/Miller) (according to: (Bertani, 1951; Luria and Burrous, 1957; Luria et al., 1960); modified by: Miller (1972))

Sodium chloride (NaCl)	10 g/L
Tryptone	10 g/L
Yeast extract	5 g/L

Ad 1 L deionized H_2O (dH_2O).

LB agar (Luria/Miller)

NaCl	10 g/L
Tryptone	10 g/L
Yeast extract	5 g/L

Agar-Agar	15 g/L

Ad 1 L dH_2O.

Super Optimal Broth (SOB)

Bacto tryptone	20 g/L
Yeast extract	5 g/L
NaCl	0.5 g/L
Potassium chloride (KCl)	2.5 mM
2 M Mg^{2+}-stock solution	1 % (add after autoclaving)

pH 7.0 was adjusted with NaOH. Ad 1 L dH_2O.

Yeast extract broth (YEB)

Beef extract	5 g/L
Yeast extract	1 g/L
Peptone	5 g/L
Sucrose	5 g/L
$MgCl_2$	0.5 g/L

Ad 1 L dH_2O.

5.1.9.1.2 Plant growth media

Plant growth media according to Murashige and Skoog (1962).

Table 7: Murashige and Skoog media used during thesis

Plant media	V or g used for ½ MS	source
Murashige and Skoog basal salt	2.13 g/L	DUCHEFA Biochemie B.V. (Haarlem, the Netherlands)
Murashige and Skoog micronutrient solution	50 mL/L	Sigma Aldrich (Carlsbad, USA)
Murashige and Skoog nitrogen-free basal salt	0.39 g/L	bioPLUS from bioWORLD (Dublin, USA)

Used macronutrient solutions to generate ½ MS with differing N concentrations

Table 8: Macronutrient solutions used for ½ MS with differing N concentrations

component	Concentration stock	Final concentration in ½ MS		
		19.7 mM N	4.93 mM N	0 mM N
	M	mM	mM	mM
Ammonium nitrate (NH_4NO_3)	0.206	10.3	2.58	0
Potassium nitrate (KNO_3)	0.188	9.4	2.34	0
Potassium hydroxide (KOH)	0.188	---	7.06	9.4
Calcium chloride ($CaCl_2$ x 2 H_2O)	0.300	1.5	1.5	1.5
Magnesium sulfate ($MgSO_4$ x 7 H_2O)	0.150	0.750	0.750	0.750

Potassium dihydrogen phosphate (KH_2PO_4)	0.080	0.625	0.625	0.625

Optional component:

Sucrose 1 %

Additional component in solid MS media:

Phytoagar 10 g/L

pH 5.7 was adjusted with KOH. Ad 1 L dH_2O.

5.1.9.1.3 Solutions for L-AA sensitivity screens

50 mM L-Glu

L-Glu 50 mM

pH 7.0 was adjusted with KOH. Ad 1 L dH_2O before sterile filtration.

50 mM L-Gln

L-Gln 50 mM

pH 7.0 was adjusted with KOH and HCl. Ad 1 L dH_2O before sterile filtration.

50 mM L-Arg

L-Arg 50 mM

pH 7.0 was adjusted with HCl. Ad 1 L dH_2O before sterile filtration.

5.1.9.1.4 Antibiotics

Table 9: Antibiotics used during thesis

	Concentration *E. coli* (µg/mL)	**Concentration *A. tumefaciens* (µg/mL)**	**Concentration plants (µg/mL)**
Ampicillin	50	-	
Kanamycin	50	50	50
Spectinomycin	50	50-100	-
Chloramphenicol	25	-	-
Rifampicin (DMSO)	-	100	-
Gentamycin	-	40	-
Hygromycin	-	-	25

5.1.9.2 Solutions and media

If not stated otherwise, all solutions were adjusted to designated final volume with dH_2O.

5.1.9.2.1 Solutions for generation of competent cells

5.1.9.2.1.1 Solutions for generation of competent *E. coli*

2 M Mg^{2+}-stock solution

$MgCl_2$ 1 M

$MgSO_4$ 1 M

Solution was sterile filtration and stored at 4°C.

RF1

Rubidium chloride (RbCl)	100mM
Manganese chloride ($MnCl_2$)	50mM
Potassium acetate	30mM
$CaCl_2$	10mM
Glycerol	15%

pH 5.8 was adjusted with acetic acid. Solution was sterile filtration and stored at 4°C.

RF2

3-(N-morpholino)propanesulfonic acid (MOPS)	10mM
RbCl	10mM
$CaCl_2$	75mM
Glycerol	15%

pH 6,1 – 6,4 was adjusted with KOH or HCl. Solution was sterile filtration and stored at 4°C.

5.1.9.2.1.2 Solutions for generation of competent *A. tumefaciens*

150 mM $CaCl_2$ solution

$CaCl_2$	150mM

Designated final volume was adjusted with dH_2O.

20 mM $CaCl_2$ solution

$CaCl_2$	20mM

5.1.9.2.2 Solutions for work with DNA

5.1.9.2.2.1 Solutions for gDNA extraction

CTAB for gDNA extraction

TRIS, pH 8.0 with HCl	100 mM
NaCl	1.4 M
EDTA	30 mM
CTAB	2% (w/v)

Edwards buffer (Edwards et al., 1991)

TRIS, pH 7.5 with HCl	200 mM
EDTA	25 mM
NaCl	250 mM
SDS	0.5 %

5.1.9.2.2.2 Nucleotide solution

dNTPs (10 mM)

dCTP	10 mM
dATP	10 mM
dGTP	10 mM
dTTP	10 mM

5.1.9.2.2.3 Solutions for small scale plasmid preparation

Mini I

Glucose	100 mM
TRIS, pH 8.0 with HCl	50 mM
EDTA, pH 8.0	10 mM

RNase A was added to a final concentration of 10 µg/mL after autoclaving.

Mini II

Sodium hydroxide (NaOH)	0.2 M
SDS	1 %

Mini III

Potassium acetate (CH_3CO_2K)	3 M

pH was adjusted to pH 5.5 with acetic acid.

5.1.9.2.3 Solutions for chloroplast isolation

Isolation medium

Sorbitol	0.3 M
$MgCl_2$	5 mM
Ethylene glycol-bis(β-aminoethyl ether)-N,N,N′,N′-tetraacetic acid (EGTA)	5 mM
EDTA	5 mM
4-(2-hydroxyethyl)-1-piperazineethanesulfonic acid (HEPES), pH 8 with KOH	20 mM
Sodium hydrogen carbonate ($NaHCO_3$)	10 mM

Gradient mix

HEPES, pH 8 with NaOH	25 mM
EDTA	10 mM
Sorbitol	3 % (w/v)

Percoll solution

Bovine serum albumin (BSA)	1 %
Polyethylene glycol (PEG) 3350	3 %
Ficoll 400	1 %
Percoll® (Amersham biosciences, GE healthcare (Chicago, USA))	95 % (w/v)

85 % Percoll solution

Percoll solution	85 %
Gradient mix	15 %

42 % Percoll solution

Percoll solution	42 %
Gradient mix	58 %

HEPES-Sorbitol-medium

Sorbitol	0.3 M
HEPES	50 mM

5.1.9.2.4 Solutions for work with proteins

5.1.9.2.4.1 Solutions for GFP/RFP-trap

Lysis buffer

TRIS, pH 7.5 with HCl	10 mM
NaCl	150 mM
EDTA	0.5 mM
NP-40 (Igepal CA-630)	0.5 %
To 10 mL Lysis buffer:	
Complete Protease-Inhibitor	1 tablet
Phenylmethylsulfonyl fluoride (PMSF)	1 mM

Wash buffer

TRIS, pH 7.5 with HCl	10 mM
NaCl	150 mM
EDTA	0.5 mM

5.1.9.2.5 Solutions for electrophoresis

5.1.9.2.5.1 Solutions for DNA agarose gel-electrophoresis and agarose gel

50 X TAE

TRIS	2 M

Acetic acid	1 M
EDTA	50 mM
pH 8.0	

1 X TAE

TRIS	40 mM
Acetic acid	20 mM
EDTA	1 mM

1 % Agarose gel

Agarose	1 % (w/v)

1 X TAE was added to designated final volume. Gel was boiled and supplemented with 1-2 drops of 0.07 % ethidium bromide (EtBr) solution (AppliChem GmbH (Darmstadt, Germany)).

2 % Agarose gel

Agarose	2 % (w/v)

1 X TAE was added to designated final volume. Gel was boiled and supplemented with 1-2 drops of EtBr solution.

5.1.9.2.5.2 Size standards

5.1.9.2.5.2.1 DNA size standard

λ-PstI DNA marker

λ-DNA (0.3 µg/µL)	415 µL
PstI	5 µL
Orange buffer	83 µL
dH_2O	327 µL

Incubation overnight at 37 °C. After incubation, addition of:

Orange Dye	415 µL

Heat inactivation at 65 °C for 10 min. Storage at -20°C.

5.1.9.2.5.2.2 Protein size standard

Spectra™ Multicolor Broad Range Protein Ladder was used for SDS-PAGE and was purchased from Thermo Fisher Scientific.

5.1.9.2.5.3 Loading dyes for gel-electrophoresis

5.1.9.2.5.3.1 Loading dye for DNA agarose-gel-electrophoresis

Orange Dye

Glycerol	60 %

2-Amino-2-(hydroxymethyl)propane-1,3-diol (TRIS)-HCl	10 mM
Orange G	0.15 %
Ethylenediaminetetraacetic acid (EDTA)	60 mM

5.1.9.2.5.3.2 Loading dyes for protein gel-electrophoresis

2X sample buffer (according to ChromoTek manual for RFP-Trap)

TRIS, pH 6.8 with HCl	120 mM
Glycerol	20%
Sodium dodecyl sulfate (SDS)	4%
Bromophenol blue	0.04%
β-mercaptoethanol	10%

2X sample buffer containing dithiothreitol (DTT)

TRIS, pH 6.8 with HCl	100 mM
Glycerol	20%
SDS	4%
Bromophenol blue	0.2%
DTT	200 mM

Designated final volume was adjusted with dH_2O.

5.1.9.2.5.4 Solutions for SDS-Polyacrylamide gel electrophoresis (PAGE)

Bottom buffer

TRIS, pH 8.8	1 M
SDS	0.27 %

Buffer was sterile filtrated.

Upper buffer

TRIS, pH 6.8	0.25 M
SDS	0.2 %

Buffer was sterile filtrated.

Acrylamide running gel (1 gel)

Table 10: SDS-Polyacrylamide running gel compositions used during thesis

Ingredient	12.5 % acrylamide	10 % acrylamide
30% acrylamide/bis-acrylamide (37.5:1) solution	2.5 mL	2 mL
H_2O	1.2 mL	1.7 mL
Bottom buffer	2.25 mL	2.25 mL
10 % ammonium persulfate (APS)	50 µL	50 µL
Tetramethylethylenediamine (TEMED)	4 µL	4 µL

Acrylamide stacking gel (1 gel)

Table 11: SDS-Polyacrylamide stacking gel composition used during thesis

Ingredient	4.5 % acrylamide
30% acrylamide/bis-acrylamide (37.5:1) solution	0.3 mL
H_2O	0.7 mL
Upper buffer	1 mL
10 % ammonium persulfate (APS)	10 µL
Tetramethylethylenediamine (TEMED)	2 µL

10 X SDS running buffer

TRIS	250 mM
Glycine	2.5 M
SDS	1 %

1 X SDS running buffer

TRIS	25 mM
Glycine	0.25 M
SDS	0.1 %

5.1.9.2.5.5 Coomassie staining of SDS-polyacrylamide gel

Coomassie staining solution

Coomassie Brilliant Blue R-250	0.05% (w/v)
2-propanol	25 % (v/v)
Acetic acid	10 % (v/v)
dH_2O	65 % (v/v)

Coomassie destainer

Acetic acid	10 %

5.1.9.2.6 Western blot buffer and solutions

10 X Transfer buffer

TRIS. pH 8.8 with HCl	250 mM
Glycine	1.92 M

1 X Transfer buffer

TRIS	25 mM
Glycine	192 mM
Ethanol	20 %

TRIS-buffered saline (TBS)

TRIS-HCl, pH 7.5	50 mM
NaCl	150 mM

TBS-Tween

Added to TBS	
Tween-20	0.05 %

Blocking solution

Skim milk powder	5 %

Alkaline Phosphatase (AP) buffer

TRIS	12.144 g/L
NaCl	5.844 g/L
$MgCl_2$	1.0165 g/L

pH was adjusted to 9.5 with NaOH/HCl.

Nitro blue tetrazolium chloride (NBT) (5%)

NBT	5%

Solved in 70% Dimethylformamide (DMF)

5-Bromo-4-chloro-3-indolyl phosphate (BCIP) (5 %)

BCIP (5%)	5%

Solved in 100 % DMF

Detection buffer for AP

AP-buffer	10 mL
NBT (5 %)	66 µL
BCIP (5 %)	33 µL

Detection buffer of horseradish peroxidase (HRP)

Detection of HRP was performed with Amersham ECL™ Prime Western blotting detection reagent solution A (Luminol Solution) and solution B (peroxide solution) according to manufacturer's manual.

5.1.9.3 Solutions and buffer for work with plants

5.1.9.3.1 Solutions for transient infiltration of *N. benthamiana* leaves

Stock solutions for AS medium

2-morpholin-4-ylethanesulfonic acid (MES)-KOH buffer, pH 5.8	1 M in dH_2O
Magnesium chloride ($MgCl_3$)	1 M in dH_2O
4'-Hydroxy-3',5'-dimethoxyacetophenone (Acetosyringone)	150 mM in DMSO

AS medium

1M MES-KOH buffer, pH 5.8	1 % (v/v)

1M $MgCl_3$	1 % (v/v)
150 mM Acetosyringone	0.1 % (v/v)

5.1.9.3.2 Solutions for stable transformation of *A. thaliana*

AraAS medium

Sucrose	5 %
Silwett L-77	0.01 %
200 mM Acetosyringone	0.05 %
(Glucose	tip of spatula)
$MgSO_4$	tip of spatula

5.1.9.3.3 Sterilisation of *A. thaliana* seeds

5.1.9.3.3.1 Sterilisation of *A. thaliana* seeds using Ethanol

70 % Ethanol supplemented with Triton X-100

Ethanol	70 %
Triton X-100	0.05 %

5.1.9.3.3.2 Sterilisation of *A. thaliana* seeds using chloric gas

Sodium hypochlorite/ HCl solution

37 % HCl	1.5 mL
12 % Sodium hypochlorite (NaClO)	50 mL

5.1.9.3.4 Solutions and buffer for GUS staining:

Phosphate buffer for GUS-assay

Sodium hydrogen phosphate (Na_2HPO_4)	34.2 mM
Sodium dihydrogen phosphate (NaH_2PO_4)	15.8 mM
Triton X-100	0.25 %

5-Bromo-4-chloro-1*H*-indol-3-yl β-D-glucopyranosiduronic acid (X-Gluc) solution

Potassium ferrocyanide	0.5 mM
Potassium ferricyanide	0.5 mM
X-Gluc	1 mM

5.1.9.3.5 Solutions for DAPI and YO-PRO™-1 iodide staining

20 X Sodium chloride sodium citrate (SSC) solution

NaCl	3 M
Sodium citrate	300 mM

2 X SSC

NaCl	0.3 M
Sodium citrate	30 mM
pH 7.0	

2 X SSC with 4 % Formaldehyde

NaCl	0.3 M
Sodium citrate	30 mM
Formaldehyde	4 %
pH 7.0	

SSC/glycerol solution

2 X SSC	50%
Glycerol	50 %

5.1.10 Equipment

For most experiments, standard equipment of a molecular biology laboratory was used. For imaging of dark grown seedlings (Figure 5) NightShade LB 985 from Berthold Technologies GmbH & Co.KG (Bad Wildbad, Germany) was used.

5.1.11 Software

Matlab	The MathWorks Inc. (Natick, USA)

Box plots of hypocotyl and root growth, flowering time, and FLIM measurements were generated with Matlab. Script written with the help of Xuan Tran Vi Le and MathWorks forum.

Adobe Creative Suite CS6 Design Standard	Adobe Inc. (San Jóse, USA)
Adobe Acrobat Reader DC	Adobe Inc. (San Jóse, USA)
GIMP	The GIMP Developer
ImageJ	Wayne Rasband, National institute of Health
Fiji (Fiji is just ImageJ)	Schindelin et al. (2012), based on ImageJ
ZEN	Carl Zeiss Microscopy GmbH (Jena, Germany)
Leica Application Suite X (LAS X)	Leica Microsystems GmbH (Wetzlar, Germany)
Leica Application Suite AF Lite (LAS AF Lite)	Leica Microsystems GmbH (Wetzlar, Germany)

CLC Main Workbench 8	CLC bio, Qiagen (Aarhus, Denmark)
ApE (A plasmid Editor)	M. Wayne Davis

5.1.12 Internet Resources

PubMed, BLAST	National Center for Biotechnology Information (NCBI)
Information about *Arabidopsis* genes and lines	www.arabidopsis.org (TAIR)
Information about *Arabidopsis* expression profiles	Arabidopsis eFP Browser, https://bar.utoronto.ca/efp/cgi-bin/efpWeb.cgi
Information about Rice genes	http://rice.plantbiology.msu.edu/; Rice genome annotation project, Kawahara et al. (2013)
MS-Fit ProteinProspector	http://prospector.ucsf.edu
ChloroP 1.1	Emanuelsson et al. (1999)
TargetP 2.0	Almagro Armenteros et al. (2019)
Spectral information	Spectra-Viewer from Thermo Fisher Scientific (Karlsruhe, Germany)

5.1.13 Stereomicroscopy

Leica MZFLIII fluorescence stereomicroscope	Leica Microsystems GmbH (Wetzlar, Germany)

5.1.14 Laser scanning confocal microscopy

For confocal imaging, three Laser scanning confocal microscopy systems were used:

Zeiss LSM880 Airyscan	Carl Zeiss Microscopy GmbH (Jena, Germany)
Leica TCS SP2	Leica Microsystems GmbH (Wetzlar, Germany)
Leica TCS SP8	Leica Microsystems GmbH (Wetzlar, Germany)

5.2 Methods

5.2.1 Cell biological techniques

5.2.1.1 Work with *E. coli*

Growth conditions of used organisms are specified below.

5.2.1.1.1 Growth conditions for *E. coli*

E. coli was grown either in liquid LB media on a rotator or on LB agar plates containing appropriate antibiotics at 37°C overnight.

5.2.1.1.2 Generation of chemical competent *E. coli* cells

Chemical competent *E. coli* cells were generated according to protocol described in Dautel (2016) based on protocols described by Hanahan (1983); Hanahan et al. (1991).

5.2.1.1.3 Transformation of chemical competent *E. coli* cells

Transformation of chemical competent *E. coli* cells was performed with modifications according to protocol I in Sambrook et al. (1989); Froger and Hall (2007). Following modifications were applied: 950 µL LB media was used instead of 500 µL SOB or SOC media. Transformed cells were incubated at 37°C for 1 h prior to platting on LB plates.

5.2.1.2 Work with *A. tumefaciens*

5.2.1.2.1 Growth conditions for *A. tumefaciens* GV3101

A. tumefaciens was grown either in liquid LB media in a rotator at 28°C overnight or on LB agar plates containing appropriate antibiotics at 28°C for two to three days.

5.2.1.2.2 Generation of chemical competent *A. tumefaciens* GV3101 cells

Chemical competent *A. tumefaciens* GV3101 cells were generated according to protocol from Dautel (2016).

5.2.1.2.3 Transformation of chemical competent *A. tumefaciens* GV3101

Transformation of chemical competent *A. tumefaciens* GV3101 cells was performed according to protocol from Dautel (2016) with the modification that LB medium was used instead of YEB medium.

5.2.1.2.4 Glycerol stocks of transformed *A. tumefaciens* GV3101

Cryotubes (1.5 mL) were filled with 0.5 mL glycerol, before autoclaving. 0.5 mL of an overnight culture of *A. tumefaciens* GV3101 strains were pipetted into cryotube

with glycerol and were mixed. Cryotubes were closed, frozen in liquid N_2 and stored at -80°C.

5.2.1.2.5 Verification of positive transformants in *A. tumefaciens* GV3101

Single colonies were either subjected to PCR or inoculated in LB media. Inoculated LB media was placed in a rotator overnight at 28°C. Small scale plasmid preparation was performed (see section 5.2.2.3) followed by transformation in chemical competent *E. coli* cells (see section 5.2.1.1.3), and inoculation of E. coli overnight cultures of single colonies at 37°C. Small scale plasmid preparation was performed (see section 5.2.2.3) prior to restriction site analyses (see section 5.2.2.5.4), and DNA agarose gel-electrophoresis (see section 5.2.2.5.5).

5.2.1.3 Work with *A. thaliana*

5.2.1.3.1 Sterilisation of *A. thaliana* seeds

5.2.1.3.1.1 Sterilisation of *A. thaliana* seeds using chloric gas

Seeds of *A. thaliana* were filled into 1.5 mL Eppendorf tubes until maximum fill of 500 µL. Tubes were placed in desiccator with open lids. 50 mL of 12 % NaClO and 1.5 mL 37 % HCl were filled in a beaker in the desiccator. Afterwards, the lid of the desiccator was closed, and samples incubated for 3 h in chloric gas. Vents were opened, allowing gas exchange until the next day. Tubes were taken out and were closed properly the next day.

5.2.1.3.1.2 Sterilisation of *A. thaliana* seeds using Ethanol

Seeds of *A. thaliana* were filled into 1.5 mL Eppendorf tubes. 1 mL of 70% Ethanol+0.05 % Triton X-100 were added, and tubes were shaking for 20 to 30 min. Ethanol was replaced by 100% Ethanol and were shook for 8 min. Seeds were pipetted on sterile filter paper and were dried.

5.2.1.3.2 General growth conditions for *A. thaliana*

A. thaliana was grown in the green house under long day conditions (16 h/light at 18°C, 8 h/dark at 15°C, humidity: 55-60%) on T- and R-soil mixed with sand (10:10:1) according to central facility manual.

5.2.1.3.3 Stable transformation of *A. thaliana* using floral dipping

Stable transformation of *A. thaliana* was performed according to the “floral dip method” from Clough and Bent (1998). The Floral Dipping procedure was done twice within two to three days.

5.2.1.3.4 Screen for T-DNA insertions

A. thaliana seeds were sown on ½ MS plates containing appropriate antibiotics, for selection of T-DNA insertion, and were stratified for two to three days in dark at 4°C. Seedlings were grown under constant light at 22°C and were analysed by fluorescence using a stereomicroscope with UV-lamp, or by PCR using gDNA extracts (see section 5.2.2.2, 5.2.2.4).

5.2.1.3.5 Sensitivity screens

L-AA sensitivity screens were performed according to protocol described by Gördes et al. (2013) with following modifications. For L-AA sensitivity screens, one seed per well of *A. thaliana* Col-0 or *PIIS2*, was sown in 96-well microtiter plates containing 150 µL of liquid ½ MS media +/- N (according to Table 7, and Table 8) +/- L-Glu, L-Gln, and L-Arg, respectively, prior to stratification for two days at 4°C in dark. After stratification, seedlings were grown under long day conditions (16 h day/ 8 h night) at ~22°C for 14 days.

For minimal N concentration in ½ MS media, a dilution series of ½ MS+1% sucrose with self-made ½ MS-N+1% sucrose in a ratio from 1:1 from lane to lane was prepared. Lane one contained ½ MS+1% sucrose, and lane twelve ½ MS- N+1% sucrose. Sowing and germination of seeds took place as described in the preceding paragraph.

5.2.1.3.6 Hypocotyl and root growth analyses

For phenotypic analyses of *A. thaliana* Col-0 and *PIIS2*, seeds were sown on plates containing solid ½ MS media +/- N (according to Table 7, and Table 8) and +/- 1% sucrose and were stratified in darkness at 4°C. After two days, one set of plates were either placed in constant light, long day (16h light/ 8h dark), short day (8h light/ 16h dark) or darkness, respectively. For dark treatment, plates of the first approach (Figure 4) were placed in a dark chamber. For the second approach, plates were placed in NightShade LB 985 (Figure 5). First approach: light grown seedlings were scanned every day for 10 days, dark grown seedlings were marked and scanned at day 0 and 10. Second approach: light grown seedlings were scanned every day until day 5, afterwards at day 7, 8 and 10. Dark grown seedlings were imaged every day in the NightShade, and were scanned at day 0 and 10. Statistical analysis was performed using two-sided Student's t-test in Microsoft Excel and Matlab. Box plots were generated in Matlab.

5.2.1.3.7 Phenotypic analyses

For phenotypic analyses of *A. thaliana* Col-0, *PIIS2*, and overexpression lines in *PIIS2* or Col-0 background, seeds were sown on ½ MS media and were stratified in dark at 4°C. After two days, plates were placed in a long day phytochamber (16 h light at 20°C, 8 h dark at 18°C, humidity: 40%) for 11 days. Overexpression lines were screened for GFP-fluorescence using a stereomicroscope consisting of a UV-lamp. Single seedlings were pricked in pots with GS90 soil supplemented with Confidor, were covered with a hood for three days, and placed again in the long day phytochamber. Plants were marked at starting point of flowering and imaged regularly using a Canon PowerShot SX150 IS.

5.2.1.3.8 Light and temperature treatment

A. thaliana line Col-0 x *pUBQ::gAtPII-GFP* T2 10.2 was sown on ½ MS media and stratified in dark at 4°C for one night. Plates were grown for one day in constant light at 23°C. Afterwards, plates were placed in black boxes in constant light at 22°C for three days. One plate per condition was placed for temperature treatment in dark at 8°C, 23°C, and 37°C, and for light treatments in BL (23°C), GL, RL (22°C), and FRL (23°C). Each treatment was performed for 24 h. Seedlings were harvested, pre-fixed for 4 h in 2 X SSC+4% Formaldehyde, fixed by vacuum infiltration three times for 15 sec, and additionally incubated for 30 min. Seedlings were transferred to 6-well plate containing 2 X SSC and were washed over night. After overnight wash step, seedlings were washed twice with 2 X SSC for 1 h and mounted on dH_2O on object slides and were covered with cover glasses. Imaging was performed at Zeiss LSM880, see section 5.2.1.7. Growth conditions and light treatment according to Sweere et al. (2001).

5.2.1.3.9 Histochemical GUS-Assay

Histochemical GUS-assays were performed according to Martin et al. (1992) and Naleway (1992).

A. thaliana seedlings stably transformed with the GUS gene under the endogenous PII promoter or the 35S promoter were grown for 14 days under constant light at ~21°C on ½ MS media +/- N and +/- sucrose. Seedlings were harvested, were placed in 6-well plates with 3 mL X-Gluc solution and vacuum infiltrated three times for 15 sec at 300 mbar. Then these plates were taken out, closed and sealed with Parafilm. Seedlings were incubated in X-Gluc solution for 42 h at 37°C. After incubation time, X-Gluc solution was removed, and 70 % Ethanol was added to

destain the seedlings. Plates were sealed again with Parafilm and were placed at 37°C. Destaining was repeated three times. Seedlings were mounted on SSC/glycerol solution on object slides and were covered with cover slips. Seedlings were imaged with a Canon D80 camera.

5.2.1.3.10 Chloroplast isolation

Chloroplast isolation of *A. thaliana* was performed according to protocols described by Somerville et al. (1981); Bartlett et al. (1982); Meurer et al. (1996); Meurer et al. (2002).

Leaf material of *A. thaliana* was harvested in 50 mL Falcon tubes and was placed on ice. 10 mL Isolation medium was added, and leaf material was homogenised with an IKA ULTRA-TURRAX® for 1 sec on ice. Homogenised material was filtered through gauze (16 µm pore width) and was collected in a fresh 50 mL Falcon tube. Intact leaf material was collected from gauze and homogenisation steps were repeated. Falcon tubes harbouring samples were tared with Isolation medium and centrifuged at 368.9 g for 6 min at 4°C without break. Supernatant was discarded; pellet was resuspended in remaining liquid, and tube was placed on ice. Percoll gradient was prepared in 15 mL Falcon tubes consisting of 3 mL 85 % Percoll solution overlaid with 7 mL 42% Percoll solution. Resuspended pellet was pipetted on Percoll gradient and centrifuged at 1475 g for 12 min at 4°C without brake. Intact chloroplasts were pipetted carefully into fresh 15 mL Falcon tube, supplemented with Isolation medium and inverted carefully. Sample was centrifuged at 4°C at 370 g for 8 min without brake. Supernatant was discarded. Pellet was resuspended in 100 µL HEPES/Sorbitol medium and frozen in liquid N_2. Samples were stored at -80°C.

5.2.1.4 Work with *N. benthamiana*

5.2.1.4.1 Growth conditions for *N. benthamiana*

N. benthamiana plants, used for transient infiltration, were grown in the green house under long day conditions (14 h light at 23°C, 10 h dark at 20°C, humidity: 60%) on P-soil.

5.2.1.4.2 Transient transformation of *N. benthamiana* leaves with *A. tumefaciens*

Leaves of three to four week old *N. benthamiana* were transiently transformed with *A. tumefaciens* GV3101 (Koncz and Schell, 1986) carrying plasmids of interest using syringe mediated infiltration (Schöb et al., 1997; Sparkes et al., 2006). Growth

of *A. tumefaciens* and infiltration was performed according to protocol described in Hecker et al. (2015) derived from protocols of Schöb et al. (1997); Sparkes et al. (2006); Grefen et al. (2008); Blatt and Grefen (2014) with following modifications. Cells were not washed with sterile H_2O before resuspension in AS medium. Transiently transformed leaves were imaged with Leica TCS SP8 and Zeiss LSM880 Airyscan after two to three days of infiltration (see section 5.2.1.7).

5.2.1.5 DAPI staining

DAPI staining was performed modified according to Newell et al. (2012). Seedlings stably transformed with pFRET-PII-NAGK were vacuum infiltrated three times for 15 sec at 300 mbar prior to 15 min incubation.

5.2.1.6 DAPI and YO-PRO™-1 iodide staining

Modified YO-PRO™-1 iodide staining was performed according to Krupinska et al. (2014). Small leaf disks of transiently transformed leaves of *N. benthamiana* with PII-RFP+P19 or P19 (see section 5.2.1.4.2) were cut out three days after infiltration and incubated in 2 X SSC +/- RNase A (10 µg/mL), or 2 X SSC+1 X DNase I buffer + DNase I (100 U/mL), in for 4 h at 37°C. Leaf disks were vacuum infiltrated three times for 15 sec at 300 mbar in 2 X SSC+4% formaldehyde and further incubated for 15 min. Leaf disks were washed three times in 2 X SSC and stained with DAPI (1:1000)/ YO-PRO™-1 iodide (5 µg/mL) in 2 X SSC overnight. Stained leaf disks were washed 1 X with 1 X SSC, were mounted on SSC/glycerol solution on object slides and were covered with cover slips. Imaging was performed with Zeiss LSM880 Airyscan.

5.2.1.7 Confocal laser scanning microscopy

5.2.1.7.1 Imaging of fluorophores

Confocal imaging was performed with Leica TCS SP8 and Zeiss LSM880 Airyscan with a 63X/NA1.2 objective. An Argon laser was used for excitation of GFP/ YO-PRO™-1 iodide at 488 nm and YFP at 514 nm. For excitation of mCherry, RFP and Chlorophyll, a DPSS 561 nm laser was used. DAPI was excited with a 405 nm diode laser.

Emission was usually detected at following spectra:

DAPI	418-446 nm
GFP	499-544 nm
YO-PRO™-1 iodide	499-526 nm
YFP	517-553 nm

mCherry/RFP	591-618 nm
Chlorophyll	651-735 nm

Images were processed using Fiji.

5.2.1.7.2 Interaction studies

5.2.1.7.2.1 BiFC

BiFC measurements were performed with transiently transformed *N. benthamiana* leaves (see section 5.2.1.4.2) expressing 2in1 pBiFC vectors carrying genes of interest (see Table 21) three days after infiltration according to modified protocol of Grefen and Blatt (2012). Internal RFP control was not used for ratiomeric measurements but as transformation control. Images were processed using Fiji.

5.2.1.7.2.2 FRET-FLIM

FRET-FLIM measurements were performed with Leica TCS SP8 equipped with SymPhoTime software (PicoQuant GmbH (Berlin, Germany)) using transiently transformed *N. benthamiana* leaves with *A. tumefaciens* GV3101 (see section 5.2.1.4.2) carrying 2in1 pFRET vectors with C-terminally GFP-tagged PII and C-terminally mCherry-tagged known and novel interaction partners (see Table 20). FLIM measurements were performed according to Ladwig et al. (2015) and Hecker et al. (2015). FLIM measurements of two biological replicates were performed for five to six regions containing plastids in the epidermis until acquisition of 700 photons in the brightest point (Figure 31). For FastFLIM measurements using rapidFLIM two biological replicates were performed for five to six regions containing plastids in the epidermis until acquisition of 1000 photons in the brightest point (Figure 32). Statistical analyses were performed using two-sided Student's t-test in Microsoft Excel and Matlab. Box plots were generated in Matlab. Images were processed using Fiji.

5.2.2 Molecular biological techniques

5.2.2.1 RNA extraction and cDNA synthesis

5.2.2.1.1 RNA extraction

Plant leaves of wild type and mutant lines in *A. thaliana* Col-0 ecotype were frozen in liquid N_2 and shred with glass beads (Ø 2.1 mm). For the extraction the Zymo Quick-RNA MiniPrep Kit was used according to manufacturer's protocol.

5.2.2.1.2 cDNA synthesis

For cDNA synthesis of RNA extracts was performed with Oligo(dT)18 Primer (Thermo Fisher Scientific (Waltham, USA)) were applied. First strand synthesis was performed according to the first two steps of “First Strand cDNA Synthesis Protocols (E6300)” from New England Biolabs GmbH (Frankfurt am Main, Germany). Further protocol for cDNA synthesis using RevertAid H Minus Reverse Transcriptase was performed according to manufacturer’s protocol.

5.2.2.2 gDNA extraction

Genomic DNA of wild type and mutant lines in *A. thaliana* Col-0 ecotype were extracted according to protocol for gDNA extraction using Edwards buffer by Edwards et al. (1991), or using the CTAB method by Doyle and Doyle (1987).

5.2.2.3 Small scale plasmid preparation

Small scale plasmid preparation was performed according to modified alkaline lysis protocol originally derived from Bimboim and Doly (1979).

5.2.2.4 Polymerase chain reaction (PCR)

5.2.2.4.1 Amplification of fragments using polymerase chain reaction

DNA-Fragments were amplified from either cDNA or gDNA of *A. thaliana* Col-0 or mutant lines, or from vectors containing sequence of interest. For classical cloning, fragments were amplified with restriction sites of interest. PCR pipetting schemes and programs according to manufacturer’s manual of used DNA polymerases.

5.2.2.4.2 Site directed mutagenesis

Site directed mutagenesis was performed according to protocol in Heunemann (2016).

Two single PCR approaches with only primer were set up using Phusion polymerase with an annealing time at 65°C (manual see Thermo Fisher Scientific (Waltham, USA)). Each approach was set in the thermocycler for 5 cycles. Afterwards, both PCR approaches were fused and were placed back in the thermocycler for additional 15 cycles. 1 µL of *Dpn*I was added to PCR approach and was digested overnight at 37°C. 5 µL of PCR product was transformed in *E. coli* DH5α.

5.2.2.5 Cloning procedures

5.2.2.5.1 pENTR™/D-TOPO® reaction

pENTR™/D-TOPO® reaction was performed according to the pENTR™ Directional TOPO® Cloning Kits manual from Invitrogen, a Thermo Fisher Scientific brand (Carlsbad, USA), using ¼ of the designated volumes.

5.2.2.5.2 Classical cloning

5.2.2.5.2.1 Restriction digest of fragments

Fragments were either amplified before restriction digest or generated by restriction digest of vectors harbouring fragment of interest with respective restriction sites. Restriction digest was performed according to manufacturer's manual from Thermo Fisher Scientific (Waltham, USA). For pipetting scheme of restriction digest of vectors see section 5.2.2.5.4. For restriction digest of fragments generated by PCR, 5 µL of PCR product was used instead of 1 µL plasmid DNA, remaining contents see section 5.2.2.5.4.

5.2.2.5.2.2 Gel elution

Gel elution of digested fragments was performed according to manufacturer's manual for Gel extraction MiniPrep Kit from Genaxxon, or for GeneJET Gel Extraction Kit from Thermo Fisher Scientific, respectively.

5.2.2.5.2.3 Generation of blunt ends for ligation

Gel eluate fraction of fragment of interest was supplied with T4 DNA polymerase according to manufacturer's manual using the 3'-5' exonuclease activity to generate blunt ends.

5.2.2.5.2.4 Dephosphorylation of fragments

One fragment was dephosphorylated prior to ligation using Shrimp Alkaline Phosphatase according to manufacturer's manual from Thermo Fisher Scientific (Waltham, USA).

5.2.2.5.2.5 Ligation

Fragments were ligated with T4 DNA ligase in an insert to vector ratio of 5:1 for up to three days at 16°C according to manufacturer's manual from Thermo Fisher Scientific (Waltham, USA), prior to transformation of 5 µL into *E. coli*.

5.2.2.5.3 Gateway® cloning

Gateway® cloning was performed according to the Gateway® Technology manual from Invitrogen, a Thermo Fisher Scientific brand (Carlsbad, USA).

5.2.2.5.3.1 Amplification of attB-sites

Primer containing designated attB-sites with flanking 18 bp of gene of interest were ordered from biomers.net GmbH (Ulm, Germany). Amplification of attB-site containing fragments was performed according to manufacturer's manual for KOD Hot Start DNA Polymerase, from Novagen®, trademark of Merck KGaA (Darmstadt, Germany).

5.2.2.5.3.2 BP reaction

Gateway® BP reaction performed according to the Gateway® Technology manual from Invitrogen, a Thermo Fisher Scientific brand (Carlsbad, USA), using ¼ of the designated volumes, and dH_2O instead of TE.

5.2.2.5.3.3 LR reaction

Gateway® BP reaction performed according to the Gateway® Technology manual from Invitrogen, a Thermo Fisher Scientific brand (Carlsbad, USA), using ¼ of the designated volumes, and dH_2O instead of TE.

5.2.2.5.3.4 Multisite LR reaction

Multisite LR reaction was performed for FRET-FLIM and BiFC constructs according to Grefen and Blatt (2012).

5.2.2.5.4 Restriction site analyses

Restriction site analyses according to manufacturer's manual from Thermo Fisher Scientific (Waltham, USA) and New England Biolabs GmbH.

5.2.2.5.5 DNA agarose gel-electrophoresis

DNA agarose gel-electrophoresis was performed according to Sambrook et al. (1989).

5.2.2.6 Plant protein purification

Plant material was harvested in 2-mL Eppendorf tubes with six glass beads (Ø 2.1 mm) and frozen in liquid N_2 before storage at -80°C. Frozen samples were shredded using the universal mixer Silamat® S6.

5.2.2.6.1 GFP/RFP-trap

GFP/RFP-trap was performed with ChromoTek GFP-Trap® Magnetic Agarose or RFP-Trap® Magnetic Agarose according to manufacturer's manual with following modifications. Shredded frozen plant material was supplemented with 1 mL Lysis buffer, was mixed and was incubated on ice for 1 h. Lysate was centrifuged at 16100 g for 10 min at 4°C. 1 mL of supernatant was transferred to equilibrated magnetic

agarose beads. Sample of each fraction was supplemented with 2X sample buffer and was boiled at 65°C for 15 min.

5.2.2.6.2 SDS-PAGE

SDS-PAGE was performed according to Laemmli (1970). SDS-Polyacrylamide gel was stained with Coomassie staining overnight and was destained with Destainer solution until gel background showed no blue colour.

5.2.2.6.3 Western blot using PVDF membranes

Western blot was performed with wet blot analyses using PVDF membranes based on protocol by Towbin et al. (1979).

Detection was performed either with detection buffer for AP or for HRP. For detection of AP, detection buffer of AP was mixed, was spilled on membrane and was incubated in dark until bands were visible. Reaction was stopped after washing the membrane 2-3 times with H_2O. For detection of HRP, Amersham ECL™ Prime Western blotting detection reagent solution A (Luminol Solution) and solution B (peroxide solution) were mixed according to manufacturer's manual. Membrane was placed in a bag and was floated with detection buffer. Membrane was placed in chemiluminescence detection chamber and was excited until signal was detectable.

5.2.2.6.4 MassSpec analyses

MassSpec analyses was performed by Dr. Edda von Roepenack-Lahaye (ZMBP Central facilities, University of Tübingen) with single bands of sizes of interest according to size of known and putative new interaction partners (see 7.17) in eluate fractions cut out from SDS-Polyacrylamide gel after Coomassie staining.

Single bands were crumbled using a 1000 µL tip and was washed once for 15 min with 300 µL 5 mM ammonium bicarbonate (ABC) buffer in 50 % acetonitrile in an ultra-sonic bath. Afterwards, sample was washed once for 10 min in 300 µL acetonitrile. To reduce disulphide (S-S) bridges, sample was supplemented with 100 µL 20 mM ABC buffer + 10 mM DTT for 45 min at 56°C. To alkylate the thiol (-SH) groups, first, DTT was removed by addition of 100 µL 55 mM iodoacetamide in 20 mM ABC buffer for 30 min at RT in dark. Sample was washed with 300 µL 5 mM ABC buffer in 50% acetonitrile for 15 min in an ultra-sonic bath and further with 300 µL acetonitrile for 10 min.

Digestion of pelleted samples was performed with 13 µL 0.02 µg/µL trypsin in 40 mM ABC buffer in 9% acetonitrile until gel crumbles were swollen. 12 µL 40 mM

ABC buffer in 9% acetonitrile was added and samples were placed at 37°C overnight. Samples were cooled down in the fridge the next morning, were centrifuged and were transferred to LCMS-inserts. 15 µL of 50 % acetonitrile with 0.1 % formaldehyde and 3.6 µM Leu-enkephalin were added to remaining pellet crumbles, were incubated in the ultra-sonic bath for 5 min, were centrifuged and transferred to LCMS-inserts harbouring the remaining sample. LC-MS of samples was performed with ESI-Q-TOF tune-file metabolomics positive mode, inlet proteomics and MS proteomics, with water files in between the digest samples.
Dr. Edda von Roepenack-Lahaye performed analysis of MS-data. Masses detected by MS were analysed further with MS-Fit ProteinProspector (http://prospector.ucsf.ed) using SwissProt.2017.11.01 database according to Jiménez et al. (1998).

6 References

Adler SP, Purich D, Stadtman ER (1975) Cascade control of Escherichia coli glutamine synthetase. Properties of the PII regulatory protein and the uridylyltransferase-uridylyl-removing enzyme. Journal of Biological Chemistry **250:** 6264-6272

Allen JF, Bennett J, Steinback KE, Arntzen CJ (1981) Chloroplast protein phosphorylation couples plastoquinone redox state to distribution of excitation energy between photosystems. Nature **291:** 25-29

Almagro Armenteros JJ, Salvatore M, Emanuelsson O, Winther O, von Heijne G, Elofsson A, Nielsen H (2019) Detecting sequence signals in targeting peptides using deep learning. Life Science Alliance **2:** e201900429

Anderson WB, Hennig SB, Ginsburg A, Stadtman ER (1970) Association of ATP: Glutamine Synthetase Adenylyltransferase Activity with the PI Component of the Glutamine Synthetase Deadenylylation System. Proceedings of the National Academy of Sciences **67:** 1417

Arcondéguy T, Jack R, Merrick M (2001) PII Signal Transduction Proteins, Pivotal Players in Microbial Nitrogen Control. Microbiology and Molecular Biology Reviews **65:** 80

Atkinson MR, Kamberov ES, Weiss RL, Ninfa AJ (1994) Reversible uridylylation of the Escherichia coli PII signal transduction protein regulates its ability to stimulate the dephosphorylation of the transcription factor nitrogen regulator I (NRI or NtrC). Journal of Biological Chemistry **269:** 28288-28293

Ball SG, van de Wal MHBJ, Visser RGF (1998) Progress in understanding the biosynthesis of amylose. Trends in Plant Science **3:** 462-467

Bartlett SG, Grossman AR, Chua NH (1982) In vitro synthesis and uptake of cytoplasmically-synthesized chloroplast proteins. Methods in chloroplast molecular biology

Baud S, Feria Bourrellier AB, Azzopardi M, Berger A, Dechorgnat J, Daniel-Vedele F, Lepiniec L, Miquel M, Rochat C, Hodges M, Ferrario-Mery S (2010) PII is induced by WRINKLED1 and fine-tunes fatty acid composition in seeds of Arabidopsis thaliana. Plant J **64:** 291-303

Beez S, Fokina O, Herrmann C, Forchhammer K (2009) N-acetyl-L-glutamate kinase (NAGK) from oxygenic phototrophs: P(II) signal transduction across domains of life reveals novel insights in NAGK control. J Mol Biol **389:** 748-758

Bertani G (1951) Studies on lysogenesis. I. The mode of phage liberation by lysogenic Escherichia coli. Journal of bacteriology **62:** 293-300

Bimboim HC, Doly J (1979) A rapid alkaline extraction procedure for screening recombinant plasmid DNA. Nucleic Acids Research **7:** 1513-1523

Blatt MR, Grefen C (2014) Applications of Fluorescent Marker Proteins in Plant Cell Biology. *In* JJ Sanchez-Serrano, J Salinas, eds, Arabidopsis Protocols. Humana Press, Totowa, NJ, pp 487-507

Bleckmann A, Weidtkamp-Peters S, Seidel CA, Simon R (2010) Stem cell signaling in Arabidopsis requires CRN to localize CLV2 to the plasma membrane. Plant Physiol **152:** 166-176

Bracher A, Whitney SM, Hartl FU, Hayer-Hartl M (2017) Biogenesis and Metabolic Maintenance of Rubisco. Annual Review of Plant Biology **68:** 29-60

Brown MS, Segal A, Stadtman ER (1971) Modulation of Glutamine Synthetase Adenylylation and Deadenylylation Is Mediated by Metabolic Transformation of the PII-Regulatory Protein. Proceedings of the National Academy of Sciences **68:** 2949

Bücherl CA, Bader A, Westphal AH, Laptenok SP, Borst JW (2014) FRET-FLIM applications in plant systems. Protoplasma **251:** 383-394

Bueno R, Pahel G, Magasanik B (1985) Role of glnB and glnD gene products in regulation of the glnALG operon of Escherichia coli. Journal of Bacteriology **164:** 816-822

Burillo S, Luque I, Fuentes I, Contreras A (2004) Interactions between the nitrogen signal transduction protein PII and N-acetyl glutamate kinase in organisms that perform oxygenic photosynthesis. J Bacteriol **186:** 3346-3354

Caldovic L, Tuchman M (2003) N-Acetylglutamate and its changing role through evolution. Biochemical Journal **372:** 279-290

Carr PD, Cheah E, Suffolk PM, Vasudevan SG, Dixon NE, Ollis DL (1996) X-ray structure of the signal transduction protein from Escherichia coli at 1.9 A. Acta Crystallographica Section D **52:** 93-104

Chellamuthu VR, Alva V, Forchhammer K (2013) From cyanobacteria to plants: conservation of PII functions during plastid evolution. Planta **237:** 451-462

Chellamuthu VR, Ermilova E, Lapina T, Luddecke J, Minaeva E, Herrmann C, Hartmann MD, Forchhammer K (2014) A widespread glutamine-sensing mechanism in the plant kingdom. Cell **159:** 1188-1199

Chen YM, Ferrar TS, Lohmeier-Vogel EM, Morrice N, Mizuno Y, Berenger B, Ng KK, Muench DG, Moorhead GB (2006) The PII signal transduction protein of Arabidopsis thaliana forms an arginine-regulated complex with plastid N-acetyl glutamate kinase. J Biol Chem **281:** 5726-5733

Chiba A, Ishida H, Nishizawa NK, Makino A, Mae T (2003) Exclusion of ribulose-1,5-bisphosphate carboxylase/oxygenase from chloroplasts by specific bodies in naturally senescing leaves of wheat. Plant and Cell Physiology **44:** 914-921

Clough SJ, Bent AF (1998) Floral dip: a simplified method for Agrobacterium - mediated transformation of Arabidopsis thaliana. The Plant Journal **16:** 735-743

Cohen RD, Pielak GJ (2017) A cell is more than the sum of its (dilute) parts: A brief history of quinary structure. Protein Science **26:** 403-413

Commichau FM, Forchhammer K, Stülke J (2006) Regulatory links between carbon and nitrogen metabolism. Current Opinion in Microbiology **9:** 167-172

Contento AL, Xiong Y, Bassham DC (2005) Visualization of autophagy in Arabidopsis using the fluorescent dye monodansylcadaverine and a GFP-AtATG8e fusion protein. Plant J **42:** 598-608

Cunin R, Glansdorff N, Piérard A, Stalon V (1986) Biosynthesis and metabolism of arginine in bacteria. Microbiological reviews **50:** 314-352

Curtis MD, Grossniklaus U (2003) A Gateway Cloning Vector Set for High-Throughput Functional Analysis of Genes in Planta. Plant Physiology **133:** 462-469

D'Apuzzo E, Valkov VT, Parlati A, Omrane S, Barbulova A, Sainz MM, Lentini M, Esposito S, Rogato A, Chiurazzi M (2015) PII Overexpression in Lotus japonicus Affects Nodule Activity in Permissive Low-Nitrogen Conditions and Increases Nodule Numbers in High Nitrogen Treated Plants. Mol Plant Microbe Interact **28:** 432-442

da Rocha RA, Weschenfelder TA, de Castilhos F, de Souza EM, Huergo LF, Mitchell DA (2013) Mathematical Model of the Binding of Allosteric Effectors to the Escherichia coli PII Signal Transduction Protein GlnB. Biochemistry **52:** 2683-2693

Dai G-Z, Qiu B-S, Forchhammer K (2014) Ammonium tolerance in the cyanobacterium Synechocystis sp. strain PCC 6803 and the role of the psbA multigene family. Plant, Cell & Environment **37:** 840-851

Dautel R (2016) MOLECULAR CHARACTERIZATION OF THE ARABIDOPSIS THALIANA HISTIDINE KINASE 1 AND TRANSITIONS FROM THE MULTISTEP PHOSPHORELAY SYSTEM TO SER/THR/TYR PHOSPHORYLATION. Dissertation. Eberhard Karls Universität Tübingen

de Mel VSJ, Kamberov ES, Martin PD, Zhang J, Ninfa AJ, Edwards BFP (1994) Preliminary X-ray diffraction analysis of crystals of the PII protein from Escherichia coli. Journal of Molecular Biology **243:** 796-798

Dedonder A, Rethy R, Fredericq H, Van Montagu M, Krebbers E (1993) Arabidopsis rbcS Genes Are Differentially Regulated by Light. Plant Physiology **101:** 801

Doyle JJ, Doyle JL (1987) A rapid DNA isolation procedure for small quantities of fresh leaf tissue. PHYTOCHEMICAL BULLETIN **19:** 11-15

Drath M, Kloft N, Batschauer A, Marin K, Novak J, Forchhammer K (2008) Ammonia Triggers Photodamage of Photosystem II in the Cyanobacterium Synechocystis sp. Strain PCC 6803. Plant Physiology **147:** 206-215

Edwards K, Johnstone C, Thompson C (1991) A simple and rapid method for the preparation of plant genomic DNA for PCR analysis. Nucleic acids research **19:** 1349-1349

Emanuelsson O, Nielsen H, Brunak S, von Heijne G (2000) Predicting subcellular localization of proteins based on their N-terminal amino acid sequence. J Mol Biol **300:** 1005-1016

Emanuelsson O, Nielsen H, Heijne GV (1999) ChloroP, a neural network-based method for predicting chloroplast transit peptides and their cleavage sites. Protein Science **8:** 978-984

Engleman EG, Francis SH (1978) Cascade control of E. coli glutamine synthetase: II. Metabolite regulation of the enzymes in the cascade. Archives of Biochemistry and Biophysics **191:** 602-612

Ermilova E, Lapina T, Zalutskaya Z, Minaeva E, Fokina O, Forchhammer K (2013) PII Signal Transduction Protein in Chlamydomonas reinhardtii: Localization and Expression Pattern. Protist **164:** 49-59

Espinosa J, Forchhammer K, Burillo S, Contreras A (2006) Interaction network in cyanobacterial nitrogen regulation: PipX, a protein that interacts in a 2-oxoglutarate dependent manner with PII and NtcA. Mol Microbiol **61:** 457-469

Espinosa J, Forchhammer K, Contreras A (2007) Role of the Synechococcus PCC 7942 nitrogen regulator protein PipX in NtcA-controlled processes. Microbiology **153:** 711-718

Espinosa J, Labella JI, Cantos R, Contreras A (2018) Energy drives the dynamic localization of cyanobacterial nitrogen regulators during diurnal cycles. Environ Microbiol **20:** 1240-1252

Feria Bourrellier AB, Ferrario-Mery S, Vidal J, Hodges M (2009) Metabolite regulation of the interaction between Arabidopsis thaliana PII and N-acetyl-l-glutamate kinase. Biochem Biophys Res Commun **387:** 700-704

Feria Bourrellier AB, Valot B, Guillot A, Ambard-Bretteville F, Vidal J, Hodges M (2010) Chloroplast acetyl-CoA carboxylase activity is 2-oxoglutarate-regulated by interaction of PII with the biotin carboxyl carrier subunit. Proc Natl Acad Sci U S A **107:** 502-507

Ferrario-Mery S, Besin E, Pichon O, Meyer C, Hodges M (2006) The regulatory PII protein controls arginine biosynthesis in Arabidopsis. FEBS Lett **580:** 2015-2020

Ferrario-Mery S, Bouvet M, Leleu O, Savino G, Hodges M, Meyer C (2005) Physiological characterisation of Arabidopsis mutants affected in the expression of the putative regulatory protein PII. Planta **223:** 28-39

Ferrario-Mery S, Meyer C, Hodges M (2008) Chloroplast nitrite uptake is enhanced in Arabidopsis PII mutants. FEBS Lett **582:** 1061-1066

Fokina O, Chellamuthu V-R, Forchhammer K, Zeth K (2010) Mechanism of 2-oxoglutarate signaling by the Synechococcus elongatus PII signal transduction protein. Proceedings of the National Academy of Sciences **107:** 19760-19765

Forchhammer K (2004) Global carbon/nitrogen control by PII signal transduction in cyanobacteria: from signals to targets. FEMS Microbiology Reviews **28:** 319-333

Forchhammer K (2008) P(II) signal transducers: novel functional and structural insights. Trends Microbiol **16:** 65-72

Forchhammer K, Hedler A, Strobel H, Weiss V (1999) Heterotrimerization of PII-like signalling proteins: implications for PII-mediated signal transduction systems. Molecular Microbiology **33:** 338-349

Forchhammer K, Selim KA (2019) Carbon/nitrogen homeostasis control in cyanobacteria. FEMS Microbiology Reviews

Forchhammer K, Tandeau de Marsac N (1994) The PII protein in the cyanobacterium Synechococcus sp. strain PCC 7942 is modified by serine phosphorylation and signals the cellular N-status. Journal of Bacteriology **176:** 84

Forchhammer K, Tandeau de Marsac N (1995) Phosphorylation of the PII protein (glnB gene product) in the cyanobacterium Synechococcus sp. strain PCC 7942: analysis of in vitro kinase activity. Journal of Bacteriology **177:** 5812

Forchhammer K, Tandeau de Marsac N (1995a) Functional analysis of the phosphoprotein PII (glnB gene product) in the cyanobacterium Synechococcus sp. strain PCC 7942. Journal of Bacteriology **177:** 2033-2040

Forster T (1946) Energiewanderung und Fluoreszenz. Naturwissenschaften **33:** 166-175

Francis SH, Engleman EG (1978) Cascade control of E. coli glutamine synthetase: I. Studies on the uridylyl transferase and uridylyl removing enzyme(s) from E. coli. Archives of Biochemistry and Biophysics **191:** 590-601

Froger A, Hall JE (2007) Transformation of plasmid DNA into E. coli using the heat shock method. J Vis Exp**:** 253

Garcia E, Rhee SG (1983) Cascade control of Escherichia coli glutamine synthetase. Purification and properties of PII uridylyltransferase and uridylyl-removing enzyme. Journal of Biological Chemistry **258:** 2246-2253

Gerhardt EC, Rodrigues TE, Muller-Santos M, Pedrosa FO, Souza EM, Forchhammer K, Huergo LF (2015) The bacterial signal transduction protein GlnB regulates the committed step in fatty acid biosynthesis by acting as a dissociable regulatory subunit of acetyl-CoA carboxylase. Mol Microbiol **95:** 1025-1035

Giner-Lamia J, Robles-Rengel R, Hernández-Prieto MA, Muro-Pastor MI, Florencio FJ, Futschik ME (2017) Identification of the direct regulon of NtcA during early acclimation to nitrogen starvation in the cyanobacterium Synechocystis sp. PCC 6803. Nucleic Acids Research **45:** 11800-11820

Gördes D, Koch G, Thurow K, Kolukisaoglu Ü (2013) Analyses of Arabidopsis ecotypes reveal metabolic diversity to convert D-amino acids. SpringerPlus **2:** 559

Grefen C, Blatt MR (2012) A 2in1 cloning system enables ratiometric bimolecular fluorescence complementation (rBiFC). Biotechniques **53:** 311-314

Grefen C, Städele K, Růžička K, Obrdlik P, Harter K, Horák J (2008) Subcellular Localization and In Vivo Interactions of the Arabidopsis thaliana Ethylene Receptor Family Members. Molecular Plant **1:** 308-320

Gutscher M, Pauleau A-L, Marty L, Brach T, Wabnitz GH, Samstag Y, Meyer AJ, Dick TP (2008) Real-time imaging of the intracellular glutathione redox potential. Nature Methods **5:** 553-559

Hafren A, Ustun S, Hochmuth A, Svenning S, Johansen T, Hofius D (2018) Turnip Mosaic Virus Counteracts Selective Autophagy of the Viral Silencing Suppressor HCpro. Plant Physiol **176:** 649-662

Hanahan D (1983) Studies on transformation of Escherichia coli with plasmids. Journal of Molecular Biology **166:** 557-580

Hanahan D, Jessee J, Bloom FR (1991) [4] Plasmid transformation of Escherichia coli and other bacteria. *In* Methods in Enzymology, Vol 204. Academic Press, pp 63-113

Harrison MA, Keen JN, Findlay JBC, Allen JF (1990) Modification of a gInB-like gene product by photosynthetic electron transport in the cyanobacterium Synechococcus 6301. FEBS Letters **264:** 25-28

Harter K, Meixner AJ, Schleifenbaum F (2012) Spectro-Microscopy of Living Plant Cells. Molecular Plant **5:** 14-26

Hauf W, Schmid K, Gerhardt ECM, Huergo LF, Forchhammer K (2016) Interaction of the Nitrogen Regulatory Protein GlnB (PII) with Biotin Carboxyl Carrier Protein (BCCP) Controls Acetyl-CoA Levels in the Cyanobacterium Synechocystis sp. PCC 6803. Frontiers in Microbiology **7**

Hecker A, Wallmeroth N, Peter S, Blatt MR, Harter K, Grefen C (2015) Binary 2in1 Vectors Improve in Planta (Co)localization and Dynamic Protein Interaction Studies. Plant Physiol **168:** 776-787

Heinrich A, Maheswaran M, Ruppert U, Forchhammer K (2004) The Synechococcus elongatus PII signal transduction protein controls arginine synthesis by complex formation with N-acetyl-l-glutamate kinase. Molecular Microbiology **52:** 1303-1314

Heunemann M (2016) H_2O_2-Perzeption und Signaltransduktion: Funktionelle und strukturelle Charakterisierung der Arabidopsis Histidinkinase 5 (AHK5). Dissertation. Eberhard Karls Universität Tübingen

Hisbergues M, Jeanjean R, Joset F, Tandeau de Marsac N, Bédu S (1999) Protein PII regulates both inorganic carbon and nitrate uptake and is modified by a redox signal in Synechocystis PCC 6803. FEBS Letters **463:** 216-220

Hsieh MH, Lam HM, van de Loo FJ, Coruzzi G (1998) A PII-like protein in Arabidopsis: putative role in nitrogen sensing. Proc Natl Acad Sci U S A **95:** 13965-13970

Hu C-D, Chinenov Y, Kerppola TK (2002) Visualization of Interactions among bZIP and Rel Family Proteins in Living Cells Using Bimolecular Fluorescence Complementation. Molecular Cell **9:** 789-798

Huang J, Chen D, Yan H, Xie F, Yu Y, Zhang L, Sun M, Peng X (2017) Acetylglutamate kinase is required for both gametophyte function and embryo development in Arabidopsis thaliana. Journal of Integrative Plant Biology **59:** 642-656

Huergo LF, Chandra G, Merrick M (2013) PII signal transduction proteins: nitrogen regulation and beyond. FEMS Microbiology Reviews **37:** 251-283

Irmler A, Sanner S, Dierks H, Forchhammer K (1997) Dephosphorylation of the phosphoprotein PII in Synechococcus PCC 7942: identification of an ATP and 2-oxoglutarate-regulated phosphatase activity. Molecular Microbiology **26:** 81-90

Ishida H, Yoshimoto K, Izumi M, Reisen D, Yano Y, Makino A, Ohsumi Y, Hanson MR, Mae T (2008) Mobilization of rubisco and stroma-localized fluorescent

proteins of chloroplasts to the vacuole by an ATG gene-dependent autophagic process. Plant Physiol **148:** 142-155

Ishikawa-Ankerhold HC, Ankerhold R, Drummen GPC (2012) Advanced Fluorescence Microscopy Techniques—FRAP, FLIP, FLAP, FRET and FLIM. Molecules **17:** 4047-4132

Izumi M, Wada S, Makino A, Ishida H (2010) The autophagic degradation of chloroplasts via rubisco-containing bodies is specifically linked to leaf carbon status but not nitrogen status in Arabidopsis. Plant Physiol **154:** 1196-1209

Jiang P, Ninfa AJ (2009) Sensation and Signaling of α-Ketoglutarate and Adenylylate Energy Charge by the Escherichia coli PII Signal Transduction Protein Require Cooperation of the Three Ligand-Binding Sites within the PII Trimer. Biochemistry **48:** 11522-11531

Jiang P, Zucker P, Atkinson MR, Kamberov ES, Tirasophon W, Chandran P, Schefke BR, Ninfa AJ (1997) Structure/function analysis of the PII signal transduction protein of Escherichia coli: genetic separation of interactions with protein receptors. Journal of Bacteriology **179:** 4342-4353

Jiang P, Zucker P, Ninfa AJ (1997) Probing interactions of the homotrimeric PII signal transduction protein with its receptors by use of PII heterotrimers formed in vitro from wild-type and mutant subunits. Journal of Bacteriology **179:** 4354-4360

Jiménez CR, Huang L, Qiu Y, Burlingame AL (1998) Searching Sequence Databases Over the Internet: Protein Identification Using MS-Fit. Current Protocols in Protein Science **14:** 16.15.11-16.15.16

Kamberov ES, Atkinson MR, Feng J, Chandran P, Ninfa AJ (1994) Sensory components controlling bacterial nitrogen assimilation. Cell Mol Biol Res **40:** 175-191

Kamberov ES, Atkinson MR, Ninfa AJ (1995) The Escherichia coli PII Signal Transduction Protein Is Activated upon Binding 2-Ketoglutarate and ATP. Journal of Biological Chemistry **270:** 17797-17807

Karimi M, Inzé D, Depicker A (2002) GATEWAY™ vectors for Agrobacterium-mediated plant transformation. Trends in Plant Science **7:** 193-195

Kawahara Y, de la Bastide M, Hamilton JP, Kanamori H, McCombie WR, Ouyang S, Schwartz DC, Tanaka T, Wu J, Zhou S, Childs KL, Davidson RM, Lin H, Quesada-Ocampo L, Vaillancourt B, Sakai H, Lee SS, Kim J, Numa H, Itoh T, Buell CR, Matsumoto T (2013) Improvement of the Oryza sativa Nipponbare reference genome using next generation sequence and optical map data. Rice **6:** 4

Keereetaweep J, Liu H, Zhai Z, Shanklin J (2018) Biotin Attachment Domain-Containing Proteins Irreversibly Inhibit Acetyl CoA Carboxylase. Plant Physiol **177:** 208-215

Kirchhoff H, Haferkamp S, Allen JF, Epstein DBA, Mullineaux CW (2008) Protein Diffusion and Macromolecular Crowding in Thylakoid Membranes. Plant Physiology **146:** 1571-1578

Kloft N, Rasch G, Forchhammer K (2005) Protein phosphatase PphA from Synechocystis sp. PCC 6803: the physiological framework of PII-P dephosphorylation. Microbiology **151:** 1275-1283

Koncz C, Schell J (1986) The promoter of TL-DNA gene 5 controls the tissue-specific expression of chimaeric genes carried by a novel type of Agrobacterium binary vector. Molecular and General Genetics MGG **204:** 383-396

Krebbers E, Seurinck J, Herdies L, Cashmore AR, Timko MP (1988) Four genes in two diverged subfamilies encode the ribulose-1,5-bisphosphate carboxylase

small subunit polypeptides of Arabidopsis thaliana. Plant Molecular Biology **11:** 745-759

Krupinska K, Oetke S, Desel C, Mulisch M, Schafer A, Hollmann J, Kumlehn J, Hensel G (2014) WHIRLY1 is a major organizer of chloroplast nucleoids. Front Plant Sci **5:** 432

Ladwig F, Dahlke RI, Stührwohldt N, Hartmann J, Harter K, Sauter M (2015) Phytosulfokine Regulates Growth in Arabidopsis through a Response Module at the Plasma Membrane That Includes CYCLIC NUCLEOTIDE-GATED CHANNEL17, H+-ATPase, and BAK1. The Plant Cell **27:** 1718-1729

Laemmli UK (1970) Cleavage of Structural Proteins during the Assembly of the Head of Bacteriophage T4. Nature **227:** 680-685

Lapina T, Selim KA, Forchhammer K, Ermilova E (2018) The PII signaling protein from red algae represents an evolutionary link between cyanobacterial and Chloroplastida PII proteins. Scientific Reports **8:** 790

Laptenok SP, Snellenburg JJ, Bücherl CA, Konrad KR, Borst JW (2014) Global Analysis of FRET–FLIM Data in Live Plant Cells. *In* Y Engelborghs, AJWG Visser, eds, Fluorescence Spectroscopy and Microscopy: Methods and Protocols. Humana Press, Totowa, NJ, pp 481-502

Leigh JA, Dodsworth JA (2007) Nitrogen Regulation in Bacteria and Archaea. Annual Review of Microbiology **61:** 349-377

Li X, Ilarslan H, Brachova L, Qian HR, Li L, Che P, Wurtele ES, Nikolau BJ (2011) Reverse-genetic analysis of the two biotin-containing subunit genes of the heteromeric acetyl-coenzyme A carboxylase in Arabidopsis indicates a unidirectional functional redundancy. Plant Physiol **155:** 293-314

Li Y, Liu W, Sun L-P, Zhou Z-G (2017) Evidence for PII with NAGK interaction that regulates Arg synthesis in the microalga Myrmecia incisa in response to nitrogen starvation. Scientific reports **7:** 16291-16291

Liu J, Magasanik B (1993) The glnB region of the Escherichia coli chromosome. Journal of Bacteriology **175:** 7441-7449

Llácer JL, Contreras A, Forchhammer K, Marco-Marín C, Gil-Ortiz F, Maldonado R, Fita I, Rubio V (2007) The crystal structure of the complex of PII and acetylglutamate kinase reveals how PII controls the storage of nitrogen as arginine. Proceedings of the National Academy of Sciences **104:** 17644

Llácer JL, Espinosa J, Castells MA, Contreras A, Forchhammer K, Rubio V (2010) Structural basis for the regulation of NtcA-dependent transcription by proteins PipX and PII. Proceedings of the National Academy of Sciences **107:** 15397-15402

Luddecke J, Forchhammer K (2015) Energy Sensing versus 2-Oxoglutarate Dependent ATPase Switch in the Control of Synechococcus PII Interaction with Its Targets NAGK and PipX. PLoS One **10:** e0137114

Lundquist PK, Poliakov A, Bhuiyan NH, Zybailov B, Sun Q, van Wijk KJ (2012) The Functional Network of the Arabidopsis Plastoglobule Proteome Based on Quantitative Proteomics and Genome-Wide Coexpression Analysis. Plant Physiology **158:** 1172-1192

Luria SE, Adams JN, Ting RC (1960) Transduction of lactose-utilizing ability among strains of E. coli and S. dysenteriae and the properties of the transducing phage particles. Virology **12:** 348-390

Luria SE, Burrous JW (1957) Hybridization between Escherichia coli and Shigella. Journal of bacteriology **74:** 461-476

Maheswaran M, Urbanke C, Forchhammer K (2004) Complex Formation and Catalytic Activation by the PII Signaling Protein of N-Acetyl-l-glutamate Kinase

from Synechococcus elongatus Strain PCC 7942. Journal of Biological Chemistry **279:** 55202-55210

Mangum JH, Magni G, Stadtman ER (1973) Regulation of glutamine synthetase adenylylation and deadenylylation by the enzymatic uridylylation and deuridylylation of the PII regulatory protein. Archives of Biochemistry and Biophysics **158:** 514-525

Martin T, Wöhner R-V, Hummel S, Willmitzer L, Frommer WB (1992) 2 - The GUS Reporter System as a Tool to Study Plant Gene Expression. *In* SR Gallagher, ed, Gus Protocols. Academic Press, San Diego, pp 23-43

McNeill LA, Bethge L, Hewitson KS, Schofield CJ (2005) A fluorescence-based assay for 2-oxoglutarate-dependent oxygenases. Analytical Biochemistry **336:** 125-131

Meurer J, Berger A, Westhoff P (1996) A nuclear mutant of Arabidopsis with impaired stability on distinct transcripts of the plastid psbB, psbD/C, ndhH, and ndhC operons. The Plant Cell **8:** 1193-1207

Meurer J, Lezhneva L, Amann K, Gödel M, Bezhani S, Sherameti I, Oelmüller R (2002) A Peptide Chain Release Factor 2 Affects the Stability of UGA-Containing Transcripts in Arabidopsis Chloroplasts. The Plant Cell **14:** 3255-3269

Meyer AJ, Brach T, Marty L, Kreye S, Rouhier N, Jacquot J-P, Hell R (2007) Redox-sensitive GFP in Arabidopsis thaliana is a quantitative biosensor for the redox potential of the cellular glutathione redox buffer. The Plant Journal **52:** 973-986

Miller J (1972) Experiments in molecular genetics. [Cold Spring Harbor, N. Y.] Cold Spring Harbor Laboratory, 1972.

Mizuno Y, Moorhead GBG, Ng KKS (2007) Structural Basis for the Regulation of N-Acetylglutamate Kinase by PII in Arabidopsis thaliana. Journal of Biological Chemistry **282:** 35733-35740

Mura U, Chock PB, Stadtman ER (1981) Allosteric regulation of the state of adenylylation of glutamine synthetase in permeabilized cell preparations of Escherichia coli. Studies of monocyclic and bicyclic interconvertible enzyme cascades, in situ. Journal of Biological Chemistry **256:** 13022-13029

Mura U, Stadtman ER (1981) Glutamine synthetase adenylylation in permeabilized cells of Escherichia coli. Journal of Biological Chemistry **256:** 13014-13021

Murashige T, Skoog F (1962) A Revised Medium for Rapid Growth and Bio Assays with Tobacco Tissue Cultures. Physiologia Plantarum **15:** 473-497

Naleway JJ (1992) 4 - Histochemical, Spectrophotometric, and Fluorometric GUS Substrates. *In* SR Gallagher, ed, Gus Protocols. Academic Press, San Diego, pp 61-76

Nelson BK, Cai X, Nebenfuhr A (2007) A multicolored set of in vivo organelle markers for co-localization studies in Arabidopsis and other plants. Plant J **51:** 1126-1136

Nelson OE, Rines HW (1962) The enzymatic deficiency in the waxy mutant of maize. Biochemical and Biophysical Research Communications **9:** 297-300

Newell CA, Natesan SKA, Sullivan JA, Jouhet J, Kavanagh TA, Gray JC (2012) Exclusion of plastid nucleoids and ribosomes from stromules in tobacco and Arabidopsis. The Plant Journal **69:** 399-410

Nielsen H, Engelbrecht J, Brunak S, von Heijne G (1997) Identification of prokaryotic and eukaryotic signal peptides and prediction of their cleavage sites. Protein Engineering **10:** 1-6

Ninfa AJ, Atkinson MR (2000) PII signal transduction proteins. Trends in Microbiology **8:** 172-179

Ninfa AJ, Bennett RL (1991) Identification of the site of autophosphorylation of the bacterial protein kinase/phosphatase NRII. Journal of Biological Chemistry **266:** 6888-6893

Ninfa AJ, Jiang P (2005) PII signal transduction proteins: sensors of alpha-ketoglutarate that regulate nitrogen metabolism. Curr Opin Microbiol **8:** 168-173

Ninfa AJ, Magasanik B (1986) Covalent modification of the glnG product, NRI, by the glnL product, NRII, regulates the transcription of the glnALG operon in Escherichia coli. Proceedings of the National Academy of Sciences **83:** 5909

Ninfa EG, Atkinson MR, Kamberov ES, Ninfa AJ (1993) Mechanism of autophosphorylation of Escherichia coli nitrogen regulator II (NRII or NtrB): trans-phosphorylation between subunits. Journal of Bacteriology **175:** 7024-7032

Perello C, Llamas E, Burlat V, Ortiz-Alcaide M, Phillips MA, Pulido P, Rodriguez-Concepcion M (2016) Differential Subplastidial Localization and Turnover of Enzymes Involved in Isoprenoid Biosynthesis in Chloroplasts. PLoS One **11:** e0150539

Peter S, Harter K, Schleifenbaum F (2014) Fluorescence Microscopy. *In* JJ Sanchez-Serrano, J Salinas, eds, Arabidopsis Protocols. Humana Press, Totowa, NJ, pp 429-452

Pulido P, Llamas E, Llorente B, Ventura S, Wright LP, Rodriguez-Concepcion M (2016) Specific Hsp100 Chaperones Determine the Fate of the First Enzyme of the Plastidial Isoprenoid Pathway for Either Refolding or Degradation by the Stromal Clp Protease in Arabidopsis. PLoS Genet **12:** e1005824

Pulido P, Toledo-Ortiz G, Phillips MA, Wright LP, Rodriguez-Concepcion M (2013) Arabidopsis J-protein J20 delivers the first enzyme of the plastidial isoprenoid pathway to protein quality control. Plant Cell **25:** 4183-4194

Ramón-Maiques S, Fernández-Murga ML, Gil-Ortiz F, Vagin A, Fita I, Rubio V (2006) Structural Bases of Feed-back Control of Arginine Biosynthesis, Revealed by the Structures of Two Hexameric N-Acetylglutamate Kinases, from Thermotoga maritima and Pseudomonas aeruginosa. Journal of Molecular Biology **356:** 695-713

Reith M, Munholland J (1993) A High-Resolution Gene Map of the Chloroplast Genome of the Red Alga Porphyra purpurea. The Plant Cell **5:** 465-475

Rhee SG, Park R, Chock PB, Stadtman ER (1978) Allosteric regulation of monocyclic interconvertible enzyme cascade systems: use of Escherichia coli glutamine synthetase as an experimental model. Proceedings of the National Academy of Sciences of the United States of America **75:** 3138-3142

Rodrigues TE, Gerhardt EC, Oliveira MA, Chubatsu LS, Pedrosa FO, Souza EM, Souza GA, Muller-Santos M, Huergo LF (2014) Search for novel targets of the PII signal transduction protein in Bacteria identifies the BCCP component of acetyl-CoA carboxylase as a PII binding partner. Mol Microbiol **91:** 751-761

Salie MJ, Zhang N, Lancikova V, Xu D, Thelen JJ (2016) A Family of Negative Regulators Targets the Committed Step of de Novo Fatty Acid Biosynthesis. Plant Cell **28:** 2312-2325

Sambrook J, Fritsch EF, Maniatis T (1989) Molecular cloning: a laboratory manual. Cold Spring Harbor Laboratory Press, Cold Spring Harbor, NY

Sant'Anna FH, Trentini DB, de Souto Weber S, Cecagno R, da Silva SC, Schrank IS (2009) The PII Superfamily Revised: A Novel Group and Evolutionary Insights. Journal of Molecular Evolution **68:** 322-336

Schindelin J, Arganda-Carreras I, Frise E, Kaynig V, Longair M, Pietzsch T, Preibisch S, Rueden C, Saalfeld S, Schmid B, Tinevez J-Y, White DJ,

Hartenstein V, Eliceiri K, Tomancak P, Cardona A (2012) Fiji: an open-source platform for biological-image analysis. Nature Methods **9:** 676-682

Schöb H, Kunz C, Meins Jr F (1997) Silencing of transgenes introduced into leaves by agroinfiltration: a simple, rapid method for investigating sequence requirements for gene silencing. Molecular and General Genetics MGG **256:** 581-585

Selim KA, Lapina T, Forchhammer K, Ermilova E (2019) Interaction of N-acetyl-l-glutamate kinase with the PII signal transducer in the non-photosynthetic alga Polytomella parva: Co-evolution towards a hetero-oligomeric enzyme. The FEBS Journal **n/a**

Seung D, Soyk S, Coiro M, Maier BA, Eicke S, Zeeman SC (2015) PROTEIN TARGETING TO STARCH is required for localising GRANULE-BOUND STARCH SYNTHASE to starch granules and for normal amylose synthesis in Arabidopsis. PLoS Biol **13:** e1002080

Shapiro BM (1969) Glutamine synthetase deadenylylating enzyme system from Escherichia coli. Resolution into two components, specific nucleotide stimulation, and cofactor requirements. Biochemistry **8:** 659-670

Smith CS, Morrice NA, Moorhead GBG (2004) Lack of evidence for phosphorylation of Arabidopsis thaliana PII: implications for plastid carbon and nitrogen signaling. Biochimica et Biophysica Acta (BBA) - Proteins and Proteomics **1699:** 145-154

Somerville CR, Somerville SC, Ogren WL (1981) Isolation of photosynthetically active protoplasts and chloroplasts from Arabidopsis thaliana. Plant Science Letters **21:** 89-96

Son HS, Rhee SG (1987) Cascade control of Escherichia coli glutamine synthetase. Purification and properties of PII protein and nucleotide sequence of its structural gene. Journal of Biological Chemistry **262:** 8690-8695

Sparkes IA, Runions J, Kearns A, Hawes C (2006) Rapid, transient expression of fluorescent fusion proteins in tobacco plants and generation of stably transformed plants. Nature Protocols **1:** 2019-2025

Spät P, Maček B, Forchhammer K (2015) Phosphoproteome of the cyanobacterium Synechocystis sp. PCC 6803 and its dynamics during nitrogen starvation. Frontiers in Microbiology **6**

Suarez J, Hener C, Lehnhardt V-A, Hummel S, Stahl M, Kolukisaoglu Ü (2019) AtDAT1 Is a Key Enzyme of D-Amino Acid Stimulated Ethylene Production in Arabidopsis thaliana. Frontiers in Plant Science **10**

Sugiyama K, Hayakawa T, Kudo T, Ito T, Yamaya T (2004) Interaction of N-Acetylglutamate Kinase with a PII-Like Protein in Rice. Plant and Cell Physiology **45:** 1768-1778

Sweere U, Eichenberg K, Lohrmann J, Mira-Rodado V, Bäurle I, Kudla J, Nagy F, Schäfer E, Harter K (2001) Interaction of the Response Regulator ARR4 with Phytochrome B in Modulating Red Light Signaling. Science **294:** 1108-1111

Szydlowski N, Ragel P, Hennen-Bierwagen TA, Planchot V, Myers AM, Merida A, d'Hulst C, Wattebled F (2011) Integrated functions among multiple starch synthases determine both amylopectin chain length and branch linkage location in Arabidopsis leaf starch. J Exp Bot **62:** 4547-4559

Szydlowski N, Ragel P, Raynaud S, Lucas MM, Roldan I, Montero M, Munoz FJ, Ovecka M, Bahaji A, Planchot V, Pozueta-Romero J, D'Hulst C, Merida A (2009) Starch granule initiation in Arabidopsis requires the presence of either class IV or class III starch synthases. Plant Cell **21:** 2443-2457

Tenorio G, Orea A, Romero JM, Mérida Á (2003) Oscillation of mRNA level and activity of granule-bound starch synthase I in Arabidopsis leaves during the day/night cycle. Plant Molecular Biology **51:** 949-958

Thomas G, Coutts G, Merrick M (2000) The glnKamtB operon: a conserved gene pair in prokaryotes. Trends in Genetics **16:** 11-14

Towbin H, Staehelin T, Gordon J (1979) Electrophoretic transfer of proteins from polyacrylamide gels to nitrocellulose sheets: procedure and some applications. Proceedings of the National Academy of Sciences of the United States of America **76:** 4350-4354

Tsinoremas NF, Castets AM, Harrison MA, Allen JF, Tandeau de Marsac N (1991) Photosynthetic electron transport controls nitrogen assimilation in cyanobacteria by means of posttranslational modification of the glnB gene product. Proceedings of the National Academy of Sciences **88:** 4565-4569

Uhrig RG, Ng KK, Moorhead GB (2009) PII in higher plants: a modern role for an ancient protein. Trends Plant Sci **14:** 505-511

Ustun S, Hafren A, Liu Q, Marshall RS, Minina EA, Bozhkov PV, Vierstra RD, Hofius D (2018) Bacteria Exploit Autophagy for Proteasome Degradation and Enhanced Virulence in Plants. Plant Cell **30:** 668-685

van Heeswijk WC, Hoving S, Molenaar D, Stegeman B, Kahn D, Westerhoff HV (1996) An alternative PII protein in the regulation of glutamine synthetase in Escherichia coli. Molecular Microbiology **21:** 133-146

van Heeswijk WC, Stegeman B, Hoving S, Molenaar D, Kahn D, Westerhoff HV (1995) An additional PII in Escherichia coli: a new regulatory protein in the glutamine synthetase cascade. FEMS Microbiology Letters **132:** 153-157

Verma E, Chakraborty S, Tiwari B, Mishra AK (2018) Transcriptional regulation of acetyl CoA and lipid synthesis by PII protein in Synechococcus PCC 7942. Journal of Basic Microbiology **58:** 187-197

Wang S, Blumwald E (2014) Stress-induced chloroplast degradation in Arabidopsis is regulated via a process independent of autophagy and senescence-associated vacuoles. Plant Cell **26:** 4875-4888

Weiss V, Magasanik B (1988) Phosphorylation of nitrogen regulator I (NRI) of Escherichia coli. Proceedings of the National Academy of Sciences **85:** 8919-8923

Wirth AJ, Gruebele M (2013) Quinary protein structure and the consequences of crowding in living cells: Leaving the test-tube behind. BioEssays **35:** 984-993

Xu J, Huang X, Lan H, Zhang H, Huang J (2016) Rearrangement of nitrogen metabolism in rice (Oryza sativa L.) under salt stress. Plant Signal Behav **11:** e1138194

Xu Y, Cheah E, Carr PD, van Heeswijk WC, Westerhoff HV, Vasudevan SG, Ollis DL (1998) GlnK, a PII-homologue: structure reveals ATP binding site and indicates how the T-loops may be involved in molecular recognition11Edited by R. Huber. Journal of Molecular Biology **282:** 149-165

Yu X, Pasternak T, Eiblmeier M, Ditengou F, Kochersperger P, Sun J, Wang H, Rennenberg H, Teale W, Paponov I, Zhou W, Li C, Li X, Palme K (2013) Plastid-Localized Glutathione Reductase2–Regulated Glutathione Redox Status Is Essential for Arabidopsis Root Apical Meristem Maintenance. The Plant Cell **25:** 4451-4468

Zalutskaya Z, Kharatyan N, Forchhammer K, Ermilova E (2015) Reduction of PII signaling protein enhances lipid body production in Chlamydomonas reinhardtii. Plant Science **240:** 1-9

Zeth K, Fokina O, Forchhammer K (2014) Structural Basis and Target-specific Modulation of ADP Sensing by the Synechococcus elongatus PII Signaling Protein. Journal of Biological Chemistry **289:** 8960-8972

7 Appendix

7.1 Primers used during thesis

7.1.1 Primers for amplification of gene of interest followed by cloning into pENTR™/D-TOPO® or classical cloning into pENTR-MCS

Table 12: Primers used for amplification for cloning into pENTR™/D-TOPO® and pENTR-MCS during thesis

Primer name	Sequence 5'-3'	usage
AtGLB1-Start	5'-caccATGGCGGCGTCAATGACGAAAC-3'	Amplification of *cPII gPII* or *cTP$_{PII}$* for cloning into pENTR™/D-TOPO®
NK_AtGLB1-Start	5'-caccATGGCGGCGTCAATGACGAAAC-3'	Amplification of *cPII* or *gPII* for cloning into pENTR™/D-TOPO®, genotyping and cDNA level in *PIIS2* and Col-0
AtGLB1-End	5'-AGACGGTGAAAGCATATCACCAG-3'	Amplification of c*PII*, *gPII* or *pAtPII::gAtPII* without stop codon for cloning into pENTR™/D-TOPO®, genotyping and cDNA level in PIIS2 and Col-0
NK_proAtPIIstart	5'-caccTTTTGTTTCACCTTAACCAG-3'	Amplification of *pPII* or *pPII::gPII* for cloning into pENTR™/D-TOPO®
NK_proATPIIend	5'-CCATGATTCTAGTTTTTTTTTTAACAC-3'	Amplification of *pPII* for cloning into pENTR™/D-TOPO®
NK_AtPIIdelta-start2	5'-CACCATGCAAATATCTTCTGATTATATTCC-3'	Amplification of Δ*AtPII* lacking *cTP$_{PII}$* with ATG start codon for cloning into pENTR™/D-TOPO®
AtNAGK-Start	5'-caccACCGTATCAACACCACCTTC-3'	Amplification of *NAGK* for cloning into pENTR™/D-TOPO®
AtNAGK-End	5'-TCCAGTAATCATAGTTCCAGCTC-3'	Amplification of *NAGK* without stop codon for cloning into pENTR™/D-TOPO®
NK_AtNAGKstart	5'-caccATGGCCACCGTCACATCCAATGCTTC-3'	Amplification of *NAGK* for cloning into pENTR™/D-TOPO®
NK_AtNAGKend	5'-TCCAGTAATCATAGTTCCAGCTCCTTC-3'	Amplification of *NAGK* without stop codon for cloning into pENTR™/D-TOPO®
NK_AtNAGKstop	5'-TTATCCAGTAATCATAGTTCCAGCTCCTTC-3'	Amplification of *NAGK* for cloning into pENTR™/D-TOPO®
NK_AtBCCP1start	5'-ATGGCGTCTTCGTCGTTCTCAGTCACATCT-3'	Amplification of *BCCP1* for cloning into pENTR™/D-TOPO®
NK_AtBCCP1start-2	5'-caccATGGCGTCTTCGTCGTTCTCAGTCAC-3'	Amplification of *BCCP1* for cloning into pENTR™/D-TOPO®
NK-BCCP1end	5'-CGGTTGAACCACAAACAGAGGAGTGTC-3'	Amplification of *BCCP1* for cloning into pENTR™/D-TOPO®
NK_At1g52670-start	5'-caccATGAATTCCTGTAGCTTAGGAG-3'	Amplification of *BADC2 (At1g52670)* for cloning into pENTR™/D-TOPO®
NK_At1g52670-end	5'-CTGAAGCTTCTTGATGCCAGGA-3'	Amplification of *BADC2 (At1g52670)* for cloning into pENTR™/D-TOPO®
NK_At3g56130-start	5'-caccATGGCGTCTTCTGCAGCTC-3'	Amplification of *BADC3 (At3g15690.2)* for cloning into pENTR™/D-TOPO®
NK_At3g56130-end	5'-CTGGATGTTGATGTCGTGGA-3'	Amplification of *BADC3 (At3g15690.2)* for cloning into pENTR™/D-TOPO®
NK_RGCS1A-FP	5'-caccATGGCTTCCTCTATGCTCTCTTCCG-3'	Amplification of *RBCS3B.1* (At5g38410.1) for cloning into pENTR™/D-TOPO®

NK_RGCS1A-RP	5'-ACCGGTGAAGCTTGGTGGCTTGTAGG-3'	Amplification of *RBCS3B.1* (At5g38410.1) for cloning into pENTR™/D-TOPO®
NK_U6-FP	5'-caccAGAAATCTCAAAATTCCGGCA-3'	Amplification of *Construct1* and *Construct 2* of *PII* and *DAT1* CRISPR/Cas constructs for cloning into pENTR™/D-TOPO®
NK_sg-RP	5'-TAATGCCAACTTTGTACAAGAAAGC-3'	Amplification of *Construct1* and *Construct 2* of *PII* and *DAT1* CRISPR/Cas constructs for cloning into pENTR™/D-TOPO®
NK_Sac-D1-C2-FP	5'-GGAACCCAATTCGAGCTCAGAAATCTCAAAATTCCGGCAGAAC-3'	Amplification of *Construct1* and *Construct 2* of *DAT1* CRISPR/Cas constructs containing restriction sites restriction enzyme-based cloning into pENTR-MCS
NK_Acc65I-D1-C2-RP	5'-AGGATCCCGGGTACCTAATGCCAACTTTGTACAAGAAAGC-3'	Amplification of *Construct1* and *Construct 2* of *DAT1* CRISPR/Cas constructs containing restriction sites restriction enzyme-based cloning into pENTR-MCS
NK_SacI-D1-C2-RP	5'-GCGGGAGCTCGAATTGGGTTCCTAATGCCAACTTTGTACAGGA-3'	Amplification of *Construct1* and *Construct 2* of *DAT1* CRISPR/Cas constructs containing restriction sites restriction enzyme-based cloning into pENTR-MCS
NK_EcoRI-C1-FP	5'-ACCATGGAATTCCCGCATAGAAATCTCAAAATTCCGGCAGAAC-3'	Amplification of *Construct1* and *Construct 2* of *DAT1* CRISPR/Cas constructs containing restriction sites restriction enzyme-based cloning into pENTR-MCS

7.1.2 Primers for amplification of gene of interest followed by BP reaction into pDONR221-P1P4 or pDONR221-P3P2

Table 13: Primers used for amplification of attP-site containing fragments for BP reaction into pDONR221-P1P4 and pDONR221-P3P2

Primer name	Sequence 5'-3'	usage
NK_attP2P3-PIIstart	5'-GGGGACAACTTTGTATAATAAAGTTGTAATGGCGGCGTCAATGACG-3'	Amplification of *PII* with *attP3* and *attP2* attachment sites for BP reaction into pDONR221-P3P2
NK_attP2P3-PIIend	5'-GGGGACCACTTTGTACAAGAAAGCTGGGTTAGACGGTGAAAGCATATC-3'	Amplification of *PII* with *attP3* and *attP2* attachment sites for BP reaction into pDONR221-P3P2
NK_attP1P4-PIIstart	5'-GGGGACAAGTTTGTACAAAAAAGCAGGCTTAATGGCGGCGTCAATGACG-3'	Amplification of *PII* with *attP1* and *attP4* attachment sites for BP reaction into pDONR221-P1P4
NK_attP1P4-PIIend	5'-GGGGACAACTTTGTATAGAAAAGTTGGGTGAGACGGTGAAAGCATATC-3'	Amplification of *PII* with *attP1* and *attP4* attachment sites for BP reaction into pDONR221-P1P4
NK_cTP-AtPII-P1P4-RP	5'-GGGGACAACTTTGTATAGAAAAGTTGGGTGGGCACTAACGACAGGTAA-3'	Amplification of cTP_{PII} with *attP1* and *attP4* attachment sites for BP reaction into pDONR221-P1P4
NK_attP1P4-NAGKstart	5'-GGGGACAAGTTTGTACAAAAAAGCAGGCTTAATGGCCACCGTCACATCC-3'	Amplification of *NAGK* with *attP1* and *attP4* attachment sites for BP reaction into pDONR221-P1P4
NK_attP1P4-NAGKend	5'-GGGGACAACTTTTGTATAGAAAAGTTGGGTGTCCAGTAATCATAGTTCC-3'	Amplification of *NAGK* with *attP1* and *attP4* attachment sites for BP reaction into pDONR221-P1P4
NK_attP1P4-BCCP1start	5'-GGGGACAAGTTTGTACAAAAAAGCAGGCTTAATGGCGTCTTCGTCGTTC-3'	Amplification of *BCCP1* with *attP1* and *attP4* attachment sites for BP reaction into pDONR221-P1P4
NK_attP1P4-BCCP1end	5'-GGGGACAACTTTGTATAGAAAAGTTGGGTGCGGTTGAACCACAAACAG-3'	Amplification of *BCCP1* with *attP1* and *attP4* attachment sites for BP reaction into pDONR221-P1P4

NK_P1P4-GBSSI-FP	5'-GGGGACAAGTTTGTACAAAAAAGCAGGCTTAATGGCAACTGTGACTGCT-3'	Amplification of *GBSSI* with *attP1* and *attP4* attachment sites from *pH7FWG2.0-GBSSI* for BP reaction into pDONR221-P1P4
NK_P1P4-GBSSIend-RP	5'-GGGGACAACTTTGTATAGAAAAGTTGGGTGCGGCGTCGCTACGTTCTC-3'	Amplification of *GBSSI* with *attP1* and *attP4* attachment sites from *pH7FWG2.0-GBSSI* for BP reaction into pDONR221-P1P4
NK_P1P4-DA1-FP	5'-GGGGACAAGTTTGTACAAAAAAGCAGGCTTAATGGCAGGTTTGTCGCTG-3'	Amplification of *DAT1* with *attP1* and *attP4* attachment sites from pUBQ-DAT1(Col-0)-GFP for BP reaction into pDONR221-P1P4
NK_P1P4-DA1-RP	5'-GGGGACAACTTTGTATAGAAAAGTTGGGTGGTAAGGAACAAGAACACG-3'	Amplification of *DAT1* with *attP1* and *attP4* attachment sites from pUBQ-DAT1(Col-0)-GFP for BP reaction into pDONR221-P1P4
NK_RGCS1A-P1P4-FP	5'-GGGGACAAGTTTGTACAAAAAAGCAGGCTTAATGGCTTCCTCTATGCTC-3'	Amplification of *RBCS3B.1* with *attP1* and *attP4* attachment sites from pENTR-RBCS3B.1 for BP reaction into pDONR221-P1P4
NK_RGCS1A-P1P4-RP	5'-GGGGACAACTTTGTATAGAAAAGTTGGGTGACCGGTGAAGCTTGGTGG-3'	Amplification of *RBCS3B.1* with *attP1* and *attP4* attachment sites from pENTR- RBCS3B.1 for BP reaction into pDONR221-P1P4
NK_attP1-FP-DXS	5'-GGGGACAAGTTTGTACAAAAAAGCAGGCTTAATGGCTTCTTCTGCATTT-3'	Amplification of *DXS* with *attP1* and *attP4* attachment sites from pH7FWG2,0-DXS for BP reaction into pDONR221-P1P4
NK_attP4-RP-DXS	5'-GGGGACAACTTTGTATAGAAAAGTTGGGTGAAACAGAGCTTCCCTTGG-3'	Amplification of *DXS* with *attP1* and *attP4* attachment sites from pH7FWG2,0-DXS for BP reaction into pDONR221-P1P4
NK_attP1-FP-DXR	5'-GGGGACAAGTTTGTACAAAAAAGCAGGCTTAATGACATTAAACTCACTA-3'	Amplification of *DXR* with *attP1* and *attP4* attachment sites from pH7FWG2,0-DXR for BP reaction into pDONR221-P1P4
NK_attP4-RP-DXR	5'-GGGGACAACTTTGTATAGAAAAGTTGGGTGTGCATGAACTGGCCTAGC-3'	Amplification of *DXR* with *attP1* and *attP4* attachment sites from pH7FWG2,0-DXR for BP reaction into pDONR221-P1P4
NK_attP1-FP-G11	5'-GGGGACAAGTTTGTACAAAAAAGCAGGCTTAATGGCTTCAGTGACTCTA-3'	Amplification of *GGPPS11* with *attP1* and *attP4* attachment sites from pCambia-G11 (GGPPS11) for BP reaction into pDONR221-P1P4
NK_attP4-RP-G11	5'-GGGGACAACTTTGTATAGAAAAGTTGGGTGGTTCTGTCTATAGGCAAT-3'	Amplification of *GGPPS11* with *attP1* and *attP4* attachment sites from pCambia-G11 (GGPPS11) for BP reaction into pDONR221-P1P4

7.1.3 Primers for site directed mutagenesis of AtPII to generate AtPII-OsQ

Table 14: Primers used for site directed mutagenesis of AtPII to generate AtPII-OsQ

Primer name	Sequence 5'-3'	usage
NK_AtPII-Q-FP2	5'-GGGCTAGCTGATATGCTTTCACCGTCTAAG-3'	Site directed mutagenesis of AtPII to obtain AtPII-OsQ; 3 AA were inserted
NK_AtPII-Q-RP2	5'-AGCTAGCCCACCAGTCATCTTCTCTGCTTTCTC-3'	Site directed mutagenesis of AtPII to obtain AtPII-OsQ; 3 AA were inserted

7.1.4 Primers used for genotyping and/or sequencing

Table 15: Primers used for genotyping and/or sequencing

Primer name	Sequence 5'-3'	usage
NK_AtPIIseq-start	5'-ATGGCGGCGTCAATGAC-3'	Amplification of genomic PII for sequencing of CRISPR/Cas event
NK_PIIfor2	5'-GACCAAGTGGAATCTGTAATC-3'	Amplification of CDS of PII for analysis of PII mRNA level in PIIS2

NK_PIIrev2	5'-TCACATCAGAAACAGTAACACCT-3'	Amplification of CDS of PII for analysis of PII mRNA level in PIIS2
NK_AtPIIseq-rev	5'-ACAGTAACACCTCGAATCC-3'	Amplification of genomic PII for sequencing of CRISPR/Cas event
NK_GBSSI-Fpseq	5'-CATTGCTACAAACGAGGAG-3'	Sequencing of *GBSSI*
NK_C1-2seq	5'-TCTCTCCACAACACCATT-3'	Genotyping of CRISPR/Cas plants to check for T-DNA insertion on the
NK_Bar-RP	5'-TCAGATCTCGGTGACGGGCAG-3'	Genotyping of CRISPR/Cas plants to check for T-DNA
M13-FP	5'-TGTAAAACGACGGCCAGT-3'	Sequencing of pENTR vectors
M13-RP	5'-CAGGAAACAGCTATGACC-3'	Sequencing of pENTR vectors
pc3.1GFP-Topo-RP	5'-CCCATTAACATCACC-3'	Sequencing of pUBQ vectors

7.2 Vectors used during this thesis

7.2.1 Vectors for cloning and expression in plants provided by other sources

Table 16: Vectors for cloning and expression in plants provided by other sources

Name	Resistance		Source	Usage
	Bac.	plant		
pENTR™/D-TOPO®	Kan	---	Thermo Fisher Scientific	Cloning for Destination vectors
pUBQ10-Dest (#1757)	Spec	Kan	Gateway cassette from invitrogen, generated by Achim Hahn, derived from pUGT1kan+ vector from Karin Schumacher	Expression of C-terminal GFP-tagged proteins in plants
pMDC107 (#688)	Spec	Hyg	Curtis and Grossniklaus (2003)	Expression in plants
pMDC163 (#695)	Spec	Hyg	Curtis and Grossniklaus (2003)	Expression in plants
pH7FWG2,0-Dest (#1082)	Spec	Hyg	Karimi et al. (2002)	Expression in plants
pB7RWG2,0-Dest (#999)	Spec	PPT	Karimi et al. (2002)	Expression in plants
pFRETgc-2in1-CC (#3063)	Spec	PPT	Hecker et al. (2015)	Expression in plants
pBiFCt-2in1-CC (#3068)	Spec	---	Grefen and Blatt (2012)	Expression in plants
pDONR221-P1P4 (#3061)	Kan	---	Invitrogen Thermo Fisher Scientific (Carlsbad, USA)	BP Reaction for 2in1 vectors
pDONR221-P3P2 (#3062)	Kan	---	Invitrogen Thermo Fisher Scientific (Carlsbad, USA)	BP Reaction for 2in1 vectors
MTN2966-Dest	Spec	PPT	Vector provided by J. Kieber cloned by Marc Nishimura from Dangl lab	Destination vector for LR reaction of CRISPR/Cas constructs
pDe-CAS9-FastRed-Dest	Spec	PPT	Gift from Christopher Grefen	Destination vector for LR reaction of CRISPR/Cas constructs
17ABBIGP_Construct1_pMA-T	Amp	---	Synthesized by Invitrogen Thermo Fisher Scientific (Carlsbad, USA)	Cloning of CRISPR/Cas constructs
17ABBIGP_Construct2_pMA-T	Amp	---	Synthesized by Invitrogen Thermo Fisher Scientific (Carlsbad, USA)	Cloning of CRISPR/Cas constructs
18ABOQXP_DAT1-Protospacer1_pMA-RQ	Amp	---	Synthesized by Invitrogen Thermo Fisher Scientific (Carlsbad, USA)	Cloning of CRISPR/Cas constructs
18ABOQXP_DAT1-Protospacer2_pMA-RQ	Amp	---	Synthesized by Invitrogen Thermo Fisher Scientific (Carlsbad, USA)	Cloning of CRISPR/Cas constructs
pENTR-DAT1(Col)	Kan	---	Juan Suarez	Amplification for 2in1 vectors
pUBQ10-DAT1(Col-0)-GFP	Spec	Kan	Juan Suarez	Expression in plants
pUBQ10-DAT1(Ler)-GFP	Spec	Kan	Juan Suarez	Expression in plants
pENTR-cAtPII	Kan	---	Juan Suarez, Benedikt Fischer	LR reaction in destination vector

pENTR-cAtPIIend	Kan	---	Juan Suarez, Benedikt Fischer	LR reaction in destination vector
pENTR-L1-GentR-L4	Kan	---	Grefen and Blatt (2012)	Multisite LR reaction in destination vectors pFRETgc-2in1-CC and pBiFCt-2in1-CC; generation of donor only vectors
pH7FWG2.0-GBSSIend	Spec	Hyg	Gift from Szydlowski et al. (2009)	Expression in plants
pCambia-G11 (GGPPS11)	Kan	---	Gift from Manuel Rodriguez-Concepcion; Perello et al. 2016	Expression in plants
pB7FWG2,0-DXS	Spec	Hyg	Gift from Manuel Rodriguez-Concepcion; Perello et al. 2016	Expression in plants
pB7FWG2,0-DXR	Spec	Hyg	Gift from Manuel Rodriguez-Concepcion; Perello et al. 2016	Expression in plants
CD3-999 pt-rk (Plastids, mCherry)	Kan		from Nelson et al. (2007)	Expression in plants
pABindGFP-cAtPIIend	Spec	Hyg	Marvin Braun	Localization analyses in transiently transformed *N. benthamiana* and stably transformed in *A. thaliana*
pABindmCherry-cAtPIIend	Spec	Hyg	Marvin Braun	Localization analyses in transiently transformed *N. benthamiana*
pABindmCherry-DAT1end	Spec	Hyg	Marvin Braun	Localization analyses in transiently transformed *N. benthamiana*

7.2.2 Used pENTR vectors for cloning into destination vectors generated during this thesis

Table 17: Used pENTR vectors for cloning into destination vectors generated during this thesis

Construct	Resistance bacteria	origin	usage
pENTR-pAtPII	Kan	This study	LR reaction in destination vector
pENTR-gAtPII	Kan	This study	LR reaction in destination vector
pENTR-pAtPII::gAtPII	Kan	This study	LR reaction in destination vector
pENTR-cAtPII+OsQ	Kan	This study	LR reaction in destination vector
pENTR-NAGKend	Kan	This study	LR reaction in destination vector
pENTR-BCCP1	Kan	This study	LR reaction in destination vector
pENTR-BCCP1end	Kan	This study, Benedikt Fischer	LR reaction in destination vector
pENTR-BCL1end (BADC3)	Kan	This study	LR reaction in destination vector
pENTR-BCL2end (BADC2)	Kan	This study	LR reaction in destination vector
pENTR-RBCS3B	Kan	This study	LR reaction in destination vector
pENTR-MCS	Kan	This study; derived from *Hind*III digested multiple cloning site containing pENTR-D1 (Kolukisaoglu and Krieger et al., unpublished)	Classical cloning of CRISPR/Cas constructs
pENTR-MCS-Construct 1	Kan	This study	LR reaction in destination vector
pENTR-MCS-Construct 2	Kan	This study	Classical cloning of Construct 2 into pENTR-MCS-Construct 1; LR reaction in destination vector
pENTR-MCS-Construct1-Construct2	Kan	This study, Leander K. W. Rohr	LR reaction in destination vector
pENTR-MCS-DAT1_C1-C2	Kan	This study, Xuan Tran Vi Le	LR reaction in destination vector

7.2.3 pENTR vectors derived from BP reaction of attB-site containing PCR fragments with pDONR221-P1P4 and pDONR221-P3P2 for LR in 2in1 destination vectors

Table 18: pENTR vectors derived from BP reaction of attB-site containing PCR fragments with pDONR221-P1P4 and pDONR221-P3P2 for LR in 2in1 destination vectors

Construct	Resistance bacteria	origin	usage
pENTR-L3L2-PIIend	Kan	This study, Benedikt Fischer	Multisite LR reaction in destination vectors pFRETgc-2in1-CC and pBiFCt-2in1-CC
pENTR-L1L4-PIIend	Kan	This study, Benedikt Fischer	Multisite LR reaction in destination vectors pFRETgc-2in1-CC and pBiFCt-2in1-CC
pENTR-L1L4-NAGKend	Kan	This study, Marius Harter	Multisite LR reaction in destination vectors pFRETgc-2in1-CC and pBiFCt-2in1-CC
pENTR-L1L4-BCCP1end	Kan	This study, Marius Harter	Multisite LR reaction in destination vectors pFRETgc-2in1-CC and pBiFCt-2in1-CC
pENTR-L1L4-GBSSI	Kan	This study	Multisite LR reaction in destination vectors pFRETgc-2in1-CC and pBiFCt-2in1-CC
pENTR-L1L4-DAT1	Kan	This study	Multisite LR reaction in destination vectors pFRETgc-2in1-CC and pBiFCt-2in1-CC
pENTR-L1L4-RBCS3B.1	Kan	This study	Multisite LR reaction in destination vectors pFRETgc-2in1-CC and pBiFCt-2in1-CC
pENTR-L1L4-DXS	Kan	This study	Multisite LR reaction in destination vectors pFRETgc-2in1-CC and pBiFCt-2in1-CC
pENTR-L1L4-DXR	Kan	This study	Multisite LR reaction in destination vectors pFRETgc-2in1-CC and pBiFCt-2in1-CC
pENTR-L1L4-GGPPS11 (G11)	Kan	This study	Multisite LR reaction in destination vectors pFRETgc-2in1-CC and pBiFCt-2in1-CC
pENTR-L1L4-cTP	Kan	This study	Multisite LR reaction in destination vectors pFRETgc-2in1-CC and pBiFCt-2in1-CC

7.2.4 Expression vectors for localization analyses and stable transformation into plants

Table 19: Expression vectors for localization analyses and stable transformation into plants

Construct	Resistance		origin	usage
	Bact.	plant		
pMDC107-pAtPII::gAtPII-GFP	Kan	Hyg	This study	Localization analyses in transiently transformed *N. benthamiana* and stably transformed in *A. thaliana*
pUBQ10-cAtPII-GFP	Spec	Kan	This study	Localization analyses in transiently transformed *N. benthamiana* and stably transformed in *A. thaliana*
pUBQ10-gAtPII-GFP	Spec	Kan	This study	Localization analyses in transiently transformed *N. benthamiana* and stably transformed in *A. thaliana*
pH7FWG2,0-cAtPII-GFP	Spec	Hyg	This study	Localization analyses in transiently transformed *N. benthamiana* and stably transformed in *A. thaliana*
pB7RWG2-PIIend	Spec	Hyg	This study	Localization analyses in transiently transformed *N. benthamiana* and stably transformed in *A. thaliana*

pMDC163-pAtPII::GUS	Kan	Hyg	This study	Localization analyses in transiently transformed *N. benthamiana*
pH7FWG2,0-cAtPII+OsQ-GFP	Spec	Hyg	This study	Localization analyses in transiently transformed *N. benthamiana* and stably transformed in *A. thaliana*
pB7RWG2-NAGKend	Spec	PPT	This study	Localization analyses in transiently transformed *N. benthamiana*
pB7RWG2,0-BCL1end (BADC3)	Spec	Hyg	This study, Benedikt Fischer	Localization analyses in transiently transformed *N. benthamiana*
pB7RWG2,0-BCL2end (BADC2)	Spec	Hyg	This study, Benedikt Fischer	Localization analyses in transiently transformed *N. benthamiana*
pB7RWG2,0-RBCS3B.1	Spec	PPT	This study	Localization analyses in transiently transformed *N. benthamiana*

7.2.5 Expression vectors for FRET-FLIM analyses

Table 20: Expression vectors for FRET-FLIM analyses

Construct	**Resistance**		**origin**	**usage**
	Bact.	**plant**		
pFRETcg-CC-PII-PII	Spec	PPT	This study, Benedikt Fischer	FRET-FLIM in transiently transformed *N. benthamiana*, stable transformation into *A. thaliana*
pFRETcg-CC-NAGK-PII	Spec	PPT	This study, Benedikt Fischer	FRET-FLIM in transiently transformed *N. benthamiana*, stable transformation into *A. thaliana*
pFRETcg-CC-BCCP1-PII	Spec	PPT	This study	FRET-FLIM in transiently transformed *N. benthamiana*, stable transformation into *A. thaliana*
pFRETcg-CC-GBSSI-PII	Spec	PPT	This study, Benedikt Fischer	FRET-FLIM in transiently transformed *N. benthamiana*, stable transformation into *A. thaliana*
pFRETcg-CC-DAT1-PII	Spec	PPT	This study, Benedikt Fischer	FRET-FLIM in transiently transformed *N. benthamiana* and stably transformed into *A. thaliana*
pFRETcg-CC-RBCS3B.1-PII	Spec	PPT	This study	FRET-FLIM in transiently transformed *N. benthamiana*
pFRETcg-CC-DXS-PII	Spec	PPT	This study	FRET-FLIM in transiently transformed *N. benthamiana*
pFRETcg-CC-DXR-PII	Spec	PPT	This study	FRET-FLIM in transiently transformed *N. benthamiana*
pFRETcg-CC-G11-PII	Spec	PPT	This study	FRET-FLIM in transiently transformed *N. benthamiana*
pFRETcg-CC-GentR-PII	Spec	PPT	This study, Benedikt Fischer	FRET-FLIM in transiently transformed *N. benthamiana*, stable transformation into *A. thaliana*

7.2.6 Expression vectors for BiFC analyses

Table 21: Expression vectors for BiFC analyses

Construct	**Resistance bacteria**	**origin**	**usage**
pBiFCt-CC-PII-PII	Spec	This study	BiFC analyses in transiently transformed *N. benthamiana*
pBiFCt-CC-PII-NAGK	Spec	This study	BiFC analyses in transiently transformed *N. benthamiana*
pBiFCt-CC-PII-BCCP1	Spec	This study	BiFC analyses in transiently transformed *N. benthamiana*
pBiFCt-CC-PII-GBSSI	Spec	This study, Benedikt Fischer	BiFC analyses in transiently transformed *N. benthamiana*
pBiFCt-CC-PII-DAT1	Spec	This study, Benedikt Fischer	BiFC analyses in transiently transformed *N. benthamiana*
pBiFCt-CC-PII-RBCS3B.1	Spec	This study	BiFC analyses in transiently transformed *N. benthamiana*
pBiFCt-CC-PII-DXS	Spec	This study	BiFC analyses in transiently transformed *N. benthamiana*
pBiFCt-CC-PII-DXR	Spec	This study	BiFC analyses in transiently transformed *N. benthamiana*

pBiFCt-CC-PII-G11	Spec	This study	BiFC analyses in transiently transformed *N. benthamiana*
pBiFCt-CC-PII-Gent	Spec	This study, Benedikt Fischer	BiFC analyses in transiently transformed *N. benthamiana*

7.2.7 Expression vectors for CRISPR/Cas9

Table 22: Expression vectors for CRISPR/Cas9

Construct	**Resistance**		**origin**	**usage**
	Bact.	**plant**		
MTN2966-MCS-Construct 1	Spec	PPT	This study	Genome editing of stably transformed *A. thaliana*, generate PII knock-out mutant
MTN2966-MCS-Construct 2	Spec	PPT	This study	Genome editing of stably transformed *A. thaliana*, generate PII knock-out mutant
MTN2966-MCS-Construct1-Construct2	Spec	PPT	This study, Leander K. W. Rohr	Genome editing of stably transformed *A. thaliana*, generate PII knock-out mutant
pDe-CAS9-FastRed-PII-C1-C2	Spec	PPT	This study	Genome editing of stably transformed *A. thaliana*, generate PII knock-out mutant
MTN2966-MCS-DAT1_C1-C2	Spec	PPT	This study	Genome editing of stably transformed *A. thaliana*, generate DAT1 knock-out mutant
pDe-CAS9-FastRed-DAT-C1-C2	Spec	PPT	This study	Genome editing of stably transformed *A. thaliana*, generate DAT1 knock-out mutant

7.3 *A. tumefaciens* strains obtained during thesis

Stroke out *A. tumefaciens* strains containing TagRFP-Atg8e, TagRFP-Atg8g, and NBR1-RFP were provided by Dr. Suayib Üstün (ZMBP, University of Tübingen).

7.4 Generation of pENTR-MCS-C1-C2 for CRISPR event in PII

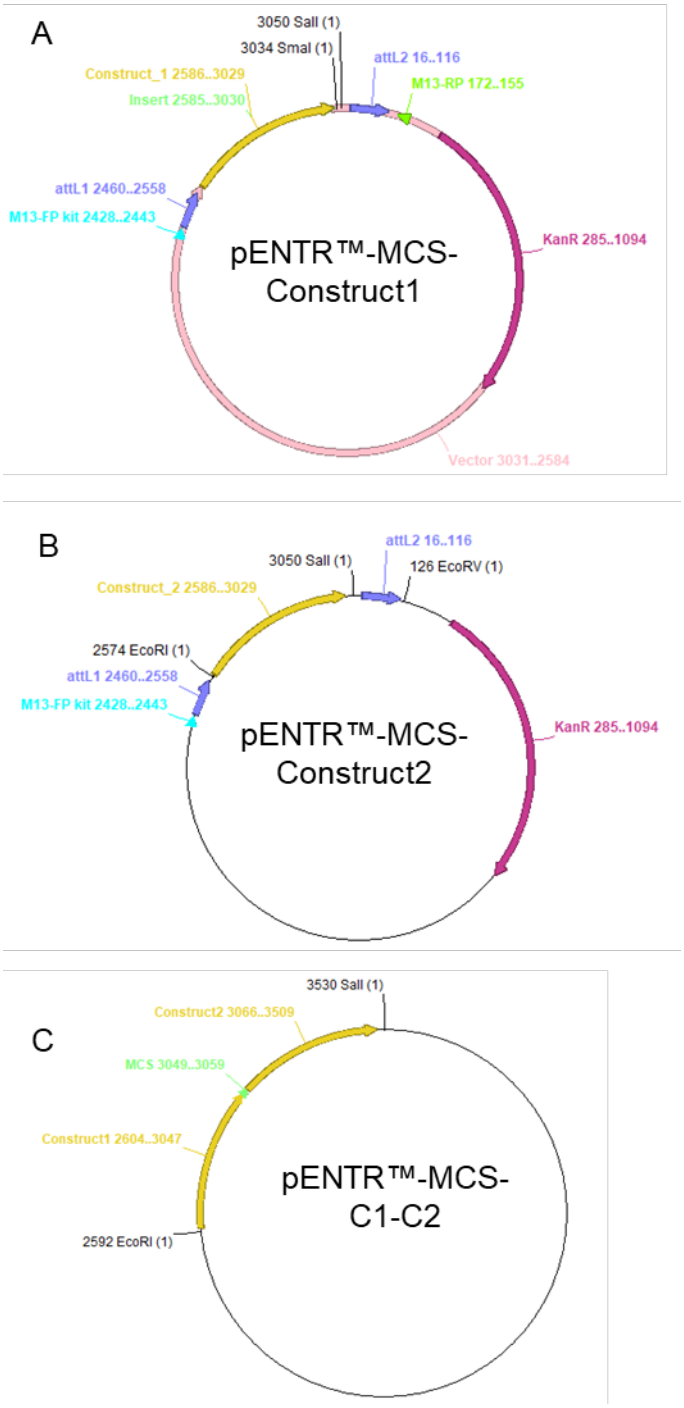

Figure A 1: Vector maps of pENTR-MCS-Construct1 and -Construct 2 to generate pENTR-MCS-C1-C2 for PII.
For generation of pENTR-MCS-C1-C2 A) pENTR-MCS-Construct1 was used as vector backbone. A) pENTR-MCS-Construct1 was digested with SmaI and SalI to linearize the vector and generate sites of interest. B) pENTR-MCS-Construct2 was digested first with EcoRI and EcoRV. After gel elution, fragment of interest was supplemented with T4 DNA Polymerase to generate a blunt end at EcoRI restriction site. Fragment was further digested with SalI.
After gel elution of A) and fragment of B), fragments were ligated to generate pENTR-MCS-C1-C2. Vector maps were generated with ApE.

7.5 Graphic map of generated pENTR vectors

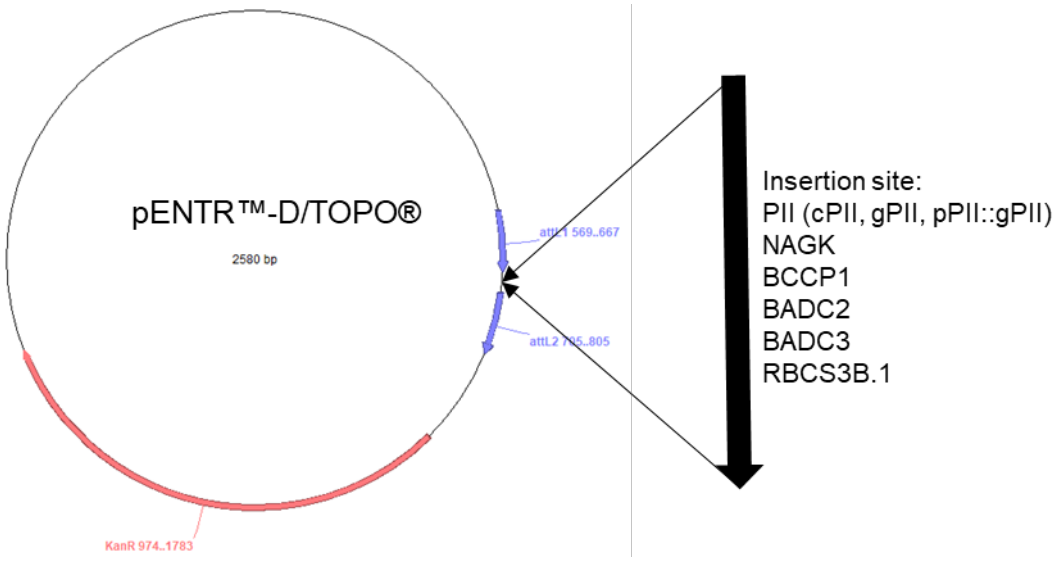

Figure A 2: pENTR™/ constructs harbouring gene of interest were generated using pENTR™/D-TOPO® with corresponding pENTR™/D-TOPO® reaction.
Single genes of interest: PII, NAGK, BCCP1, BADC2, BADC3, RBCS3B.1.
pENTR™/D-TOPO® reaction with PCR fragments of genes of interest generated from either gDNA of cDNA. Vector maps were generated with ApE.

7.6 Graphic map of generated pENTR-L1L4 and pENTR-L3L2 vectors

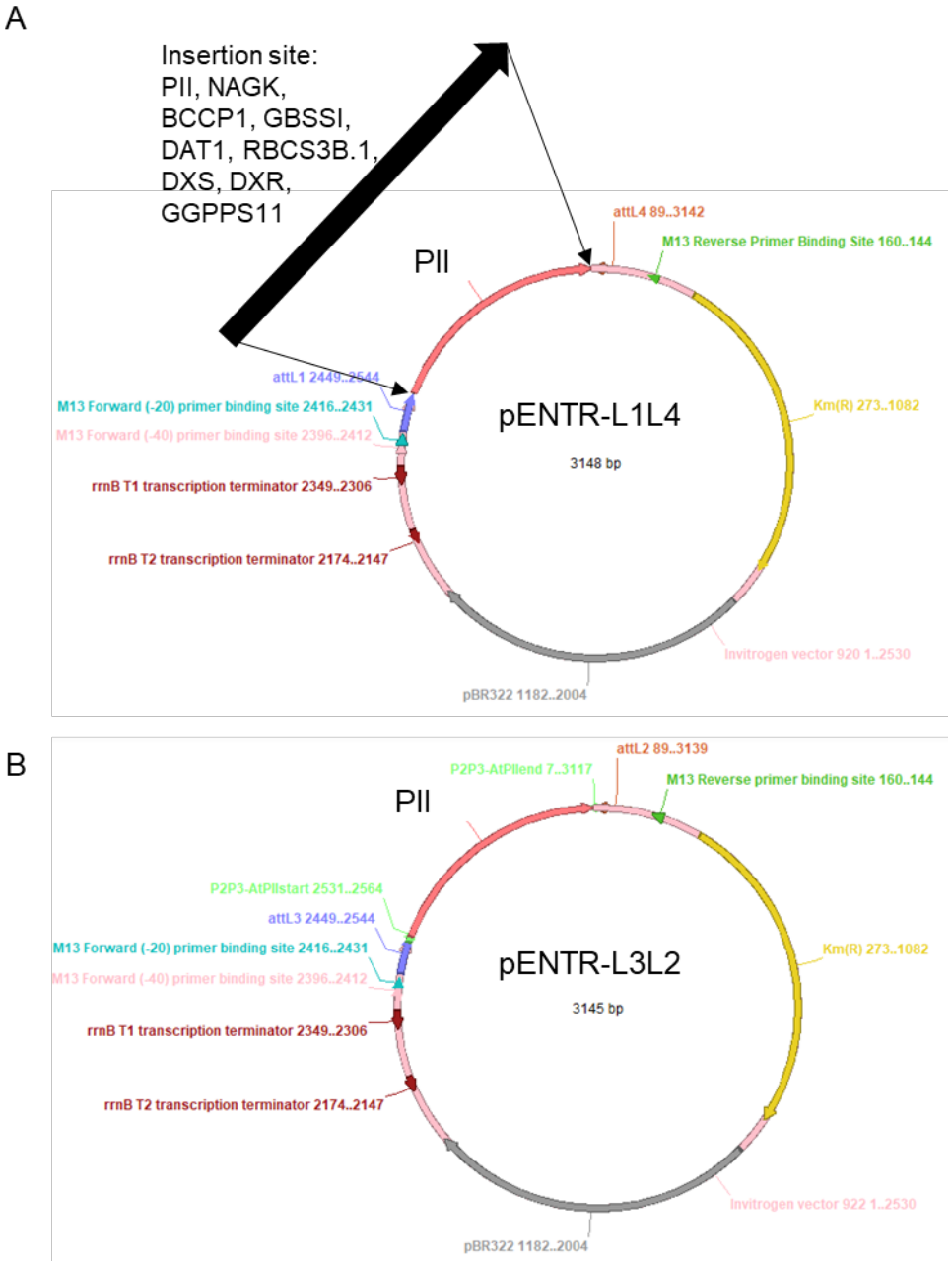

Figure A 3: Graphic map of pENTR-L1L4 and pENTR-L3L2 generated with BP reaction of pDONR221-P1P4 and pDONR221-P3P2, respectively

A) pENTR-L1L4 harbouring genes of interest for later mCherry- and cYFP-tagged constructs, respectively. Genes of interest: PII, NAGK, BCCP1, GBSSI, DAT1, RBCS3B.1, DXS, DXR and GGPPS11. B) pENTR-L3L2 harbouring PII for later GFP- and nYFP-tagged constructs, respectively. Graphic maps generated with ApE.

7.7 Overview of used expression vectors

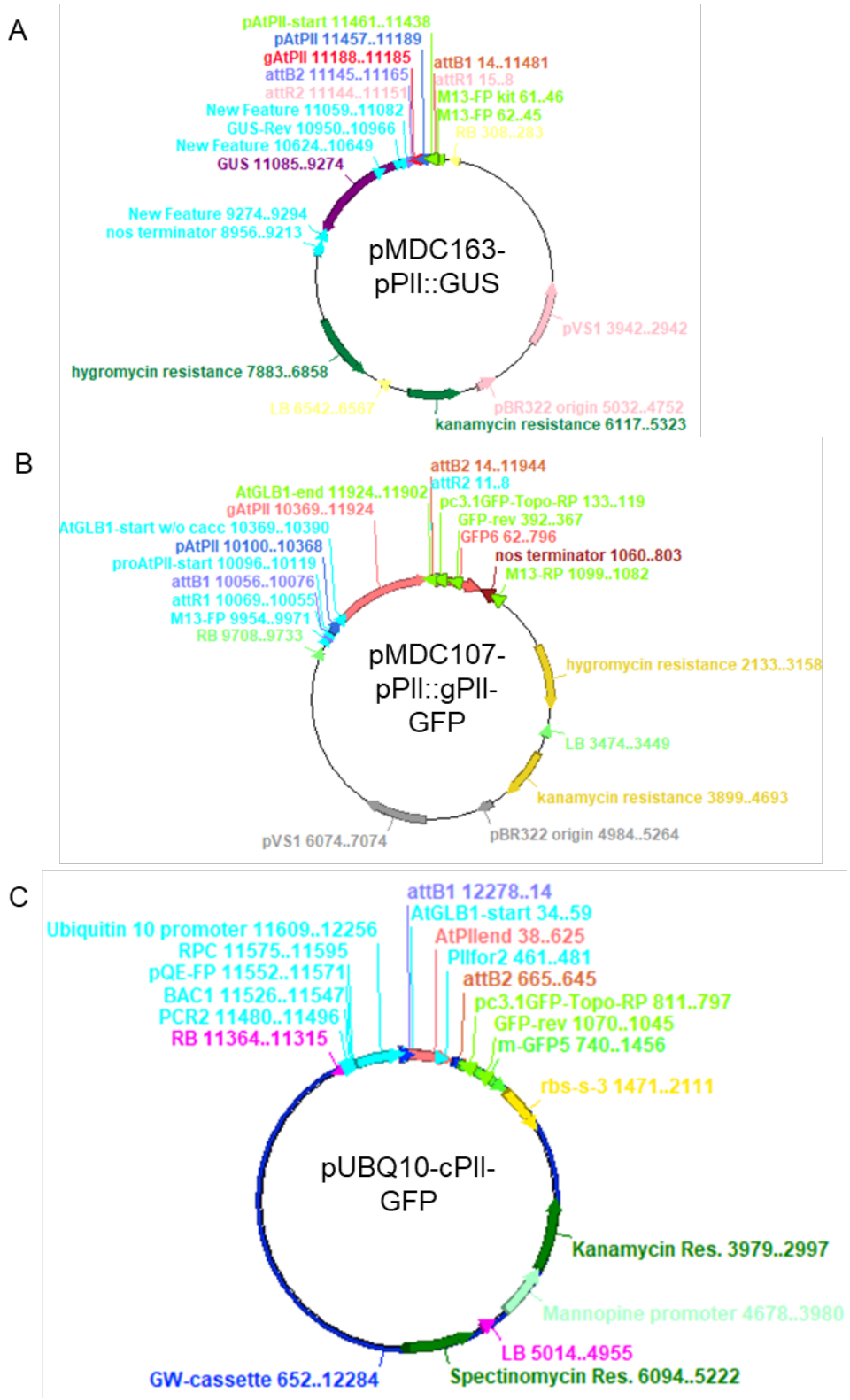

Figure A 4: Graphic maps of used pMDC163-pPII::GUS, pMDC107-pPII::gPII and pUBQ10::cPII-GFP used for expression and localization analyses, respectively.
A) pMDC163-pPII::GUS, B) pMDC107-pPII::gPII, C) pUBQ10::cPII-GFP. Graphic maps generated with ApE.

7.8 Graphic map of pFRET and pBiFC 2in1 vectors generated during thesis

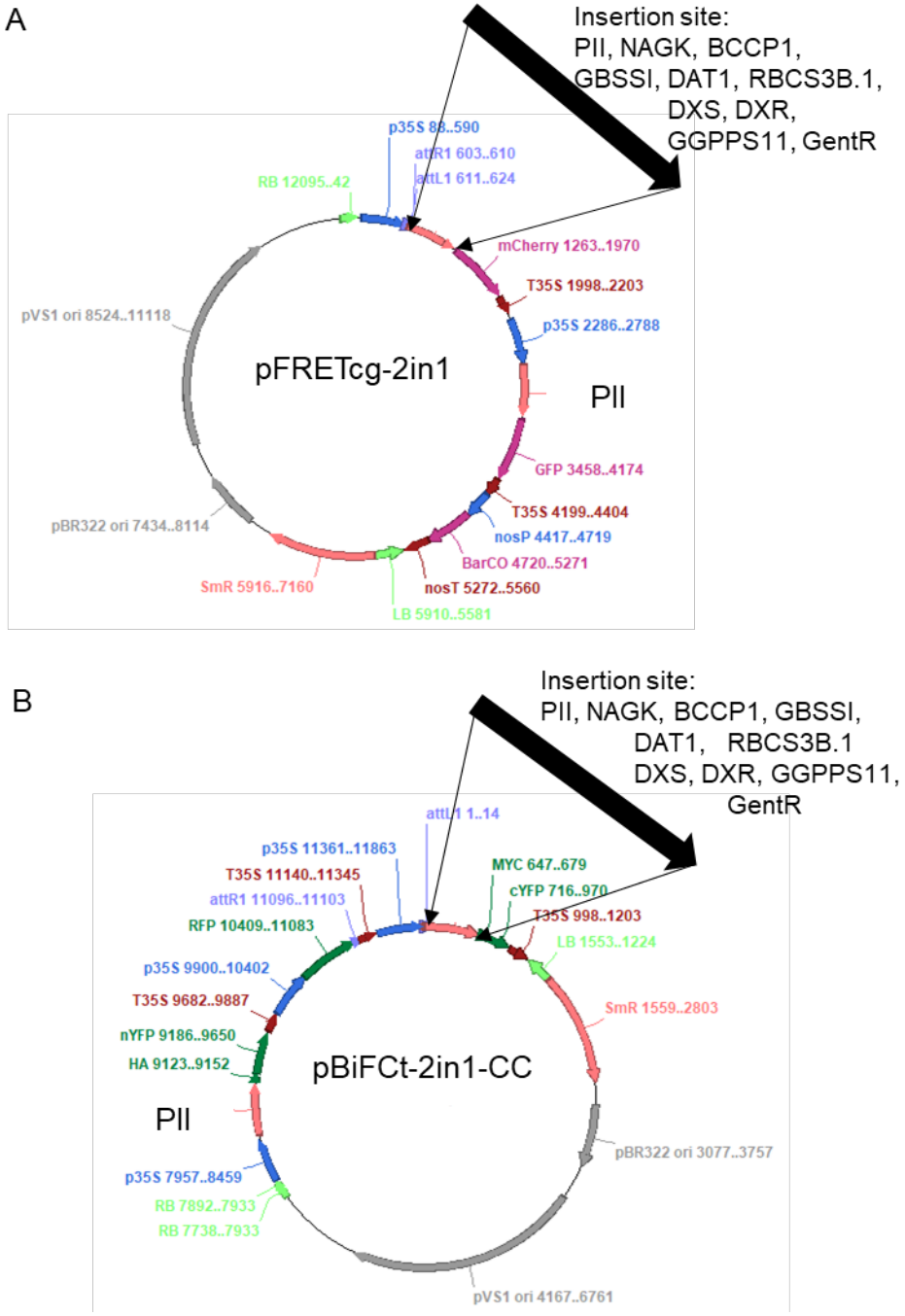

Figure A 5: Graphic map of pFRETcg-2in1 and pBiFCt-2in1-CC harbouring genes of interest A) pFRETcg-2in1 and B) pBiFCt-2in1-CC harbouring genes of interest at annotated sites. PII tagged with A) GFP, and B) nYFP, respectively. Genes of interest PII, NAGK, BCCP1, GBSSI, DAT1, RBCS3B.1, DXS, DXR, GGPPS11 and GentR tagged with A) mCherry, and B) cYFP, respectively. Graphic maps were generated with ApE.

7.9 *A. thaliana* lines used during thesis

Table 23: *A. thaliana* lines used during thesis

***A. thaliana* line**	**origin**	**usage**
Col-0	Nottingham Arabidopsis Stock Centre (NASC) or Arabidopsis Biological Resource Center (ABRC)	Phenotypic analyses, RNA extraction, amplification of genomic and coding sequences
PIIS2	SALK line from Nottingham Arabidopsis Stock Centre (NASC)	Phenotypic analyses, RNA extraction
pt-gk	From Nelson et al. (2007) provided by NASC	GFP-trap
Col-0 x *pUBQ::cAtPII-GFP* T1 #5	Stable transformation of Col-0 generated during this thesis	GFP-trap
***Col-0 x pUBQ::gAtPII-GFP* T2 10.2**	Stable transformation of Col-0 generated during this thesis	Temperature and light treatment, phenotypic analyses
***Col-0 x pAtPII::gAtPII-GFP* T2 1.5**	Stable transformation of Col-0 generated during this thesis	Localization studies
Col-0 x *pUBQ::gAtPII-GFP* T2 9.4	Stable transformation of Col-0 generated during this thesis	Phenotypic analyses
Col-0 x *pUBQ::gAtPII-GFP* T2 2.10	Stable transformation of Col-0 generated during this thesis	Phenotypic analyses
Col-0 x *pUBQ::cAtPII-GFP* T2 2.4	Stable transformation of Col-0 generated during this thesis	Phenotypic analyses
Col-0 x *pUBQ::cAtPII-GFP* T2 9.5	Stable transformation of Col-0 generated during this thesis	Phenotypic analyses
Col-0 x *pUBQ::cAtPII-GFP* T2 4.2	Stable transformation of Col-0 generated during this thesis	Phenotypic analyses
Col-0 x *pAtPII::gAtPII-GFP* T2 1.6	Stable transformation of Col-0 generated during this thesis	Phenotypic analyses
Col-0 x *pAtPII::gAtPII-GFP* T2 4.5	Stable transformation of Col-0 generated during this thesis	Phenotypic analyses
Col-0 x *p35S::cAtPII-GFP* T2 1.2.7	Stable transformation of Col-0 generated during this thesis	Phenotypic analyses
Col-0 x *p35S::cAtPII-GFP* T2 1.4.8	Stable transformation of Col-0 generated during this thesis	Phenotypic analyses
***PIIS2* x *pUBQ::gAtPII-GFP* T2 1.6**	Stable transformation of *PIIS2* generated during this thesis	Phenotypic analyses
***PIIS2* x *pUBQ::gAtPII-GFP* T2 4.3**	Stable transformation of *PIIS2* generated during this thesis	Phenotypic analyses
***PIIS2* x *pUBQ::gAtPII-GFP* T2 7.1**	Stable transformation of *PIIS2* generated during this thesis	Phenotypic analyses
***PIIS2* x *pUBQ::cAtPII-GFP* T2 1.1**	Stable transformation of *PIIS2* generated during this thesis	Phenotypic analyses
***PIIS2* x *pUBQ::cAtPII-GFP* T2 3.4**	Stable transformation of *PIIS2* generated during this thesis	Phenotypic analyses
***PIIS2* x *pAtPII::gAtPII-GFP* T2 3.3**	Stable transformation of *PIIS2* generated during this thesis	Phenotypic analyses
***PIIS2* x *pAtPII::gAtPII-GFP* T2 5.3**	Stable transformation of *PIIS2* generated during this thesis	Phenotypic analyses
***PIIS2* x *pAtPII::gAtPII-GFP* T3 2.4.1**	Stable transformation of *PIIS2* generated during this thesis	Phenotypic analyses
***PIIS2* x *pAtPII::gAtPII-GFP* T3 2.4.2**	Stable transformation of *PIIS2* generated during this thesis	Phenotypic analyses

7.10 Sensitivity screens using L-Gln as additional N source

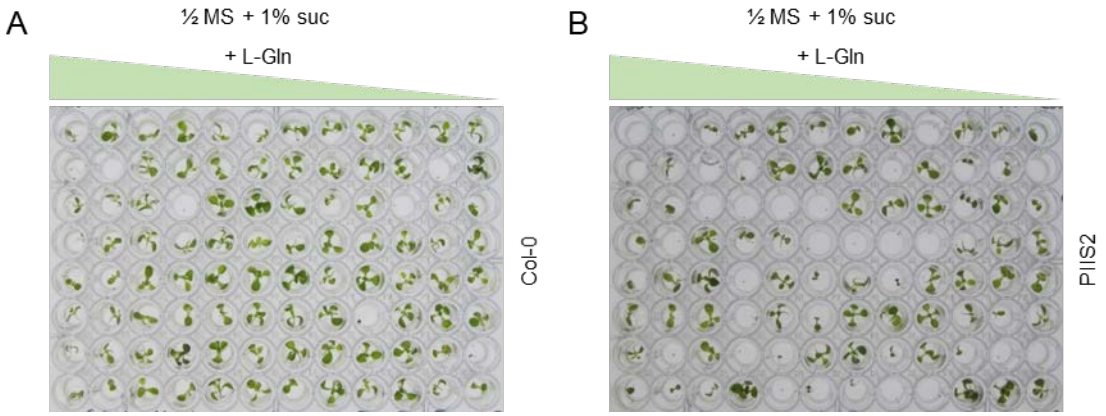

Figure A 6: Growth assay of L-Gln dilution series as additional N source.

14-day old seedlings of Col-0 (A) and *PIIS2* (B) grown on ½ MS+1% sucrose with or without L-Gln as additional N source under long day conditions. First lane represents 10 mM L-Gln. L-Gln was diluted 1:1 with ½ MS+1% sucrose from lane to lane, starting with 10 mM L-Gln to ~ 0.009 mM L-Gln in the second last lane. Last lane represents 0 mM L-Gln. A) Col-0; B) *PIIS2*.

7.11 Sensitivity screen using L-Glu, L-Gln and L-Arg as additional N source in N limiting and non-limiting media

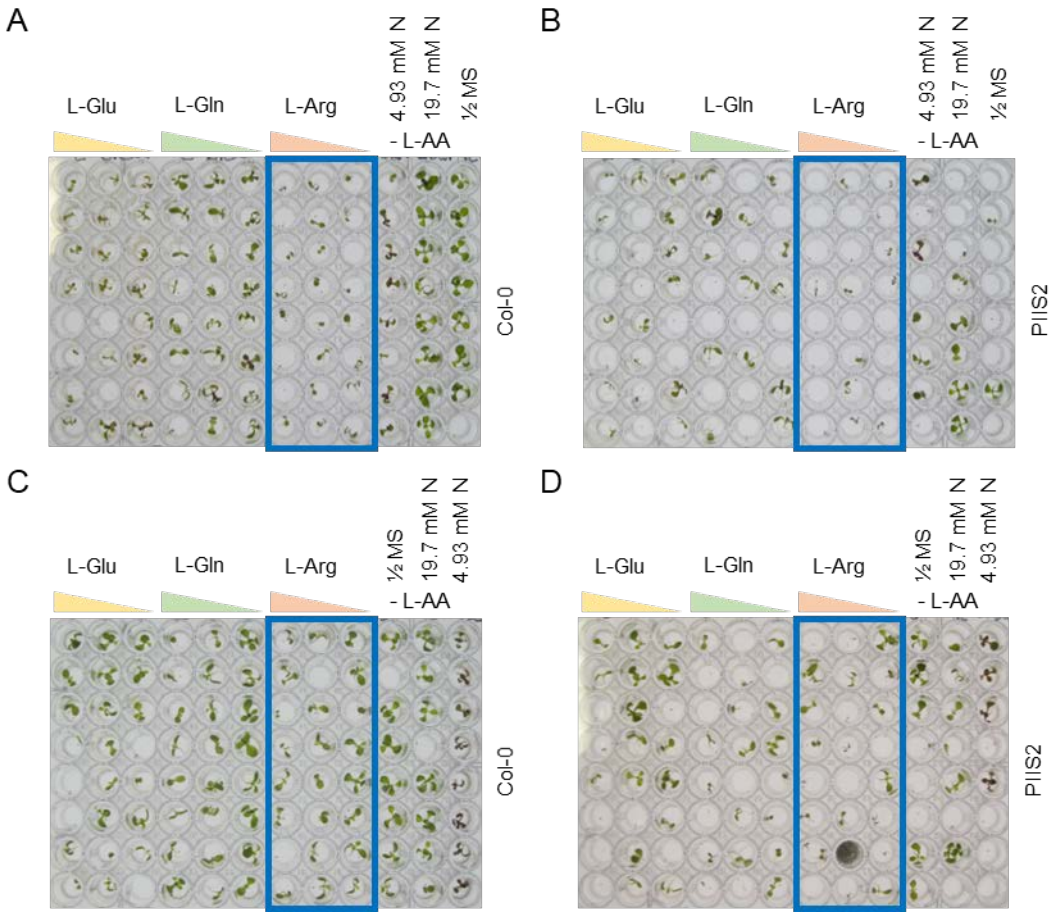

Figure A 7: Amino acid sensitivity screen using L-Glu, L-Gln or L-Arg as additional N source in N deficient or non-deficient media.

Col-0 (A, C) and *PIIS2* (B, D) grown on A)-B) 4.93 mM N in ½ MS-N+1% sucrose or C)-D) 19.7 mM N in ½ MS-N+1% sucrose with 0, 2.5, 5, and 10 mM L-Glu, L-Gln and L-Arg as additional N source. 4.93 mM N or 19.7 mM N in ½ MS-N+1% sucrose and ½ MS+1% sucrose without additional L-AA as controls.

7.12 Overview of phenotype of plants analysed during phenotypic analyses

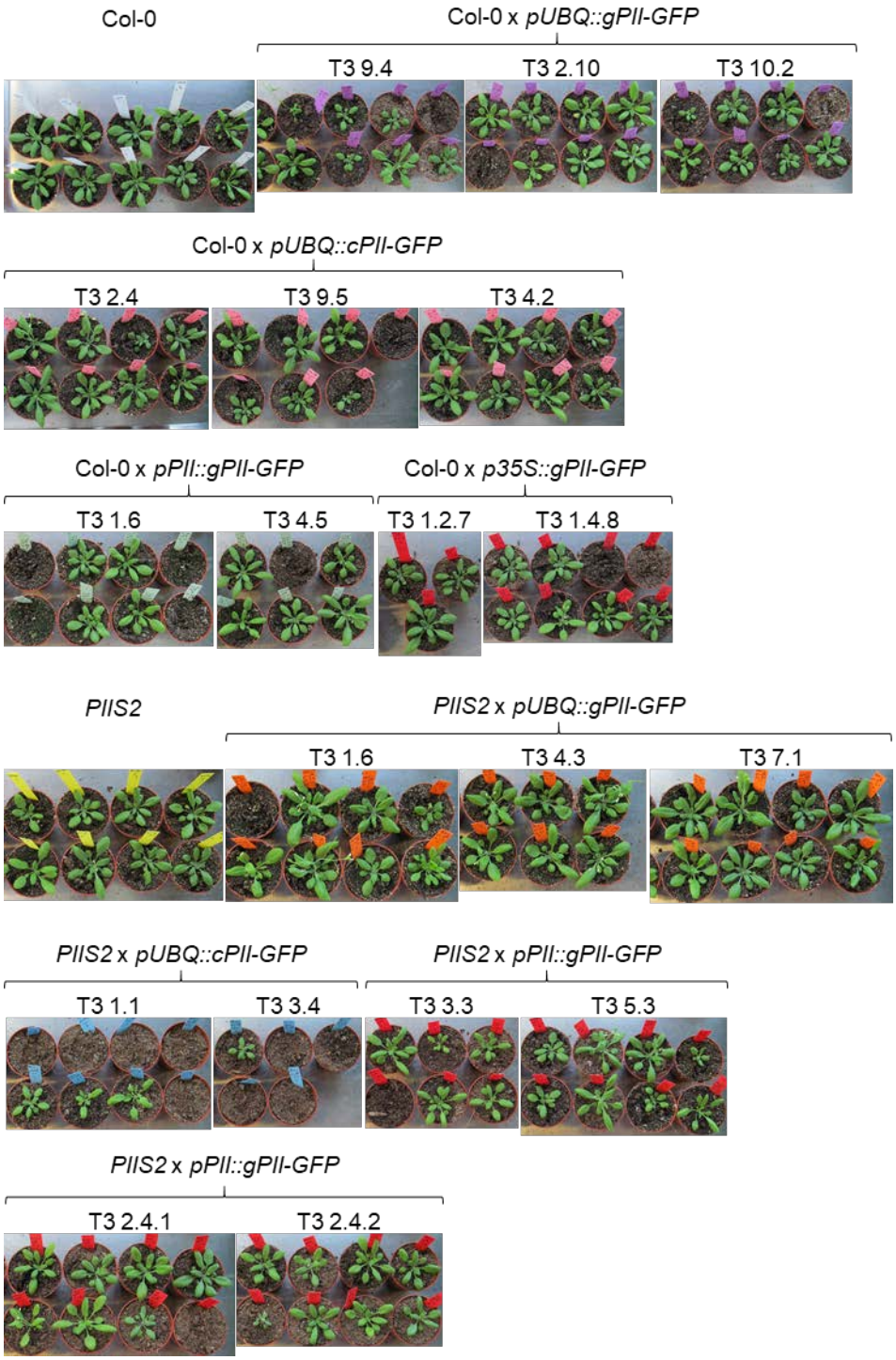

Figure A 8: Overview of T3 and T4 plants of phenotypic analysis in approach 1

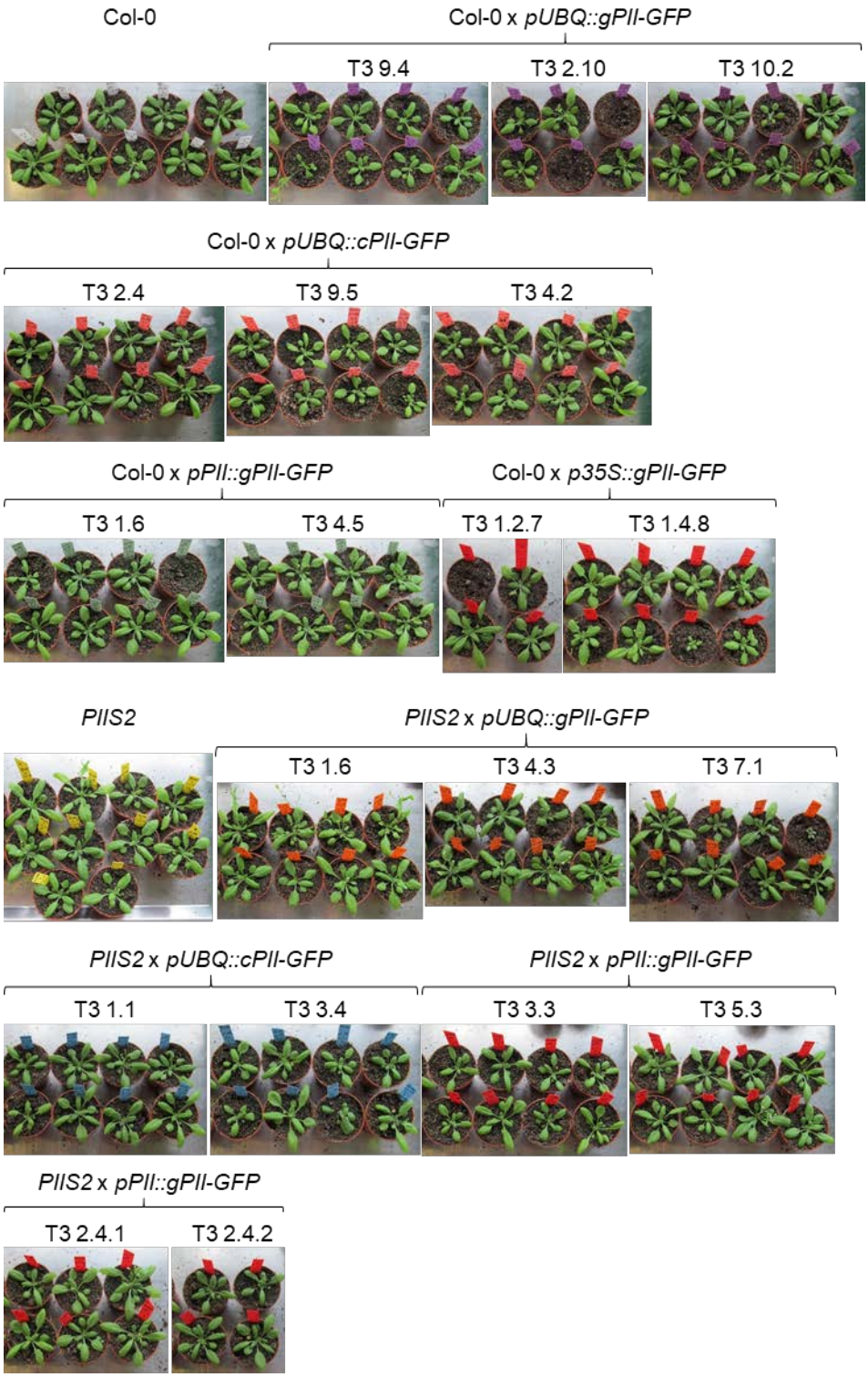

Figure A 9: Overview T3 and T4 plants of phenotypic analysis in approach two

7.13 Localization pattern of PII-OsQ-GFP under control of the 35S promoter in transiently transformed *N. benthamiana*

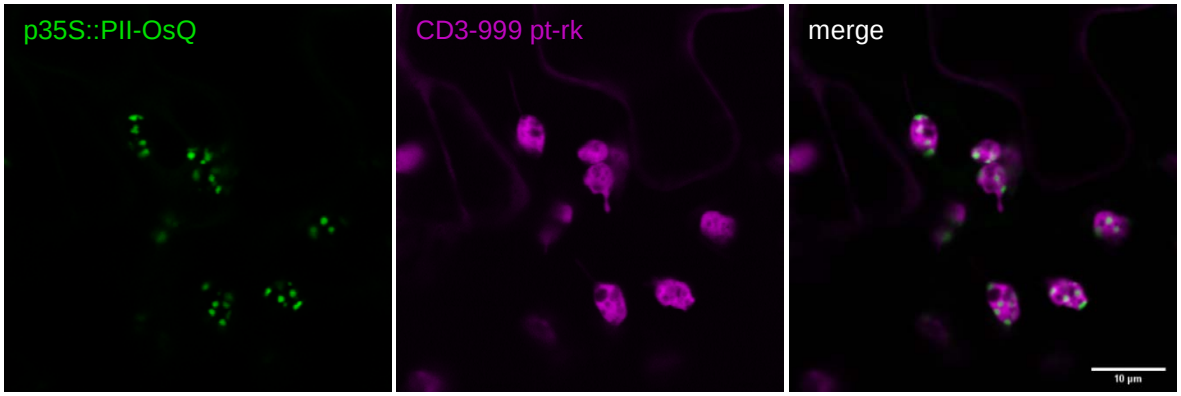

Figure A 10: PII-OsQ-GFP localizes in foci in leaves of transiently transformed *N. benthamiana* PII with reconstituted three amino acids of the Oryza sativa Q-loop tagged with GFP co-expressed with CD3-999 pt-gk localizes to plastids. Confocal images were taken three days after transient infiltration in N. benthamiana leaves.

7.14 Localization of GBSSI-GFP, DAT1-GFP and RBCS3B

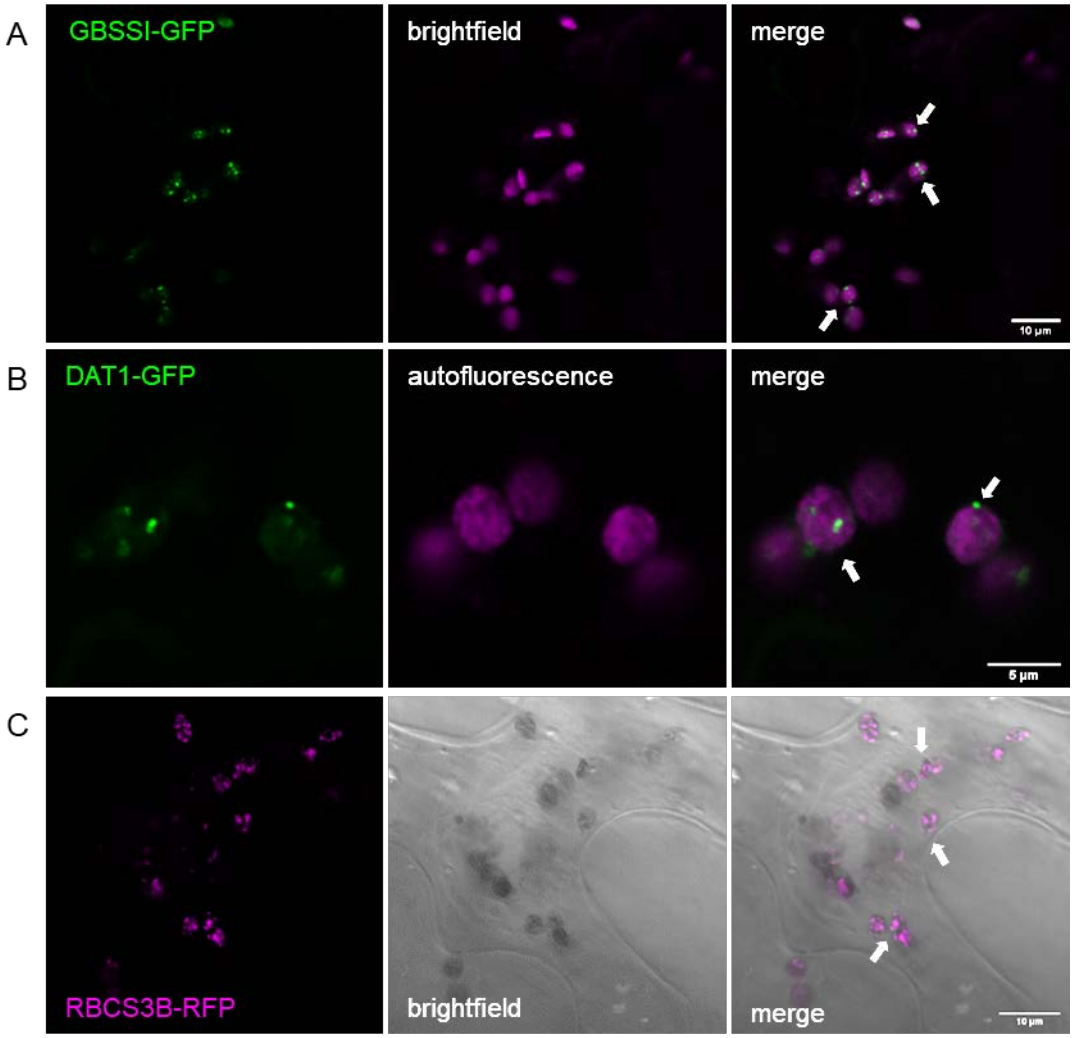

Figure A 11: GBSSI-GFP, DAT1-GFP and RBCS3B-RFP localize in aggregates to plastids of transiently transformed *N. benthamiana* leaf cells.

A) GBSSI-GFP localizes to plastids. Expression under the control of the *p35S*. B) DAT1-GFP localizes to plastids. Expression under the control of the *pUBQ*. C) RBCS3B-RFP localizes to plastids. *RBCS3B-RFP* was expressed under the control of the *p35S*.

White arrows: aggregates in plastids. Scale bars A) and C) 10 µm, B) 5 µm. Confocal images were taken 2 days after transient transformation of *N. benthamiana.*

7.15 Localization of PII-GFP after temperature and light treatment

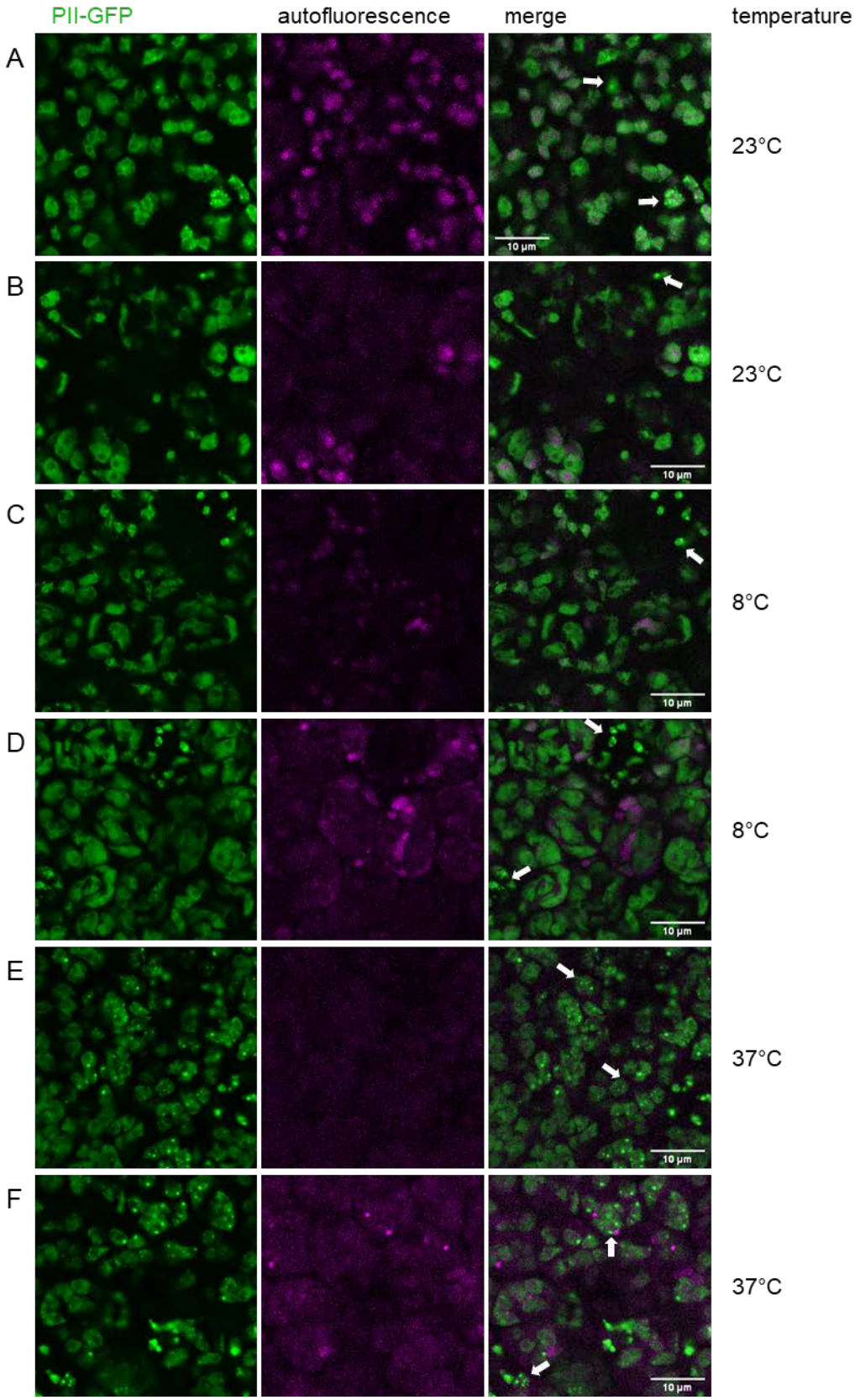

Figure A 12: PII-GFP localization changes slightly in 6-day old seedlings after 24h in varying temperature conditions in *A. thaliana* expressing PII-GFP under the control of *pUBQ*.
A) – B) PII-GFP localization after 24h in dark at 23°C. C) – D) PII-GFP localization after 24h in dark at 8°C. E) – F) PII-GFP localization after 24h in dark at 37°C.

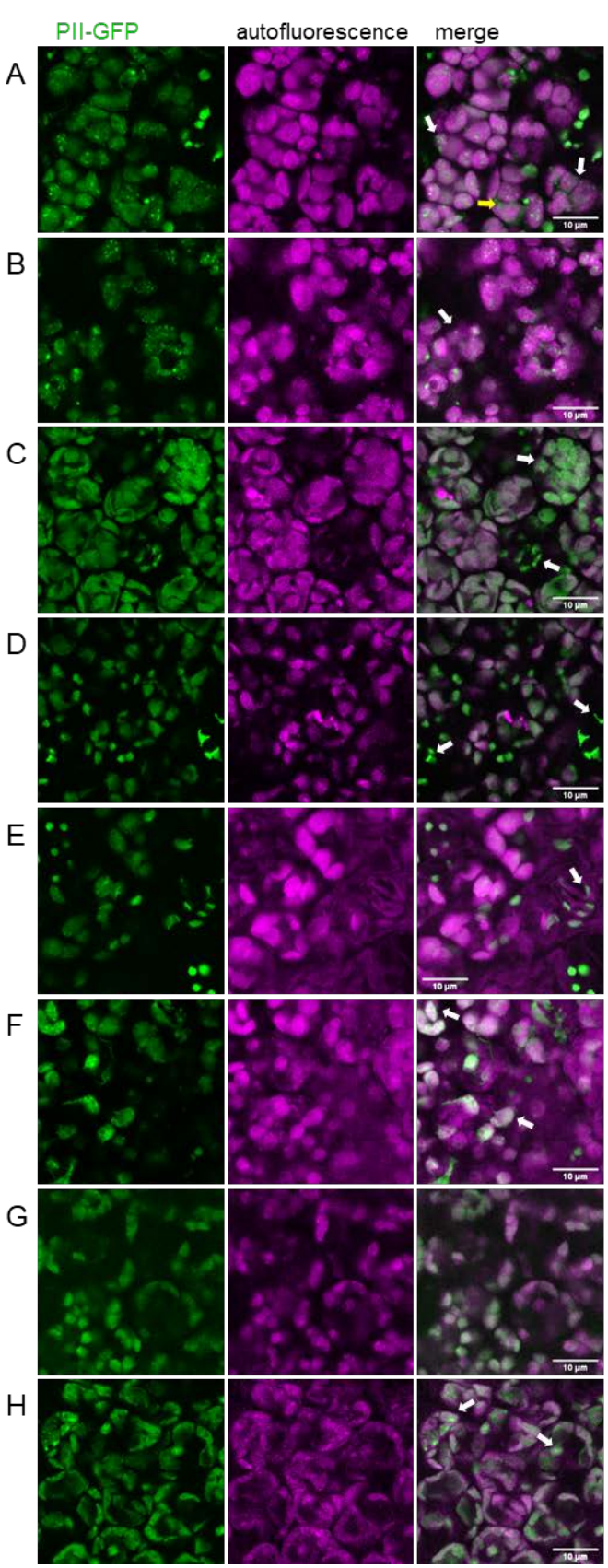

Figure A 13: PII-GFP localization changes slightly in 6-day old seedlings after 24h in varying light conditions in *A. thaliana* expressing *gPII-GFP* under control of *pUBQ*.
A)-B) PII-GFP localization after 24h under blue-light.
C)-D) PII-GFP localization after 24h under green light.
E)-F) PII-GFP localization after 24h under red light.
G)-H) PII-GFP localization after 24h under far-red light.

7.16 GFP-trap of isolated chloroplasts expressing PII-GFP

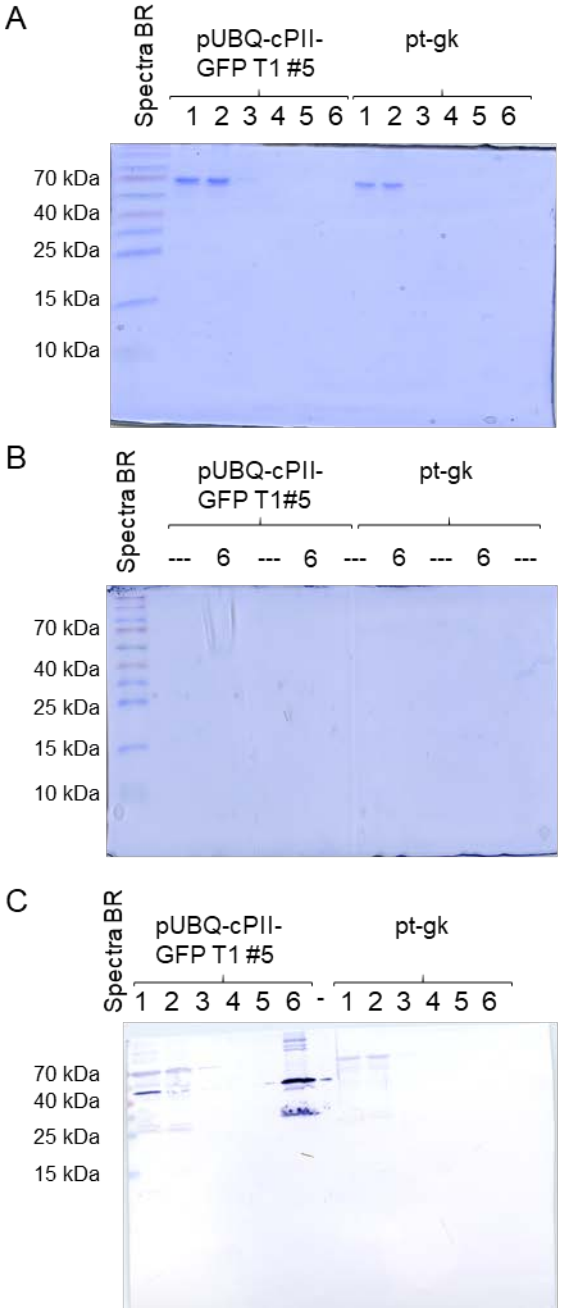

Figure A 14: SDS-PAGEs and Western blot of chloroplast extracts followed by GFP-trap from pt-gk (tobacco Rubisco cTP tagged with GFP) and *pUBQ-cPII-GFP* T1 #5 stable transformed in *A. thaliana* Col-0

A) SDS-PAGE of single fractions after GFP-trap. Signal detectable in fraction 1 and 2 for both samples at ~ 70 kDa.
B) SDS-PAGE of eluates after GFP-trap for MassSpec-analyses. No signal detectable.
C) Western blot of GFP-trapped chloroplast extracts with α-GFP. Incubation time 3h. GFP-signal detectable for cPII-GFP at ~ 45kDa in fraction 1, 2 and 6. Additional bands detectable at ~140 kDa, ~100 kDa and ~30 kDa in eluate of cPII-GFP. For pt-gk, detectable signal could be observed only at ~70 kDa and ~50 kDa in fraction 1 and 2. Same signal observed for cPII-GFP in fractions 1, 2 and 6.
Fraction 1: Input; 2: Flow-through; 3: Wash 1; 4: Wash 2; 5: Wash 3; 6: Elution. 15 µL per lane.

7.17 Predicted protein sequences of proteins of interest

Protein sequences of PII and known and putative novel interactors. Predicted cTP (TargetP and ChloroP) sequences underlined.

PII-mGFP5

Protein sequence with cTP and mGFP5 53.392 kDa (48.815 kDa without cTP):

MAASMTKPISITSLGFYSDRKNIAFSDCISICSGFRHSRPSCLDLVTKSPSNNSRVLPVVSAQISSDYIPDSKFYK
VEAIVRPWRIQQVSSALLKIGIRGVTVSDVRGFGAQGGSTERHGGSEFSEDKFVAKVKMEIVVKKDQVESVINT
IIEGARTGEIGDGKIFVLPVSDVIRVRTGERGEKAEKMTGDMLSPSKGGRADPAFLYKVVMGRPRRSTRVDSR
YPTSQIQGDIIMSKGEELFTGVVPILVELDGDVNGHKFSVSGEGEGDATYGKLTLKFICTTGKLPVPWPTLVTTF
TYGVQCFSRYPDHMKRHDFFKSAMPEGYVQERTIFFKDDGNYKTRAEVKFEGDTLVNRIELKGIDFKEDGNIL
GHKLEYNYNSHNVYIMADKQKNGIKANFKTRHNIEDGGVQLADHYQQNTPIGDGPVLLPDNHYLSTQSALSKD
PNEKRDHMVLLEFVTAAGITHGMDELYK

Free mGFP5 26,859 kDa

MSKGEELFTGVVPILVELDGDVNGHKFSVSGEGEGDATYGKLTLKFICTTGKLPVPWPTLVTTFTYGVQCFSR
YPDHMKRHDFFKSAMPEGYVQERTIFFKDDGNYKTRAEVKFEGDTLVNRIELKGIDFKEDGNILGHKLEYNYN
SHNVYIMADKQKNGIKANFKTRHNIEDGGVQLADHYQQNTPIGDGPVLLPDNHYLSTQSALSKDPNEKRDHM
VLLEFVTAAGITHGMDELYK

PII At4g01900

Protein sequence with cTP 21.276 kDa:

MAASMTKPISITSLGFYSDRKNIAFSDCISICSGFRHSRPSCLDLVTKSPSNNSRVLPVVSAQISSDYIPDSKFYK
VEAIVRPWRIQQVSSALLKIGIRGVTVSDVRGFGAQGGSTERHGGSEFSEDKFVAKVKMEIVVKKDQVESVINT
IIEGARTGEIGDGKIFVLPVSDVIRVRTGERGEKAEKMTGDMLSPS

Protein sequence without cTP according to ChloroP, 14.699 kDa:

AQISSDYIPDSKFYKVEAIVRPWRIQQVSSALLKIGIRGVTVSDVRGFGAQGGSTERHGGSEFSEDKFVAKVKM
EIVVKKDQVESVINTIIEGARTGEIGDGKIFVLPVSDVIRVRTGERGEKAEKMTGDMLSPS

NAGK At3g57560

Protein sequence with cTP 36.595 kDa (31.161 kDa without cTP):

MATVTSNASPKSFSFTVSNPFKTLIPNKSPSLCYPTRNKNHHRLGFSIKATVSTPPSIATGNAPSPDYRVEILSE
SLPFIQKFRGKTIVVKYGGAAMTSPELKSSVVSDLVLLACVGLRPILVHGGGPDINRYLKQLNIPAEFRDGLRVT
DATTMEIVSMVLVGKVNKNLVSLINAAGATAVGLSGHDGRLLTARPVPNSAQLGFVGEVARVDPSVLRPLVDY
GYIPVIASVAADDSGQAYNINADTVAGELAAALGAEKLILLTDVAGILENKEDPSSLIKEIDIKGVKKMIEDGKVAG
GMIPKVKCCIRSLAQGVKTASIIDGRRQHSLLHEIMSDEGAGTMITG

BCCP1 At5g16390

Protein sequence with cTP 29.614 kDa (21.011 kDa without cTP):

MASSSFSVTSPAAAASVYAVTQTSSHFPIQNRSRRVSFRLSAKPKLRFLSKPSRSSYPVVKAQSNKVSTGASS
NAAKVDGPSSAEGKEKNSLKESSASSPELATEESISEFLTQVTTLVKLVDSRDIVELQLKQLDCELVIRKKEALP
QPQAPASYVMMQQPNQPSYAQQMAPPAAPAAAAPAPSTPASLPPPSPPTPAKSSLPTVKSPMAGTFYRSPA
PGEPPFIKVGDKVQKGQVLCIVEAMKLMNEIESDHTGTVVDIVAEDGKPVSLDTPLFVVQP

BCCP2 At5g15530

Protein sequence with cTP 27.280 kDa (17.911 kDa without cTP):

MASLSVPCVKICALNRRVGSLPGISTQRWQPQPNGISFPSDVSQNHSAFWRLRATTNEVVSNSTPMTNGGY
MNGKAKTNVPEPAELSEFMAKVSGLLKLVDSKDIVELELKQLDCEIVIRKKEALQQAVPPAPVYHSMPPVMAD

FSMPPAQPVALPPSPTPTSTPATAKPTSAPSSSHPPLKSPMAGTFYRSPGPGEPPFVKVGDKVQKGQIVCIIE
AMKLMNEIEAEKSGTIMELLAEDGKPVSVDTPLFVIAP

BADC1 At3g56130

Protein sequence with cTP 29.577 kDa (23.565 kDa without cTP):

MASSAALGSLHQTLGSAINSQSEVHSLSGNWSASGNSCVPRWRLSNRNSNYRLVLRAKAAKSSTTTISDGSS
DASVSDGKKTVRRITFPKEVEALVHEMCDETEVAVLQLKVGDFEMNLKRKIGAATNPIPVADISPTVAPPIPSEP
MNKSASSAPSPSQAKPSSEKVSPFKNTSYGKPAKLAALEASGSTNYVLVTSPAVGKFQRSRTVKGKKQSPSC
KEGDAIKEGQVIGYLHQLGTELPVTSDVAGEVLKLLSDDGDSVGYGDPLVAVLPSFHDINIQ

BADC2 At1g52670

Protein sequence with cTP 29.575 kDa (24.221 kDa without cTP):

MNSCSLGAPKVRIFATNFSRLRCGNLLIPNNQRLFVDQSPMKYLSLRTTLRSVKAIQLSTVPPAETEAIADVKDS
DETKSTVVNTHLMPKSSEVEALISEITDSSSIAEFELKLGGFRLYVARKLTDESSPPPQQIQPVVAASATPEGVH
TNGSATSSSLAITKTSSSSADRPQTLANKAADQGLVILQSPTVGYFRRSKTIKGKRTPTICKEKDIVKEGQVLCY
IEQLGGQIPVESDVSGEIVKILREDGEPVGYNDALITVLPSFPGIKKLQ

BADC3 At3g15690.2

Protein sequence with cTP 28.170 kDa (22.224 kDa without cTP):

MASCSLGVPKIKISAVDLSRVRSGSLLIPYNQRSLLRQRPVKYLSLKTTFGSVKAVQVSTVPTAETSATIEVKDS
KEIKSSRLNAQLVPKPSEVEALVTEICDSSSIAEFELKLGGFRLYVARNIADNSSLQPPPTPAVTASNATTESPE
SNGSASSTSLAISKPASSAADQGLMILQSPKVGFFRRSKTIKGKRLPSSCKEKDQVKEGQILCYIEQLGGQFPIE
SDVTGEVVKILREDGEPVGYNDALISILPSFPGIKKLQ

GBSS1 At1g32900

Protein sequence with cTP 66.881 kDa (58.483 kDa without cTP):

MATVTASSNFVSRTSLFNNHGASSCSDVAQITLKGQSLTHCGLRSFNMVDNLQRRSQAKPVSAKSSKRSSKV
KTAGKIVCEKGMSVIFIGAEVGPWSKTGGLGDVLGGLPPALAARGHRVMTICPRYDQYKDAWDTCVVVQIKV
GDKVENVRFFHCYKRGVDRVFVDHPIFLAKVVGKTGSKIYGPITGVDYNDNQLRFSLLCQAALEAPQVLNLNS
SKYFSGPYGEDVVFVANDWHTALLPCYLKSMYQSRGVYMNAKVVFCIHNIAYQGRFAFDDYSLLNLPISFKSS
FDFMDGYEKPVKGRKINWMKAAILEAHRVLTVSPYYAQELISGVDRGVELHKYLRMKTVSGIINGMDVQEWNP
STDKYIDIKYDITTVTDAKPLIKEALQAAVGLPVDRDVPVIGFIGRLEEQKGSDILVEAISKFMGLNVQMVILGTGK
KKMEAQILELEEKFPGKAVGVAKFNVPLAHMITAGADFIIVPSRFEPCGLIQLHAMRYGTVPIVASTGGLVDTVK
DGYTGFHIGRFNVKCEVVDPDDVIATAKAVTRAVAVYGTSAMQEMVKNCMDQDFSWKGPARLWEKVLLSLN
VAGSEAGTEGEEIAPLAKENVATP

DAT1 At5g57850

Protein sequence with cTP 41.066 kDa (34.464 kDa without cTP):

MAGLSLEFTVNTWNLRSLSQVPCPLRHGFRFPRRLTRRRTILMCSDSSSQSWNVPVLSSYEVGERLKLARGG
QQFLAMYSSVVDGITTDPAAMVLPLDDHMVHRGHGVFDTALIINGYLYELDQHLDRILRSASMAKIPLPFDRETI
KRILIQTVSVSGCRDGSLRYWLSAGPGDFLLSPSQCLKPTLYAIVIKTNFAINPIGVKVVTSSIPIKPPEFATVKSV
NYLPNVLSQMEAEAKGAYAGIWVCKDGFIAEGPNMNVAFVVNGGKELVMPRFDNVLSGCTAKRTLTLAEQLV
SKGILKTVKVMDVTVEDGKKADEMMLIGSGIPIRPVIQWDEEFIGEGKEGPIAKALLDLLLEDMRSGPPSVRVLV
PY

RBCS3B At5g38410

Protein sequence with cTP 20.840 kDa (15.456 kDa without cTP):

MASSMLSSAAVVTSPAQATMVAPFTGLKSSAAFPVTRKTNKDITSIASNGGRVSCMKVWPPIGKKKFETLSYL
PDLSDVELAKEVDYLLRNKWIPCVEFELEVINTKHGFVYREHGNTPGYYDGRYWTMWKLPLFGCTDSAQVLK
EVEECKKEYPGAFIRIIGFDNTRQVQCISFIAYKPPSFTEA

DXR At5g62790

Protein sequence with cTP 54.230 kDa (44.977 kDa without cTP):

MTLNSLSPAESKAISFLDTSRFNPIPKLSGGFSLRRRNQGRGFGKGVKCSVKVQQQQQPPPAWPGRAVPEA
PRQSWDGPKPISIVGSTGSIGTQTLDIVAENPDKFRVVALAAGSNVTLLADQFSGSIISKIVLTRYVSDQTREIRR
FKPALVAVRNESLINELKEALADLDYKLEIIPGEQGVIEVARHPEAVTVVTGIVGCAGLKPTVAAIEAGKDIALAN
KETLIAGGPFVLPLANKHNVKILPADSEHSAIFQCIQGLPEGALRKIILTASGGAFRDWPVEKLKEVKVADALKH
PNWNMGKKITVDSATLFNKGLEVIEAHYLFGAEYDDIEIVIHPQSIIHSMIETQDSSVLAQLGWPDMRLPILYTMS
WPDRVPCSEVTWPRLDLCKLGSLTFKKPDNVKYPSMDLAYAAGRAGGTMTGVLSAANEKAVEMFIDEKISYL
DIFKVVELTCDKHRNELVTSPSLEEIVHYDLWAREYAANVQLSSGARPVHA

DXS At4g15560

Protein sequence with cTP 76.835 kDa (70.731 kDa without cTP):

MASSAFAFPSYIITKGGLSTDSCKSTSLSSSRSLVTDLPSPCLKPNNNSHSNRRAKVCASLAEKGEYYSNRPP
TPLLDTINYPIHMKNLSVKELKQLSDELRSDVIFNVSKTGGHLGSSLGVVELTVALHYIFNTPQDKILWDVGHQS
YPHKILTGRRGKMPTMRQTNGLSGFTKRGESEHDCFGTGHSSTTISAGLGMAVGRDLKGKNNNVVAVIGDG
AMTAGQAYEAMNNAGYLDSDMIVILNDNKQVSLPTATLDGPSPPVGALSSALSRLQSNPALRELREVAKGMT
KQIGGPMHQLAAKVDEYARGMISGTGSSLFEELGLYYIGPVDGHNIDDLVAILKEVKSTRTTGPVLIHVVTEKG
RGYPYAERADDKYHGVVKFDPATGRQFKTTNKTQSYTTYFAEALVAEAEVDKDVVAIHAAMGGGTGLNLFQR
RFPTRCFDVGIAEQHAVTFAAGLACEGLKPFCAIYSSFMQRAYDQVVHDVDLQKLPVRFAMDRAGLVGADGP
THCGAFDVTFMACLPNMIVMAPSDEADLFNMVATAVAIDDRPSCFRYPRGNGIGVALPPGNKGVPIEIGKGRIL
KEGERVALLGYGSAVQSCLGAAVMLEERGLNVTVADARFCKPLDRALIRSLAKSHEVLITVEEGSIGGFGSHV
VQFLALDGLLDGKLKWRPMVLPDRYIDHGAPADQLAEAGLMPSHIAATALNLIGAPREALF

GGPPS11 At4g36810

Protein sequence with cTP 40.175 kDa (34.029 kDa without cTP):

MASVTLGSWIVVHHHNHHHPSSILTKSRSRSCPITLTKPISFRSKRTVSSSSSIVSSSVVTKEDNLRQSEPSSFD
FMSYIITKAELVNKALDSAVPLREPLKIHEAMRYSLLAGGKRVRPVLCIAACELVGGEESTAMPAACAVEMIHT
MSLIHDDLPCMDNDDLRRGKPTNHKVFGEDVAVLAGDALLSFAFEHLASATSSDVVSPVRVVRAVGELAKAIG
TEGLVAGQVVDISSEGLDLNDVGLEHLEFIHLHKTAALLEASAVLGAIVGGGSDDEIERLRKFARCIGLLFQVVD
DILDVTKSSKELGKTAGKDLIADKLTYPKIMGLEKSREFAEKLNREARDQLLGFDSDKVAPLLALANYIAYRQN

7.18 Top hits that are not present in negative control obtained from masses of MassSpec analyses

Table 24: Hits revealed by M+H+ values obtained from MassSpec-analyses of Col-0 x *pUBQ-cPII-GFP* T1 #5 using ESI-Q-TOF, in silico analyses performed with MS-Fit ProteinProspector using SwissProt.2017.11.01 database

Protein size SDS-PAGE (kDa)	hit #	% coverage	Protein name	Protein size (kDa)
70.7	1	3.9	Protein LAZ1	54.712
	3	3.6	Protein indeterminate-domain 16	41.481
	4	2.3	Pentatricopeptide repeat-containing protein At5g27270	117.452
	5	2.7	PHD finger protein At1g33420	78.095
	6	4.6	Synaptotagmin-4	63.609
	8	3.7	Decapping nuclease DXO homolog, chloroplastic	60.382
	9	2.9	Probable indole-3-acetic acid-amido synthetase GH3.1	66.735
	10	1.9	DNA topoisomerase 1 alpha	102.800
58.5	2	11.5	Chloroplastic group IIA intron splicing facilitator CRS1, chloroplastic	83.591
	5	6.4	Kinesin-like protein KIN-6	108.254
	6	17.5	Actin-1	41.798
	7	17.5	Actin-3	41.798
	8	13.5	Mitochondrial import inner membrane translocase subunit TIM44-1	54.300
45.8	**1**	**62.8**	**PII (Nitrogen regulatory protein P-II homolog)**	**21.276**
	2	12.6	Calmodulin-interacting protein 111	111.520
	3	12.7	Kinesin-like protein KIN-7G	119.335
	4	9	Glutamate receptor 3.4	107.208
	5	7.8	ATPase 4, plasma membrane-type	105.718
	6	8.7	Kinesin-like protein KIN-7K, chloroplastic	108.468
	7	10.1	Kinesin-like protein KIN-UC	117.376
	8	17.4	Pentatricopeptide repeat-containing protein At4g21170	67.093
	9	14.2	Protein WEAK CHLOROPLAST MOVEMENT UNDER BLUE LIGHT-like 2	84.454
	10	14.8	Kinesin-like protein KIN-4B	118.763
45	**1**	**17.9**	**PII (Nitrogen regulatory protein P-II homolog)**	**21.276**
	2	8.1	Casein kinase 1-like protein 13	53.205
	3	8	Putative F-box protein At1g19160	40.402
	4	4.7	Ubiquitin-like modifier-activating enzyme atg7	76.522
	5	3.8	BTB/POZ domain-containing protein At1g67900	70.315
	6	7	Glutathione S-transferase F9	24.146
	8	5.9	Purple acid phosphatase 17	38.297
	9	4.7	Phosphate transporter PHO1 homolog 4	86.986
	10	6.9	Casein kinase 1-like protein 8	54.441
34.5	1	14	Peptide methionine sulfoxide reductase B8	15.430
	2	13.9	Peptide methionine sulfoxide reductase B7	15.457
	3	3.1	ATPase 9, plasma membrane-type	105.209

	4	6.3	PHD finger protein At1g33420	78.095
	5	4.3	DNA mismatch repair protein MSH5	91.124
	7	4.2	Pentatricopeptide repeat-containing protein At2g36980, mitochondrial	69.098
	8	6.8	Cyclic dof factor 5	44.007
	9	4.8	GTP-binding protein OBGC, chloroplastic	75.648
	10	9	F-box/kelch-repeat protein At4g39753	44.958
34	1	14	Peptide methionine sulfoxide reductase B8	15.430
	2	13.9	Peptide methionine sulfoxide reductase B7	15.457
	3	6.2	Protein LAZ1	54.712
	4	3.1	ATPase 9, plasma membrane-type	105.209
	5	6.3	PHD finger protein At1g33420	78.095
	6	4.3	DNA mismatch repair protein MSH5	91.124
	7	4.2	Pentatricopeptide repeat-containing protein At2g36980, mitochondrial	69.098
	8	6.8	Cyclic dof factor 5	44.007
	9	4.8	GTP-binding protein OBGC, chloroplastic	75.648
31.2	1	5.7	PHD finger protein At1g33420	78.095
	2	9.8	Casein kinase 1-like protein 13	53.205
	5	6	H/ACA ribonucleoprotein complex subunit 4	63.027
	6	7.4	Uridine 5'-monophosphate synthase	51.851
	7	6.9	UDP-glucuronate 4-epimerase 2	48.134
	8	8.5	Casein kinase 1-like protein 8	54.441
	9	18.9	Uncharacterized mitochondrial protein AtMg01030	12.928
	10	**16.8**	**PII (Nitrogen regulatory protein P-II homolog)**	**21.276**
24.2	3	8.3	Casein kinase 1-like protein 13	53.205
	4	13.6	Putative F-box protein At2g11200	17.671
	7	18.9	Uncharacterized mitochondrial protein AtMg01030	12.928
	8	8.1	Casein kinase 1-like protein 10	50.381
	9	3.8	DEAD-box ATP-dependent RNA helicase 13	93.987
	10	9	F-box protein At1g48060	42.267
23.6	2	5.6	GDSL esterase/lipase At2g36325	39.959
	3	3.2	Sialyltransferase-like protein 2	49.481
	4	5.4	RING-H2 finger protein ATL8	19.919
	5	4.5	F-box protein At3g60790	55.928
	6	4.2	Mitochondrial import inner membrane translocase subunit TIM44-1	54.300
	7	3.9	F-box/LRR-repeat protein At5g02910	51.847
	8	2.4	DNA topoisomerase 1 alpha	102.800
	9	4.8	Probable galacturonosyltransferase 11	61.879
	10	6.9	Methyl-CpG-binding domain-containing protein 1	23.153
22.2	1	15.7	Acetyl-coenzyme A carboxylase carboxyl transferase subunit alpha, chloroplastic	85.307
	2	10.9	Gamma-tubulin complex component 4	85.908
	4	9.4	Protein TIC110, chloroplastic	112.122
	5	23.9	Probable serine/threonine-protein kinase PBL1	43.088

Top hits that are not present in negative control obtained from masses of MassSpec analyses

	6	14.6	Protein ACTIVITY OF BC1 COMPLEX KINASE 8, chloroplastic	86.024
	7	9.9	E3 ubiquitin-protein ligase BRE1-like 2	103.397
	8	11.1	Factor of DNA methylation 4	85.868
	10	12.1	FT-interacting protein 1	91.004
21	1	13.6	Putative F-box protein At2g11200	17.671
	2	3.8	DEAD-box ATP-dependent RNA helicase 13	93.987
	6	9.7	Bet1-like protein At1g29060	15.102
	7	7.1	CRIB domain-containing protein RIC1	24.140
	8	3.5	UDP-glycosyltransferase 73B5	54.185
	9	4.7	65-kDa microtubule-associated protein 5	62.654
17.9	**1**	**20.9**	**PII (Nitrogen regulatory protein P-II homolog)**	**21.276**
	2	8	Alanine--glyoxylate aminotransferase 2 homolog 1, mitochondrial	51.953
	3	4.4	Cytochrome P450 71B35	57.322
	4	7.1	Uncharacterized protein At1g10890	33.696
	6	3.4	DEAD-box ATP-dependent RNA helicase 13	93.987
	7	4.5	Glyceraldehyde-3-phosphate dehydrogenase GAPCP1, chloroplastic	44.831
	8	5.3	Zinc finger CCCH domain-containing protein 54	28.176
	9	5.8	Uncharacterized GPI-anchored protein At5g19230	20.511
	10	5.8	CRIB domain-containing protein RIC1	24.140
15.5	**1**	**51**	**PII (Nitrogen regulatory protein P-II homolog)**	**21.276**
	2	5.7	Protein STICHEL-like 1	124.892
	3	8.4	Protein WEAK CHLOROPLAST MOVEMENT UNDER BLUE LIGHT-like 2	84.454
	5	7.5	Putative ion channel POLLUX-like 2	92.211
	6	5.5	CSC1-like protein At4g15430	87.168
	7	7.8	AP-1 complex subunit gamma-1	96.470
	8	11.1	Asparagine synthetase [glutamine-hydrolyzing] 2	65.030
	9	5.4	Phosphatidylinositol/phosphatidylcholine transfer protein SFH9	66.626
14.7	**1**	**15.3**	**PII (Nitrogen regulatory protein P-II homolog)**	**21.276**
	2	13.6	Putative F-box protein At2g11200	17.671
	4	3.8	DEAD-box ATP-dependent RNA helicase 13	93.987
	5	7.3	60S ribosomal protein L6-3	26.107
	6	5.5	AAA-ATPase At2g46620	55.911
	8	3.3	Protein STICHEL-like 1	124.892
	10	10.4	Bet1-like protein At1g29060	15.102

8 Curriculum vitae

9 Acknowledgement

Ich möchte mich besonders bei Prof. Dr. Klaus Harter und Prof. Dr. Karl Forchhammer bedanken für die Möglichkeit an diesem Projekt zu arbeiten, die Unterstützung und die Begutachtung meiner Thesis.

Ich danke dem Bundesministerium für Wissenschaft, Kunst und Forschung, und der DFG für die Förderung meiner Arbeit.

Des Weiteren möchte ich ganz besonders Dr. Üner Kolukisaoglu für die vielen Diskussionen und Anregungen, sowie für die Unterstützung während meines Projekts danken.

Zudem möchte ich allen derzeitigen und ehemaligen Kollegen von Bay 6-8, Juan, Claudi, Sabine, Nina, Rebecca, Anne, Fredi, Thomas, Stefan, Andi, Michael, Leander, Xuan und Angela, für die Diskussionen und Hilfestellungen, und die angenehme Atmosphäre in der Gruppe danken.

Ich möchte mich auch bei meinen Hiwis, Bachelorstudenten und Praktikanten, Marius, Benedikt, Xuan, Sascha, Fabienne, Marvin, Torren, Michael und Leander für ihre Unterstützung während meines Projekts bedanken.

Ich möchte allen Mitarbeitern der Zentralen Bereiche des ZMBP danken, besonders dem Gärtnerei-Team, ohne die, viele Arbeiten nicht möglich gewesen wären.

Ich danke Dr. Edda von Roepenack-Lahaye für die massenspektroskopischen Analysen.

Ich danke Dr. Suayib Üstün für die *A. tumefaciens* Linien für die Autophagie-Experimente.

Des Weiteren möchte ich mich auch bei allen weiteren Kollegen am ZMBP und der FG Forchhammer für das Beibringen von Methoden und die Diskussionen bedanken.

Ganz besonders möchte ich Nina, Rebecca und Thomas danken, die im Beruflichem und Privatem an meiner Seite stehen und standen. Danke, dass ihr in guten und schlechten Zeiten an meiner Seite steht.

Ich möchte meinen Freunden Fabi, Janina, Elena, Katja, Basti, Flo, Pablo, sowie Nina, Flo, Philipp, Anna und Arvid, danken, für die tollen Zeiten jetzt und während dem Studium.

Zum Schluss möchte ich meiner Familie und ganz besonders meinen Eltern danken, ohne deren Unterstützung ich nicht so weit gekommen wäre. Danke für alles.